ASSESSING THE ROLE OF POLYDISPERSITY AND COCRYSTALLIZATION ON CRYSTALLIZING N-ALKANES IN N-ALKANE SOLUTIONS

by

Michael John Senra

A dissertation submitted in partial fulfillment
of the requirements for the degree of
Doctor of Philosophy
(Chemical Engineering)
in the University of Michigan
2009

Doctoral Committee:

Professor H. Scott Fogler, Chair
Professor Ann Marie Sastry
Professor Johannes W. Schwank
Professor Robert M. Ziff

To my mother Suzanne and my siblings Stacy, Paul and Brian…
without them, this work is not possible

ACKNOWLEDGMENTS

The spine of this book will contain only two things: the title of this thesis and my name. However, this thesis involved more than just one person. It involved a cast of thousands providing intellectual knowledge, experimental know-how, emotional support and at times a combination of all three. I am truly indebted to so many people and these few pages are incapable of truly capturing my gratitude, but I will do my best.

First, I must acknowledge my research advisor, Professor H. Scott Fogler. Professor Fogler has been crucial in my development as a problem solver, a critical thinker and a leader. By setting high expectations for his students along with his breadth of knowledge, experience and his ability to bring the best out of his students, Professor Fogler graduates students that are able to think critically and independently and are capable of handling any technical question, even if not in their expertise. I am honored to be joining the list of proud graduates from this group who have received the fruits of spending time under his tutelage. Additionally, I am grateful to Professor Fogler for allowing me to grow as an educator. A professor with his credentials in the classroom could have just rested on his laurels and had me simply follow his way. Instead, Professor Fogler gave me significant input into the classes we taught together and treated me as an equal in the classroom and for this I will be forever grateful.

I would also like to thank Professors Ann Marie Sastry, Johannes Schwank and Robert Ziff for agreeing to serve on my dissertation committee. Their thoughts, insights and suggestions have been incorporated into this work and have greatly enhanced the quality of my thesis.

In the career of most graduate students, their funding sources act as nameless, faceless beings that you thank for money and send status updates on an agreed-upon basis. However, I have been fortunate to receive my funding primarily from petroleum companies that have provided not only financial support during my graduate studies, but also technical knowledge, support and a plethora of ideas that have moved my research forward. Particularly, I would like to thank the following people for making me feel like an equal in the world of oil although their knowledge far surpassed my own: Jefferson Creek and Rama Venkatesan at Chevron, Probjot Singh and William Thomason (retired) at ConocoPhillips and Stephan Allenson and Susan Garner at Nalco.

Further thanks go to the Flow Assurance Group at the ConocoPhillips Technology Center in Bartlesville, Oklahoma for their technical support and kindness during my internship in the blazing Oklahoma summer. Special thanks goes to Chrissy Maxey for her support, assistance and good humor while I was working on the cross polarized microscope and densitometer, vital parts of some of the research presented in this work. Further research for this thesis was done by Ekarit Paracharoensawad on the coldfinger and Tim Scholand on some of the gelation experiments. Abhishek Shetty also assisted with general issues concerning the rheometer. Without their assistance, this research would not have been completed in anything close to a timely manner.

The staff of the Chemical Engineering department at Michigan has been nothing

but hospitable, helpful and friendly towards me during my studies. Particularly, Laura Bracken has been essential with a wide number of issues dealing with the multitude of paperwork that has to be filled out and general group issues and Pablo Lavalle has helped with any questions regarding laboratory issues, whether for the research group or for the senior unit operations lab. Additionally, Leslie Cypert, Claire O'Connor, Susan Hamlin, Shelley Fellers, Linda Casto and Christine Moellering have been gracious in handling one of my numerous requests or questions whether research related, funding related or teaching related.

The Fogler research group has provided a wonderful environment not only to grow as a researcher but also to learn about a breadth of cultures and myself. The doctoral students that came before me acted as role models in both conducting quality academic research and fostering a group environment that aids in the development of great researchers and great people. Those Fogler alumni: Drs. Piyarat (Anne) Wattana, Ryan Hartman, Veerapat (Five) Tantayakom, Kristofer Paso, Hyun Su Lee, Kriangkrai Kraiwattanawong and Elizabeth Gorrepati passed their knowledge and insight to me to keep the continuity of excellence in the Fogler group. Hopefully, I have successfully completed this job. For the current graduate students: Tabish Maqbool, Zhenyu (Jason) Huang, Michael Hoepfner and Nasim Haji Akbari Balou, the baton has been passed and hopefully I could assist in your understanding of the positive aspects of belonging to the Fogler research group and pass it along to future group members. You are part of a special family and have a responsibility to continue the tradition of excellence. From the abilities that I have seen from all of you, I have full and complete confidence.

I would be remiss if I did not single out a few members of the Fogler group for

their assistance to me during this process. Ryan Hartman convinced me to become a member of this group and helped me greatly during the early years even though our research areas were drastically different. Tabish Maqbool has been an ideal group member during most of my graduate studies. Our numerous conversations about our research, teaching and his love of all things visual will be remembered... in spite of his corny sense of humor. Jason Huang has made it easy to come to work on a daily basis. His demeanor, kind heart and inquisitiveness about everything provided a perfect complement to me. These interactions will be greatly missed for I learned a great deal from them... and laughed a great deal as well.

The Fogler group is not complete without the caravan of post-docs, master's students and visiting scholars that made the group seem like a mini United Nations at times. I have had the pleasure to gain a wide number of perspectives on a wide number of issues. There are far too many people to note, but I would like to acknowledge Dr. Nihat Gurmen, Elena Mansilla Diaz, Prashant Singh, Ekarit (Ko) Paracharoensawad, Abu Hassan, Pornchai (Tee) Sae-Lim, Alejandra de Obeso, Dr. Sasanka Raha, Phathushedzho Mahvina, Shanpeng Han, Arjames (Jim) Balgoa, Pattanapong (Patt) Wongthahan, Perapat (Oat) Srikiratiwong and Satinee (Noi) Yindee.

I have been extremely fortunate and humbled to be surrounded by a unique set of individuals in Ann Arbor. Unlike my research group, these people chose to incorporate me into their inner circles and personally, I truly have no idea why.

Although he has read but a few pages of my academic work, Sean Langelier is one of the major reasons why this work has been completed. Graduate school is not a walk in the park and when the whole process seemed unberable or useless, he was always

willing to listen to me rant incessantly and provide strength and compassion when it was needed most. I have learned so much from Sean, generally about things not research related that I will never be able to repay him. Everyone should be fortunate enough to have a friend like him... in spite of his forgetfulness.

Liz Ranney has been a pillar of support to me at the latter end of my research. Her understanding, good-humor and kindness through all of the ups and downs of graduate school have been essential to me. Her loyalty is unparalleled and I hope to be as of much help to her from afar as she reaches the end of her research as she was for me.

Special thanks to Andrew (Bean) Getsoian for being an amazing human being. Joseph and Megan Mayne along with Meghan Cuddihy were caring and supportive through some of the most difficult points of graduate school. Neil Schweitzer and Daniel McNerny always provided an entertaining escape from the world of graduate school in drastically different ways. The loyalty and conversations with Siris Laursen and Phillip Christopher will not be forgotten and I greatly respect the two of them. Thanks to Ramsey Zeitoun for being himself. Additionally, Ashish Agarwal, Scott and Rebecca Ankeney, James and Amy Bucher, Lisa Colosi, Kevin Crichtley and Georgina Wilkins, Amanda Hickman, Adam Holewinski, David and Nikki Ingram, Wenyan (Grace) Ji, Daniel and Michelle Lilly, Deshpremy Mukhija, Abhishek Shetty, Stephanie Teich-McGoldrick and Thomas Westrich have all been part of making my time here one interesting experience.

Before coming to Michigan, I was fortunate to be associated with a number of wonderful people at Cornell who I am still in contact. Caleb Kovell has been nothing short of an amazing friend and some of my fondest memories during my graduate school

years are with him and his wife Lori, who deserves special recognition for being able to deal with the two of us. Caleb always provided the greatest distraction from graduate school, even if I was working in my office. My fellow graduates in chemical engineering at Cornell provided a source of inspiration with the work they have done since graduation. I am still honored to be a member of a class with such incredible talents, intellects and people. Joseph Barbi, Robert Cronin, Vincent Hull, Matthew Kemm, Richard Lee, Kevin Scelia and Brian Wong have still remained a part of my life after all of the years and I am grateful.

During my years at Cornell and Michigan, I had the chance to teach over 100 students under the supervision of the two best professors in chemical engineering in the country: Professor Scott Fogler and Professer T. Michael Duncan. Tershia Pinder-Grover and Susan Montgomery have also been great assets in my development as an educator while at Michigan. Although I learned a great deal from all of them, I arguably learned more from my students. Teaching has been one of the hallmarks of my time in academia, mainly because of the wonderful students that I have had the honor of instructing. Many of them have great abilities in so many areas and I hope that I was able in some small way to help them grow as learners and as people.

Although my surrogate families in Ithaca and Ann Arbor have been wonderful, nothing can quite compare to the family I have that is centered in New Bedford, Massachusetts. My family has been perpetually proud of me, even though they haven't a clue what this thesis is about and really just want me back home. I hopefully have represented my family well in everything I do. They most certainly deserve this much from me. Special thanks goes to my grandparents Frederick and Joanne Borges for their

love, support and all of the souvlakis and hospital food through the years.

Agradecimentos a minhas avos Angelo e Marieta Senra para seus amor e sustentação e doação-me de uma apreciação de ser português.

Finally, I would like to thank the four people to whom this thesis is dedicated. My incomparable sister Stacy has been nothing short of amazing to me. She has helped develop me into the personable human being that I never could have been if left to my own devices. All of my friends should be indebted to her because I wouldn't be who I am without her. When we were younger, she was often unfairly cast in my shadow. As time has progressed, she has stepped into her own and made a wonderful life for herself. I am excessively proud of Big Sis, her accomplishments and what she will accomplish in the future.

My wonderful brothers Paul and Brian have shown me that unconditional love does exist. They don't care about this thesis or my previous degrees or my previous successes and failures. They care about me because they know I will protect them as their big brother and will help them with their homework, make them lunch and read them stories. The smiles on their faces when I haven't seen them in a while are one thing that money can't buy. Both of them have the chance to far surpass anything that my sister and I have ever done and I will hopefully be there to see it come to fruition.

My mother Suzanne is nothing short of an inspiration to me and others. She was convinced that the best way for our family to succeed in this world was to obtain a great education. She gave me the gift of desiring knowledge, a love that I still have to this very day, which has made my life so very fulfilling. Her unselfish willingness to help people in any situation is one of numerous traits that I proudly have acquired from her. Although

this thesis represents years of work and struggle, the proudest moment I have had in my life thus far is her receiving her masters degree because of the struggle and personal sacrifice that degree required... to help not only herself but my two brothers. I have been told by numerous people that I make more sense once you have met my mother. This statement is one of the greatest compliments I can receive.

TABLE OF CONTENTS

LIST OF FIGURES

LIST OF TABLES

LIST OF APPENDICES

CHAPTER I

INTRODUCTION

Overview of Wax Deposition

The extraction, transportation and processing of crude oil are steps of crucial importance in the petroleum industry. As time has progressed, onshore oil reserves have become depleted, forcing petroleum companies to look further and further offshore for crude oil (Venkatesan et al., 2002). This offshore drilling has magnified the issues faced during oil transportation using subsea oil pipelines, the most economic and feasible means of transporting such large quantities of crude oil at a given time (Chang et al., 1999, Coutinho et al., 2006). Offshore drilling has increased the probability of wax deposition in subsea oil pipelines. Wax deposition, a function of a number of parameters including crude oil composition, temperature, pressure and fluid mechanics, can occur at sufficiently low temperatures where the liquid wax particles precipitate out of solution (Machado et al., 2001, Taraneh et al., 2008). Deposition is not limited to subsea oil pipelines: it can also occur in tankers, oil reservoir formations and process equipment (Hennessy et al., 1999, Garcia et al., 2000, Soni and Bharambe, 2006, Mehrotra and Bhat, 2007). Deposition in pipelines is arguably most the severe location, causing a reduction in the effective diameter of the pipeline for crude oil flow (Wang et al., 2003). The decrease in the effective diameter leads to a decrease in the pressure drop, which further reduces flow and stresses the pumping system (Soni and Bharambe, 2006). This situation becomes further problematic if the pipeline is allowed to become completely blocked by

a wax deposit, particularly in pipelines that are moving further and further offshore (Weispfennig, 2001). In fact, the Lasmo oil field in the United Kingdom had to be abandoned because of recurrent wax deposition causing pipeline blockage (Venkatesan et al., 2002). The United States Department of Energy estimated in 2001 that remediating blockages in subsea oil pipelines can cost $1 million/mile (Paso and Fogler, 2003). An example of a plugged pipeline can be seen in Figure 1.1.

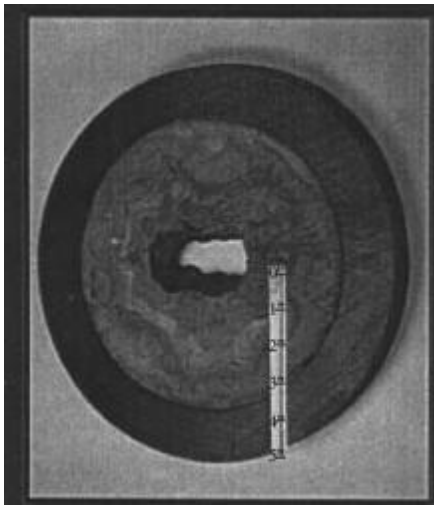

Figure 1.1: Example of a pipeline blockage (From Singh et al., 2000).

The Role of n-Alkanes in Wax Deposition

Although crude oils are a complex mixture consisting of materials such as paraffins, aromatics, naphthenes, resins, asphaltenes, sand, gas and water, it is generally accepted that the primary component of wax deposits in subsea oil pipelines are n-paraffins (Singh et al., 1999, Garcia et al., 2000, Kane et al., 2003). n-Paraffins (interchangeably referred to as n-alkanes) are the simplest hydrocarbon consisting solely of carbon-carbon single bonds having the molecular formula C_nH_{2n+2}, where n represents the carbon number of the n-alkane (Throughout this work, n-alkanes will be abbreviated

C_n.). Generally, n-paraffins are a major constituent of crude oils, typically comprising 10-20 weight % of crude oil (Kane et al., 2003). n-Alkanes with carbon numbers less than 10 typically exist in the vapor phase in subsea oil pipelines, but at reservoir conditions (70-150 °C and 8000-15000 psi), all other n-alkanes with carbon numbers as high as 90 will enter the pipeline in the liquid phase (Singh et al., 2001, Wu et al., 2002). As the crude oil leaves the reservoir and enters the pipeline, the crude oil will cool down because the pipeline temperature (as low as 4 °C in some places) is much cooler than the reservoir.

The solubility of n-paraffins in organic solvents (such as the majority of the components of crude oil) drastically decreases as a function of temperature (Singh et al., 1999). Therefore, as the crude oil progresses through the pipeline, the crude will continue to become cooler and it becomes possible that some of the n-alkanes present in the crude will reach their solubility limit. Once the n-alkanes reach their solubility limit, they will precipate out in the form of solid crystals. For the temperatures typically seen in subsea oil pipelines, these precipitated wax crystals will come from n-alkanes with a carbon number of approximately 18 or higher (Anderson et al., 2001, Coutinho et al., 2006, Bhat and Mehrotra, 2008). If this precipitation occurs close enough to the pipeline wall, deposition on the pipeline wall can result. Numerous mechanisms including molecular diffusion, shear dispersion, Brownian diffusion and gravity settling have been proposed to explain deposition in subsea oil pipelines, but it is generally accepted that deposition follows molecular diffusion (Singh et al., 2000). In developing a mechanism using molecular diffusion as the chief means of deposition, Singh outlined a five step process for wax deposition, presented below (Singh et al., 2000).

1.) Formation of an incipient gel layer on the cold surface
2.) Diffusion of select hydrocarbon molecules from the bulk fluid to the gel layer

3.) Internal diffusion of these molecules through the gel layer
4.) Precipitation of these molecules in the deposit
5.) Counterdiffusion of select hydrocarbon molecules out of the gel layer

Using this mechanism, Singh developed mass and energy balances to create a mathematical model shown to accurately predict wax deposition in small scale flow loops (Singh et al., 2000, 2001). A mass balance on wax particles equated the rate of change of wax (the left side of Equation 1.1) in the deposit to the flux of wax molecules from the bulk to the fluid-gel interface (the right side of Equation 1.1 and step 2 in the mechanism).

$$\frac{d}{dt}\left[\pi(R^2 - r^2)\overline{F}_w(t)L\rho_{gel}\right] = 2\pi r_i L k_l \left[C_{wb} - C_{ws}(T_i)\right] \tag{1.1}$$

Where: R = radius of the pipe (m)
r_i = radius of the deposit layer (m)
$\overline{F}_w$ = average mass fraction of the gel
ρ_{gel} = density of gel (kg/m^3)
L = length of the pipeline (m)
k_l = mass transfer coefficient (m/s)
C_{wb} = bulk concentration of the wax (kg/m^3)
C_{ws} = saturation concentration of the wax (kg/m^3)
T_i = interface temperature (K)

An energy balance is also performed at the bulk-gel interface where the radial convective heat flux from the bulk to the interface represents the difference of the rate of heat conduction through the deposit. The energy balance is provided in Equation 1.2.

$$2\pi r_i h_f (T_b - T_i) = \frac{2\pi k_e (T_i - T_a)}{\ln(R/r_i)} - 2\pi r_i k_l \left[C_{wb} - C_{ws}(T_i)\right]\Delta H_f \tag{1.2}$$

Where: h_f = heat transfer coefficient (W/m^2 K)
T_b = bulk temperature (K)
T_a = ambient temperature (K)
k_e = effective thermal conductivity of the gel (W/m K)
ΔH_f = heat of fusion (J/kg)

It is important to note that these deposits do not consist solely of solid wax crystals, but contain a small amount of wax (as little as 2 weight %) that entraps the liquid oil that has remained above its solubility limit (Holder and Winkler, 1965b, Singh et al., 1999). Further discussion of these wax-oil gels will occur later in the chapter.

Crystallization of n-Alkanes

Because wax deposits consist primarily of n-alkanes, it is critical to obtain an understanding of how n-alkanes crystallize to grasp how n-alkanes will crystallize in a more complex mixture. n-Alkanes are examples of rotator crystals that crystallize in distinct shapes dependent on the carbon number, molecular symmetry and temperature (Chazhengina et al., 2003). It is generally agreed that the four crystal shapes are triclinic, monoclinic, orthorhombic and hexagonal (Liu and Bennema, 1994). Although the cutoff points vary slightly in the literature, small molecules with an even carbon number ($6 \leq n \leq 26$) crystallize trinically, medium sized molecules with an even carbon number ($28 \leq n \leq 36$) crystallize monoclinically, large sized molecules with an even carbon number ($n \geq 38$) crystallize orthorhombically and all odd carbon number molecules crystallize hexagonally (Bennema, et al., 1992, Liu and Bennema, 1994, Dirand et al., 2002). In the liquid phase, n-alkanes exist as coiled molecules that undergo various conformations caused by rotations about the carbon-carbon bonds (Turner, 1971). However, as the n-alkanes reach their freezing point, the molecules become uncoiled and form a very ordered structure with the molecules exhibiting an all-trans conformation where the long axes of the carbon chains are parallel to one another and are layered one on top of the other (Turner, 1971, Dirand et al., 2002). The molecules are held together in this manner

solely from van der Waal interactions, the primary molecular force present in hydrocarbons (Liu and Bennema, 1994). From microscopic evidence and crystal modeling, crystals generally exist as a thin platelet with the (001) face being the most dominant (Bennema et al., 1992, Liu and Bennema, 1994).

However, crystal systems containing only one component are not seen in crude oil systems. Crude oils contain a broad range of n-alkanes, many of which are capable of crystallizing in conditions generally found in subsea oil pipelines. When multiple n-alkanes are capable of crystallizing from melts (i.e. no solvent), a wide number of solid solutions form dependent on the temperature and the composition of the melt. It is possible that two or more components can integrate into one common crystal structure if certain criteria are met: the molecules are sufficiently chemically similar, the molecules are of relatively the same size and the molecules self-crystallize in the same or similar crystal morphology (Turner, 1971). Kravchenko developed a prediction of mutual solubility for binary n-alkane mixtures as reported in the work of Dirand (Dirand et al., 2002).

Table 1.1: Kravchenko's predictions for miscibility of solid solutions of binary mixtures. Δn represents the difference in carbon number between the two components of the mixture (Dirand et al., 1998). [a] In order for miscibility to occur, the crystalline structures must be identical (for total miscibility) or similar (for partial miscibility)

	Miscibility of Solid Solutions		
Δn	**Total**	**Partial**	**None**
1[a]	n≥17	8<n<17	n≤7
2	n≥34	14<n<34	n≤13
4	n≥68	28<n<68	n≤27

From Table 1.1, the criteria developed by Turner can be properly assessed. The first criterion is easily met because n-alkanes are chemically identical. The second criterion is met if the two n-alkanes have similar molecular sizes. As the carbon number (C_n)

increases, the molecular size of an n-alkane with a C_n of n becomes closer to an n-alkane with a C_n of n+2, which explains the trend shown in Table 1.1 that miscibility increases with increasing carbon number for a given C_n difference. The final criterion explains the caveat in Table 1.1 for many odd and even C_n do not have similar crystal morphologies and would be unable to cocrystallize. Differences between the odd C_n alkanes and even C_n alkanes exist either at a subcell level (most odd C_n have a rhombic subcell while some even C_n alkanes have a triclinic subcell) or at a molecular level with different end group packings and/or cell symmetries (Turner, 1971).

For mixtures that satisfy all three criteria and are capable of cocrystallization, the mechanism by which the different molecules cocrystallize has been generally agreed upon (Turner, 1971, Dirand et al., 1998). In this mechanism, the larger molecules conform to the smaller molecules by bending at one end of the molecule. A schematic of this can be seen in Figure 1.2.

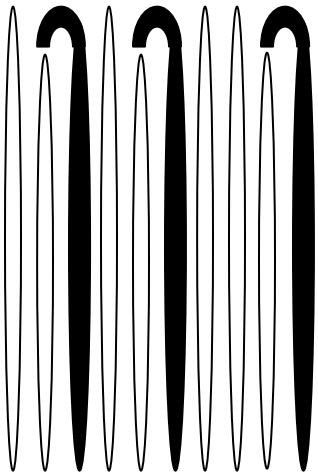

Figure 1.2: Sample molecular configuration for multiple n-alkanes cocrystallizing. The dark molecules are bending to associate with the smaller n-alkanes to form a common crystal structure.

As the carbon number difference (and thus the difference in the molecular size) increases, it becomes increasingly difficult for the end group of the longer molecule to appropriately

pack into the crystal structure. This difficulty leads to a sharp decrease in the stability of the cocrystal, preventing it from forming (Clavell-Grunbaum et al., 1997). Using Raman spectroscopy, it was shown that the longer n-alkane in binary n-alkane mixture undergoes much more conformational disorder than the shorter n-alkane, solidifying the mechanism described above (Clavell-Grunbaum et al., 1997).

Differences in n-alkane crystallization exist when comparing crystallization from the melt versus crystallization from solution. When n-alkanes crystallize in subsea oil pipelines, the solution is a complex mixture of primarily organic compounds. A major difference is that solubility must be taken into account, meaning that crystallization is now also a function of the concentration of the n-alkane in the solution and the composition of the solution in addition to temperature. Work using C_{36}, C_{32} and C_{28} as the crystallizable n-alkanes showed that crystallization occurred at far lower temperatures and some of the solid solutions present in the melt do not occur in solution because crystallization occurs at a lower temperature (Guo et al., 2004). The ability of a solvent to solvate n-alkanes is related to the intermolecular forces between the n-alkane and the solvent, intramolecular forces within the solvent and the ability of the solvent to contact the n-alkane (Jennings and Weispfennig, 2005). Because n-alkanes are very simple molecules, good solvents for n-alkanes are small molecules that contain little complexation, are non-polar and do not strongly self-associate (Alcohols and carboxylic acids are examples of compounds that strongly self-associate, primarily because of hydrogen bonding. Both are poor solvents for waxes.). For crude oils vary drastically in their composition, particularly the content of n-alkanes, branched alkanes, aromatics,

asphaltenes and resins, the temperature at which crystallization (commonly referred to as the cloud point) begins varies drastically from crude to crude.

Although a solvent has been incorporated into the system, research has shown that n-alkanes are still capable of cocrystallizing with one another and forming multicomponent solid solutions (Holder and Winkler, 1965a, Pauly et al., 1998, Briard et al., 2006). For a given solvent, the ability of an n-alkane to precipitate out of solution is based on its molecular size and its composition. The larger molecules are less soluble because it is more difficult for the solvent to completely solvate the molecule. However, longer n-alkanes are naturally present in smaller concentrations in crude oil than the shorter n-alkanes. Crude oils typically have a recurrence ratio of C_{n+1}/C_n of approximately 0.7-0.8 (Paso et al., 2005). In other words, the ratio of the mass fraction of C_{n+1} present in the purely liquid crude to the ratio of the mass fraction of C_n present in the purely liquid crude is approximately 0.7-0.8. Therefore, the least soluble n-alkane that will crystallize out at the cloud point will not necessarily be the longest n-alkane present in the crude oil as shown in Figure 1.3 below (Chevallier et al., 2000). Figure 1.3 shows that the maximum percent of a particular n-paraffin occurs around C_{30} and decreases for higher carbon numbers, indicating the trade-off between composition and molecular size.

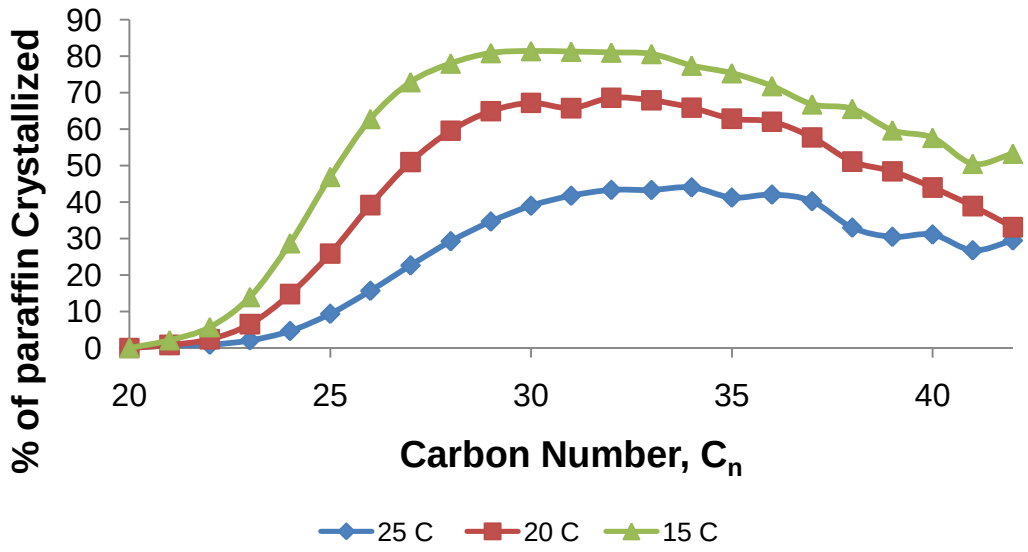

Figure 1.3: Percentage of paraffins crystallized versus carbon number for various temperatures for a multiparaffinic wax in normal tetradecane. (Data from Chevallier et al., 2000)

Depostion and Gelation in Subsea Oil Pipelines

Crystallization, although a necessary event in order for deposition to occur, does not guarantee that a deposit will form. As mentioned earlier, the deposition mechanism is a multi-step process where n-alkane precipitation is just one step. In fact, it is generally accepted that n-alkanes that precipitate in the bulk do not contribute to the wax deposits seen in subsea oil pipelines (Singh et al., 2001). Recall that wax deposits do not consist solely of solid wax particles, but are actually a wax-oil gel consisting of primarily liquid oil that is entrapped by the solid wax particles (Ronnigsen et al., 1991). Only 1-2% of wax is necessary for gelation to occur (Kane et al., 2003). In order for a gel to occur, the solid wax crystals must be capable of forming a volume spanning network. From the combination of physical contact and attractive interactions between the solid crystals, a volume spanning network can form. Figure 1.4 shows microscopic images of a case

where there are insufficient crystal-crystal interactions to form a gel (left) and a case where sufficient crystal-crystal interactions are present to form a gel.

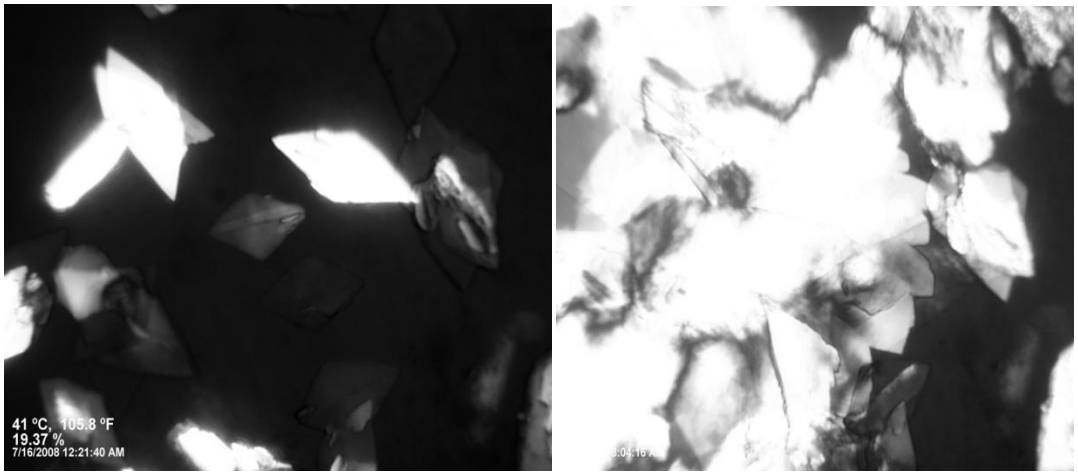

Figure 1.4: Microscopy images indicating the ability of a system to form a gel. The image on the left has insufficient interactions between the crystals to form a gel. The image on the right has sufficient interactions between the crystals to from a gel.

Two major factors dictate whether a gel deposit that forms in a subsea oil pipeline is going to be problematic: (1) the rate of growth of the deposit and (2) the strength of the deposit. If a deposit does not grow very quickly and is not very strong, the gelation will be of little interest to the petroleum industry because oil flow will not be greatly restricted and it is possible that the deposit could be broken simply by the flowing oil. The strength of a wax-oil deposit is dependent on two broad areas: (1) the operating conditions of the pipeline (i.e. internal temperature, external temperature, flow rate, etc.) and (2) the composition of the oil (i.e. wax fraction, asphaltene content, presence of inhibitors and additives, etc.) Both effects will be discussed later in the chapter. In order to understand how to compare the gels from various deposits, a few properties must be first discussed

Relevant Properties: Cloud Point, Gelation Temperature, Pour Point and Yield Stress

The cloud point has been briefly discussed earlier in the chapter and represents the solubility limit of crude oil. In other words, the cloud point represents the temperature where solid wax crystals are first created. Cloud points can vary drastically from crude oil to crude oil depending on their composition, particularly wax content, but a range for typical cloud points is 10 °C – 60 °C. Because crude oils are dark mixtures, it is impossible to evaluate crystallization with the naked eye (All work in this research utilized a clear solvent so therefore the cloud point could be obtained using visual inspection). Therefore, three other methods are generally used: (1) cross-polarized microscopy, where the solid wax crystals will reflect the cross polarized light while the crude oil will not, (2) differential scanning calorimetry, where the heat released by the phase change from liquid to solid can be detected and (3) viscometry, where the experimental viscosity deviates from an extrapolated Arrhenius viscosity curve. However, these methods can provide drastically different cloud point measurements, particularly if high cooling rates are used (Ronningsen et al., 1991). Generally, using either of the first two methods at a relatively low cooling rate will provide an accurate representation of the cloud point.

Once crystals have formed, it becomes possible for a gel to form. Two ways to measure this point are the pour point and the gelation temperature. The pour point represents the temperature when gelation occurs under static conditions (Venkatesan et al., 2002). The ASTM 97-96a standard method is used to find the gel point. In this method, the sample is cooled down and the sample is examined every 3 °C to determine if the sample is capable of moving (pouring). Therefore, the pour point represents the

lowest temperature when a waxy oil sample does not flow when cooled statically. Although a pour point must be lower than the cloud point, the pour point and cloud point are not well correlated. Depending on the oil, the difference between the cloud point of a crude oil and the pour point of a crude oil can range from 5 to 60 °C (Visintin et al., 2005). This difference seen between various crude oils is seen primarily because of the differing compositions of crude oil, particularly the ability of wax crystals to aggregate in different crudes.

The gelation temperature is closely related to the pour point except that the gelation temperature is also a function of the stress applied on the system. The pour point is the gelation temperature at a given cooling rate for a system where no stress is applied. Rheometry is typically used to evaluate a gelation temperature because it is capable of applying a stress to the wax-oil gel. Winter showed that the gel point of a cross-linking polymer could be determined by observing the crossing of G' (storage modulus) with G" (loss modulus) (Winter, 1987). The storage modulus is related to the solid-like characteristics of the system and the loss modulus is related to the liquid-like characteristics of the system. Therefore, the crossing of G' and G" represents the transition from a liquid-like system to a solid-like system. Work by Singh extended this conclusion to wax-oil gels formed from crude oils (Singh et al., 1999). Figure 1.5 shows a hypothetical oil that has been analyzed using a rheometer. The system in Figure 1.5 has gelled because of the crossing of the G' and G", a point marked as the gelation temperature.

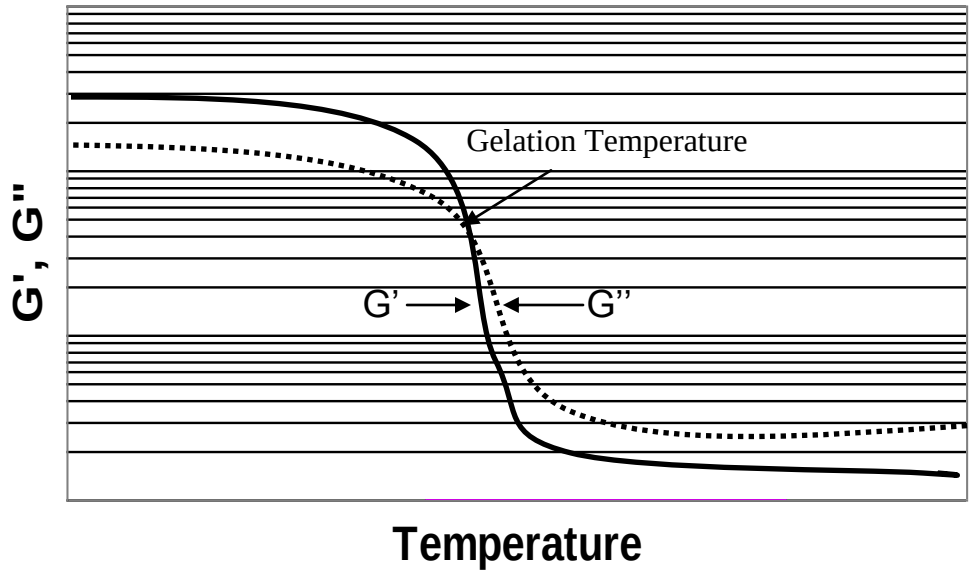

Figure 1.5: Representative rheometric results for viscoelastic fluids. In the graph, G' and G" cross over, indicating the occurrence of the formation of a gel.

The yield stress is an important variable in the petroleum industry to compare the strength of deposits and represents the amount of stress that needs to be applied in order for the forces between the wax crystals to be overcome, causing the gel to break. The yielding of crude oils is generally seen as a three step process, each with its own yield stress (Chang et al., 1999). The first step is the elastic response, where the strain linearly increases with the shear stress. At the elastic-limit yield stress, the system transitions from reversible elastic deformation to creep. When creep occurs, the linear relationship between strain and shear stress no longer exists. At the static yield stress, the gel fractures and the strain begins to rapidly increase. The final yield stress is known as the dynamic yield stress, which represents a fictitious stress used to represent the oil properties at final shear.

The yield stress is a function of the cooling rate, the stress applied to the oil and the temperature at which the stress is applied. The yield stress does not have to be

directly correlated to the pour point and/or gelation temperature: the pour point and the gelation temperature measure at what temperature the gel forms, not how strong the gel is. Similar to the gelation temperature, rheometry is generally used to measure the yield stress because a stress needs to be applied to the system. Although shear stress will be the independent variable, any number of variables can be used as the dependent variable because when the system transitions from a gel to a broken gel, numerous properties make a drastic change. Generally the dependent variable used for comparison is either the strain (as noted earlier) or viscosity, as shown in Figure 1.6.

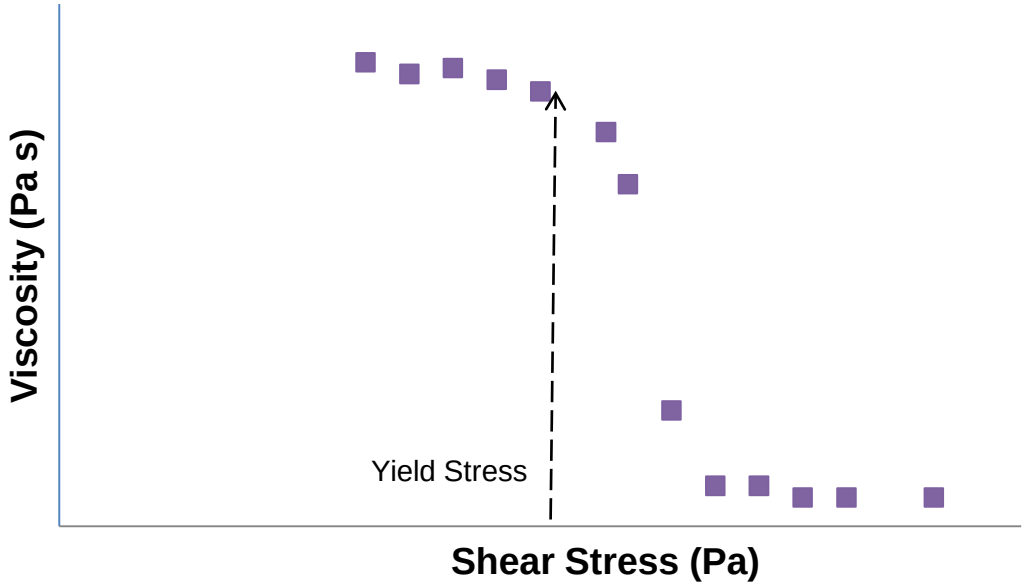

Figure 1.6: Representative rheometric results for gel yielding. The yield stress is defined as the point where the viscosity begins to deviate from the viscosity at low shear stresses.

Effect of Operating Conditions on Depositon and Gelation

A major operating condition that affects the properties of the deposit is time. Time is important because of the concluding steps of the aforementioned deposition mechanism (Singh et al., 2000). The concluding steps involve diffusion of longer carbon

number alkanes into the deposit that solidify in the deposit with the counter-diffusion of shorter carbon number alkanes that are present in the entrapped oil in the liquid phase. The ability of the molecules to diffuse and counterdiffuse out of the deposit is a strong function of the gel composition as shown in Equation 1.3 (Singh et al., 2000).

$$D_e = \frac{D_{wo}}{1+\alpha^2 F_w^2/(1-F_w)} \tag{1.3}$$

Where: D_e = effective diffusivity of wax inside the gel (m^2/s)
D_{wo} = molecular diffusivity of wax in the oil (m^2/s)
α = aspect ratio of the crystal
F_w = wax fraction inside the gel

This phenomenon has been confirmed by work using gas chromatography (Singh et al., 2001, Paso et al., 2004). In these works, the concept of a critical carbon number was proposed. The critical carbon number is defined as the carbon number where any n-alkane with a carbon number below it will counter-diffuse out of the deposit and any n-alkane with a carbon number above it will diffuse into the deposit. The addition of the larger solid n-alkanes into the gel over time causes the solid fraction of the deposit to increase. This increase in the solid fraction will only increase the physical interactions and attractive forces between the solid crystals, strengthening the gel. Venkatesan showed using rheometry that the yield stress of a model oil system was exponentially dependent on the solid content of the wax (Venkatesan et al., 2005).

Flow behavior is an exceptionally important issue in the formation of wax deposits, particularly for the ability of a gel to form. Gelation represents the crosslinking of crystals to transform a solid solution into a gel (de Carvalho and Djabourov, 1997). The crosslinking of the wax crystals can be influenced by the shear that is applied onto them by the flow of the crude oil through the pipeline. At a given cooling rate,

Venkatesan showed that the yield stress of a gel will increase as the applied stress in increased until it reaches a maximum and then the yield stress will decrease as the applied stress is increased (Venkatesan et al., 2005). Using microscopy, this result was observed by noting that the increase in the yield stress was seen because of an increase in the size of the crystal, which led to an increase in both agglomeration and the number of crystal entanglements, factors both conducive to forming a gel. However, at sufficiently high stresses, the shear will begin to break down the gel network, therefore reducing the strength of the gel. Work has also shown that as the shear rate is increased, the viscosity of the crude oil and the storage and loss modulus of the crude oil are decreased (Lorge et al., 1997, Visintin et al., 2005). Using the Einstein equation, a relationship between the shear rate and the viscosity can be derived and is shown below.

$$\frac{\eta - \eta_o}{\eta_o} \sim \phi \left[\frac{\eta_o \gamma a^3}{\Gamma_c} \right]^{-\frac{3-D}{3}} \qquad (1.4)$$

Where: η = viscosity of the suspension (Pa s)
η_o = viscosity of the solvent (Pa s)
φ = volume fraction of the particles
γ = shear rate (1/s)
a = radius of cluster (m)
D = fractal dimension
Γ_c = critical torque, the torque necessary to break the cluster into smaller particles, a function of the intraphysical interactions in the cluster.

Singh conducted extensive work using a rheometer to evaluate the effects of shear on a wax-oil gel (Singh et al., 1999). His work showed that an increase in the applied stress to the system had no effect on the cloud point, but caused a decrease in the gelation temperature. Both results are expected: the cloud point is a molecular level phenomenon that should be independent of external forces and the gelation temperature will be lowered because applying a stress will interfere with the formation of a gel,

particularly as the gel is beginning to form. If the gel is formed statically, the crystal-crystal interactions that are initially weak have the opportunity to grow in strength and eventually gel, but this formation does not happen as easily with the presence of a shear stress. In this situation, more wax crystals are needed to form the necessary interactions to form a gel, which would require a lower temperature.

Using a flow loop system and mathematical modeling, it was shown that as the flow rate is increased for a given set of thermal conditions, the thickness of the deposit decreased while the wax fraction of the deposit increased (Singh et al., 2001). The flow rate causes a decrease in the thickness because the additional stress applied onto the deposit by the flow interferes with the ability of the longer n-alkanes to deposit onto the already formed deposit onto the pipe wall. However, the thinner deposit allows for the formation of a deposit with a higher wax fraction because for a fixed temperature difference across the deposit, a thinner deposit will have a larger temperature gradient. The diffusive flux, directly related to the ability of wax to enter the deposit, is a function of the temperature gradient. Therefore, it will be easier for wax to diffuse into a thinner deposit because of the larger driving force, causing a higher wax fraction for the deposit.

The final major operating condition that greatly influences the deposit is the thermal information of the crude oil as it passes through the pipeline, which can be asseseed in two ways: temperature and cooling rate. As expected, the higher the temperature, the more difficult it is for a gel to form or maintain. A higher wall temperature for flowing systems reduces the driving force for mass transfer, which slows the rate of deposition and reduces the size of the deposit because the interface reaches the cloud point temperature at a smaller wax thickness (Singh et al., 2001). Work has shown

that as the temperature increases, both the yield stress and the viscosity decrease and that the viscosity as a function of shear stress can be expressed by the Roberts-Barnes-Carew model shown below (Chang et al., 2000, Roberts et al., 2001, Visintin et al., 2005).

$$\frac{\eta - \eta_{\infty}^{'}}{\eta_{0}^{'} - \eta_{\infty}^{'}} = \frac{\eta_0}{1 + (\sigma / \sigma_c)^m} \tag{1.5}$$

Where: η_0 = the zero-shear rate viscosity (Pa s)
$\eta_{0}^{'}$ = function of the zero-shear rate viscosity (Pa s)
$\eta_{\infty}^{'}$ = function of the infinite-shear rate viscosity (Pa s)
σ = shear stress (Pa)
σ_c = critical stress (Pa)
m = fitting parameter, typically larger than 5

The effect of cooling rate is important in gelation and deposition because cooling rate has a large effect on crystal shape and size. Using a rheometer, Singh showed that an increase in the cooling rate caused no change in the cloud point (because as mentioned earlier, the cloud point is a molecular phenomenon) and a decrease in the gelation temperature (Singh et al., 1999). Additionally, an appropriate cooling rate was determined for a flow loop system, incorporating heat transfer inside the wax deposit. The relationship is provided below.

$$CR = \frac{D_e}{(1-\phi)\xi} \frac{Nu}{R} (T_o - T_w) \tag{1.6}$$

Where: CR = cooling rate (°C/min)
ξ = thickness of cloud point layer (m)
Nu = Nusselt number
R = radius of pipeline (m)
T_w = temperature of wall (°C)

For quiescent cases, Chang and Venkatesan in separate works showed that the yield stress for two separate crude oils decreased as the cooling rate increasing (Chang et al., 2000, Venkatesan et al., 2005). Both works also showed that slower cooling rates formed the

greatest number and largest wax crystals. Venkatesan explains the result by noting that the trials with slower cooling rates have more time for their interactions to grow before they are disrupted by the presence of a stress (Venkatesan et al., 2005). However, when a constant shear stress was applied, the yield stress actually increased as the cooling rate increased. In this case, the systems at lower cooling rates are subjected to a stress for a longer period of time than the systems at higher cooling rates. Therefore, it is more likely that the crystal networks formed at lower cooling rates are degraded to a higher extent, reducing their yield stress. When the gelation stress and the cooling rate were varied, Venkatesan showed that the maximum value of the yield stress over a range of gelation stresses increased as the cooling rate decreased. Additionally, the value of the gelation stress where the maximum yield stress occurred shifted to higher gelation stresses as the cooling rate increased (Venkatesan et al., 2005). This result was explained by the fact that higher cooling rates lead to faster precipition meaning that a higher stress would be needed to aggregate crystals or break down the structure.

Effect of Additives and Composition

Any material that is present with a crystallizing compound as it crystallizes can influence crystallization (Sangwal, 1996). In crude oil, these materials include the solvent (generally shorter chained hydrocarbons) where crystallization is taking place, naturally present materials such as asphaltenes, resins and water and artificially added materials such as inhibitors and flow improvers. These materials can influence the thermodynamics and kinetics of crystal growth as well as the solubility of the crystal (Sangwal, 1996). Crystallization is the first step of the deposition mechanism, meaning that changes in

crystallization will influence deposition and gelation. Additionally, some materials that do not influence crystallization are capable of influencing the fluid flow, gelation and/or deposition of the wax crystals. Petroleum companies have dedicated a significant portion of time and money to exploit these issues in attempt to mitigate wax deposition.

Wax additives are chemical added to crude oil to improve the flow of oil through subsea oil pipelines (Kuzmic et al., 2008). Additives aid in flowabilitly by a number of different ways: lowering the cloud point of the system, modifying the crystal size and shape to retard gel formation by preventing the formation of large wax crystal lattices, reducing the oil viscosity and modifying the surface of the pipe wall to prevent deposition (Kuzmic et al., 2008, Taraneh et al., 2008, Wang et al., 2003). These additives, also referred to as wax inhibitors, pour point depressants and flow improves, are typically polymers that contain a long alkane chain to interact with the wax and side (typically polar) groups to limit cocrystallization and gelation (Kuzmic et al., 2008). Figure 1.7 shows an example of some of these side groups and copolymers.

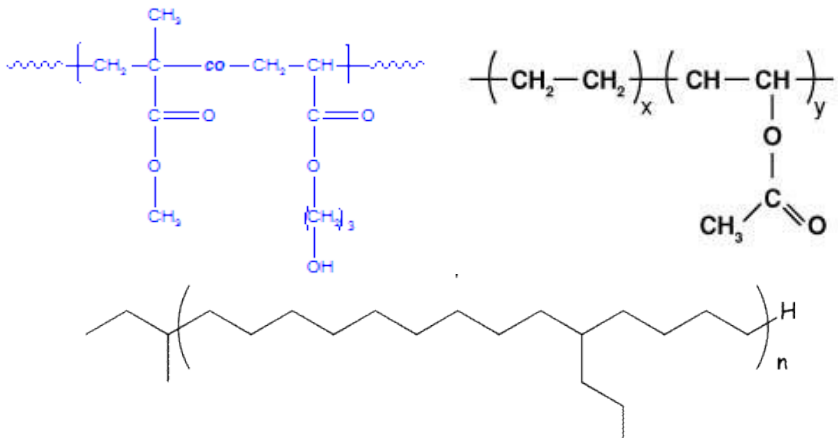

Figure 1.7: Examples of groups found in wax inhibitors. The top left is a methacrytlate group, the top right is an ethylene vinyl acetate group and the bottom is a poly(ethylene) butane copolymer.

Extensive research has been conducted on various kinds of wax inhibitors, how they mitigate wax deposition and the mechanisms by which they act. Semicrystalline random copolymers were shown to reduce the yield stress of the formation of single component wax crystals because of altering of the crystal structure by the amorphous part of the copolymer (Ashbaugh et al., 2002a). Guo presented similar results using poly(ethylene butane) also presenting micrographs that showed drastic changes in crystal size and shape because of the addition of the polymer (Guo et al., 2004, 2006). Studies on block copolymers found that wax is capable of crystallizing on the hairs of the aggregated copolymers (Leube et al., 2000). Because of the size of the copolymer (molecular weights on the order of thousands of g/mol), it becomes difficult for these wax crystals to associate with one another to form a gel (Ashbaugh et al, 2000b). EVA copolymers were observed to reduce the cloud point, viscosity and pour point of Brazilian crude oils by modifying crystals and forming weak aggregates with the wax (Machado et al., 2001). Further work with EVA copolymers with similar results was completed on five different Iranian crude oils with a wide range of oil densities, viscosities, asphaltene content and wax content (Taraneh et al., 2008). Other works have shown copolymers containing polymethacrylates and acrylic esters can also be effective wax inhibitors (Kuzmic et al., 2008, Soldi et al., 2007, Soni and Bharambe, 2006, Wang et al., 2002).

Although a wide number of polymers can be used as wax inhibitors, their efficiency is extremely sensitive to both the composition of the oil and the concentration of the additive added. Using commercially available wax inhibitors, Garcia examined their efficacy on two groups of crude oil: one group had a larger wax fraction, smaller concentration of shorter chained crystallizable n-alkanes (C_{23}-C_{48}), higher pour points

and lower API gravities than the other (Garcia, 2001). This work showed that some additives that effectively reduced the pour point for one group of oils either minimally impacted or in some cases increased the pour point for the other group oils. Similar results were seen in another study where five crude oils and five inhibitors were studied: the best inhibitor for one crude oil could be the worst inhibitor for another crude oil (Dong et al., 2001).

Further insight into why this phenomenon is occurring can be seen by looking at some of the aforementioned inhibitor studies where the functional group of the inhibitor remained basically the same but alterations to the functional groups were made (Guo et al., 2004, Kuzmic et al., 2008, Machado et al., 2001, Soldi et al, 2007, Taraneh et al., 2008). In work on EVA copolymers, it was found that copolymers with lower vinyl acetates content were more effective wax inhibitors because of its differing solubility parameter (Machado et al., 2001). Additionally, the maximium efficiency of the inhibitors occurred at intermediate concentrations because of either precipitation of the copolymer or wax nucleation induced by the copolymer. Similar results were seen when analysis was completed on two different poly(ethylene butane) copolymers that differed in the number of side groups in the inhibitor (Guo et al., 2004). The magnitude of the effect of the reduction of the yield stress for a particular copolymer was dependent on both the concentration and the n-alkane(s) crystallizing out of solution. Micrographs showed that at the optimum concentration, the crystals that formed were very small and did not aggregate very well. However, at other concentrations, the crystals were much larger (particularly at lower concentrations) and/or aggregation was more prevalent (particularly at higher concentrations). These works show that a compatibility must exist

between the n-alkane crystals and the inhibitor in order for them to be effective. Because of this fact, it is generally accepted that inhibitors can only work for a small range of crude oils, typically dependent on the carbon number distribution of the crude oil (Garcia, 2001, Garcia et al., 2000a, Wang et al., 2001).

Although a great deal of work has been dedicated to developing materials that inhibit wax deposition, very little work has been dedicated to understanding how the components already present in crude oil influence thermodynamics, gelation and deposition. Visintin explored the effect of water on the strength of gels and found that an increase in the water cut led to an increase in the pour point, yield stress, viscosity and storage modulus of the system (Visintin et al., 2008). Some work has focused on asphaltenes, the heaviest, most polar components of crude oil (Garcia et al., 2000b, Venkatesan, 2003). Garcia showed that flocculated asphaltenes will increase the cloud point of a crude oil and interfere with the mechanism of crystal inhibiton for a particular maleic anhydride wax additive (Garcia, 2000b). Using model wax-oil-asphaltene systems, Venkatesan found that adding asphaltenes reduced the gelation temperature and the yield stress when compared to the asphaltene-free model oil (Venkatesan, et al., 2003) Corresponding to the decrease in the yield stress was a change in the morphology caused by the presence of asphaltenes. Tinsley's work corresponded to Venkatesan's work, showing the adding a very small amount of asphaltenes can cause a small reduction in the cloud point and gelation temperature along with a significant decrease in the yield stress (Tinsley et al., 2009). This result is dependent upon the ratio of wax to asphaltenes: if the ratio is too high then the asphaltenes will be unable to influence the properties of the crystallizing system. However, if an excessive amount of asphaltenes are added,

asphaltene aggregates will be present before the wax precipitates out of solution. When this happens, these aggregates don not enter the crystal structure of the wax and act as nucleation sites for wax precipitation, consistent with Garcia's conclusion (Garcia, 2000b).

Although they are the major components of both crude oil and wax deposits, only a small portion of work has been dedicated to paraffins. Early work looking at binary n-paraffin mixtures showed that combining two nearby n-alkanes caused lower than expected cloud points and pour points because of the interaction effects between the two n-alkanes (Holder and Winkler, 1965a). More recent work by Paso analyzed the effect of paraffin composition on the gelation abilities of n-alkane systems (Paso et al., 2005). Solubility work showed that a polydisperse wax system had a larger supersaturation ratio at the cloud point than a monodisperse wax system. This higher supersaturation ratio indicates that the polydisperse system will have faster precipitation kinetics at the nucleation point. Further, for a given wax percentage of 0.5%, it was shown using rheometry that a monodisperse C_{36} system was unable to form a gel, whereas a polydisperse wax was able to form a gel. This phenomenon was explained by the fact that polydisperse paraffin crystals have nanoscale surface roughness to provide points of strong crystal-crystal interactions.

Research Objectives and Thesis Overview

The major overriding goal of this research is to explore how components naturally present in crude oil systems influence various properties of crude oil systems that precipitate, gel and deposit as crude oil is sent through subsea oil pipelines. A better

undertstanding of how composition (primarily n-paraffins) affect these properties is vital to appropriately develop (1) thermodynamic, deposition and gelation models for crude oils in subsea oil pipelines and (2) wax inhibitor to help mitigate wax deposition with a better fundamental understanding: most current wax inhibitor development is based on the development of similar inhibitors with only slight compositional differences and observing how the influence crude oils. Extensive further work will need to be carried out to develop the results and conclusions presented in this work because of the complexity of the crude oil. However, this work has provided a strong initial footing into obtaining a greater understanding of the effects of oil composition on crystallization, deposition and gelation.

Chapter II provides an analysis of how n-alkane composition influences the thermodynamics and deposition of petroleum-like solutions. Polydispersity and cocrystallization are shown to be major factors in these areas, particularly cocrystallization. Cocrystallization was shown to occur in solution given that certain criteria were upheld and thermodynamically influenced the solution by reducing the solubility of shorter, less soluble n-alkanes and reducing the heat released by both n-alkanes. Polydispersity slightly influenced solubility by providing heterogeneous nucleation sites for the less soluble n-alkanes. This heterogeneous nucleation also caused a reduction in the heat released by the n-alkanes during crystallization. Cocrystallization caused the formation of smaller, less waxy deposits in comparison to monodisperse systems. Polydispersity generally did not influence the longer, less soluble n-alkane, but did increase deposition for the shorter n-alkanes because of heterogeneous nucleation.

Chapter III analyzes the influence of cocrystallization and polydispersity of gelation. The pour point was shown to be dependent on the cloud point of the system and not the wax fraction of the system. This trend did not continue for polydisperse systems where adding another n-alkane actually caused a decrease in the pour point even though the total wax content of the system increased. Drastic differences were seen when cocrystallization and polydispersity were compared. The addition of only a small amount of a material that could cocrystallize with an n-alkane caused a decrease in the pour point. The pour point would reach a minimum but would begin to increase as the concentration of the shorter n-alkane was sufficiently high. Compounds that did not cocrystallize with the longer n-alkane did not influence crystallization or gelation until a threashold concentration was reached. Once this concentration was reached, the pour point exhibited a very sharp decrease and the pour point became dependent upon the shorter n-alkane and not the longer n-alkane. These results were confirmed with microscopy, which showed great changes in crystal morphology with the addition of shorter n-alkanes. These results were extended to other n-alkane systems, including those with odd carbon numbers.

Chapter IV begins to examine non n-alkanes and how they influence crystallization, deposition and gelation. An initial study was completed using stearic acid, a material that is thermodynamically similar in solvent as some of the long chained n-alkanes used in Chapters II and III. A further point of interest is that stearic acid dimerizes in solution, allowing for its molecular size to be similar to the n-alkanes. However, it is this dimerization, caused by strong hydrogen bonding, which causes the stearic acid to have no influence on the n-alkanes unless it present in sufficient amounts to precipitate before the n-alkanes.

Chapter V provides a summary of the major conclusions in Chapters II-IV and explains their relevance in the petroleum industry.

Chapter VI discusses the numerous avenues for future work that the results, analysis and conclusions have opened up for discovery. The research completed in this dissertation can provide a reasonable starting point for a number of Ph.D. theses or more practical investigations carried out by petroleum companies or chemical companies that develop wax additives.

References:

Anderson, T., Peters, H. S., Torres, R. A., Nagy, N. A., and Schruben, D. L., "Wax Crystal Size Distribution Versus Composition", *Fuel,* **80**, 1635-1638 (2001)

Ashbaugh, H. S., Radulescu, A., Prud'homme, R. K., Schwahn, D., Richter, D. and Fetters, L. J., "Interactions of Paraffin Wax Gels with Random Crystalline/Amorphous Hydrocarbon Copolymers", *Macromolecules,* **35**, 7044-7053 (2002)

Ashbaugh, H. S., Fetters, L. J., Adamson, D. H., and Prud'homme, R. K., "Flow Improvement of Waxy Oil Mediated by Self-Aggregating Partially Crystallizable Diblock Copolymets", *J. Rheol.*, **46**, 763-776 (2002)

Bennema, P., Liu, X.Y., Lewtas, K., Tack, R.D., Rijpkema, J.J.M. nd Roberts, K.J., "Morphology of Orthorhombic Long Chain Normal Alkanes: Theory and Observation", *J. Cryst. Growth*, **121**, 679-696 (1992)

Bhat, N.V. and Mehrotra, A.K., "Modeling the Effect of Shear Stress on the Composition and Growth of the Deposit Layer from "Waxy" Mixtures under Laminar Flow in a Pipeline", *Energy & Fuels,* **22**, 3237-3248 (2008)

Briard, A.-J., Bouroukba, M., Petitjean, D., Hubert, N., Moise, J.-C., and Dirand, M., "Thermodynamic and Structural Analyses and Mechanisms of the Crystallisation of Multi-Alkane Model Mixtures Similar to Petroleum Cuts", *Fuel*, **85**, 764-777 (2006)

Chang, C., Nguyen, Q.D. and Ronningsen, H.P., "Isothermal Start-Up of Pipeline Transporting Waxy Crude Oil", *J. Non-Newtonian Fluid Mech.*, **87**, 127-154 (1999)

Chang, C., Boger, D.V. and Nguyen, Q.D., "Influence of Thermal History on the Waxy Structure of Statically Cooled Waxy Crude Oil", *SPE J.*, **5**, 148-157 (2000)

Chazhengina, S.Y., Kotelnikova, E.N., Filippova, I.V. and Filatov, S.K., "Phase Transitions of n-Alkanes as Rotator Crystals", *J. Molec. Struct.,* **647**, 243-257 (2003)

Clavell-Grunbaum, D., Strauss, H.L. and Snyder, R.G., "Structure of Model Waxes: Conformational Disorder and Chain Packing in Crystalline Multicomponent n-Alkane Solid Solutions", *J. Phys. Chem. B,* **101**, 335-343 (1997)

Coutinho, J.A.P., Edmonds, B., Moorwood, T., Szczepanski, R. and Zhang, X., "Reliable Wax Predictions for Flow Assurance", *Energy & Fuels,* 20, 1081-1088 (2006)

de Carvalho, W and Djabourov, M., "Physical Gelation Under Shear for Gelatin Gels", *Rheol. Acta*, **36**, 591-609 (1997)

Dirand, M., Chevallier, V., Provost, E., Bouroukba, M., and Petitjean, M., "Multicomponent Paraffin Waxes and Petroleum Solid Deposits: Structural and Thermodynamic State", *Fuel,* **77**, 1253-1260 (1998)

Dirand, M., Bouroukba, M., Chevallier, V., Petitjean, D., Behar, E., and Ruffier-Murray, V., "Normal Alkanes, Multialkane Synthetic Model Mixtures and Real Petroleum Waxes: Crystallographic Structures, Thermodynamic Properties and Crystallization", *J. Chem. Eng. Data.,* **47**, 115-135 (2002)

Dong, L., Xie, H., and Zhang, F., "Chemical Control Techniques for the Paraffin and Asphaltene Deposition", *SPE 65380,* 1-11 (2001)

Garcia, M.d.C., "Crude Oil Wax Crystallization. The Effect of Heavy n-Paraffins and Flocculated Asphaltenes", *Energy and Fuels,* **14**, 1043-1048 (2000)

Garcia, M.d.C., Carbognani, L., Orea, M. and Urbina, A., "The Influence of Alkane Class-Types on Crude Oil Wax Crystallization and Inhibitors Efficiency", *J. Pet. Sci. & Engr.,* **25**, 99-105 (2000)

Garcia, M.d.C., "Paraffin Deposition in Oil Production", *SPE J. 64992,* 1-7 (2001)

Guo, X., Pethica, B.A., Huang, J.S., and Prud'homme, R.K., "Crystallization of Long Chain n-Paraffins from Solutions and Melts as Observed by Differential Scanning Calorimetry", Macromolecules, **15**, 5638-5645 (2004)

Guo, X., Pethica, B. A., Huang, J. S., Adamson, D. H., and Prud'homme, R. K., "Effect of Cooling Rate on Crystallization of Model Waxy Oils with Microcrystalline Poly(ethylene butane)", *Energy & Fuels,* **20**, 250-256 (2006)

Hennessy, A.J., Neville, A. and Roberts, K.J., "An Examination of Additive-Mediated Wax Nucleation in Oil Pipeline Environments", *J. Cryst. Growth,* **198/199**, 830-837 (1999)

Holder, G.A. and Winkler, J., "Wax Crystallization from Distillate Fuels: I. Cloud and Pour Phenomena Exhibited by Solutions of Binary n-Paraffin Mixtures", *J. Inst. Petrol., **51***, 228-235 (1965)

Holder, G.A. and Winkler, J., "Wax Crystallization from Distillate Fuels: II. Mechanism of Pour Depression", *J. Inst. Petrol., **51***, 235-242 (1965)

Jennings, D.W. and Weispfennig, K. "Experimental Solubility Data of Various n-Alkane Waxes: Effects of Alkane Chain Length, Alkane Odd Versus Even Carbon Number Structures and Solvent Chemistry on Solubility", *Fluid Phase Equlibria,* **227**, 27-35 (2005)

Kane, M., Djabourov, M., Volle, J-L., Lechaire, J-P., and Frebourg, G. "Morphology of Paraffin Crystals in Waxy Crude Oils Cooled in Quiescent Conditions and Under Flow", *Fuel*, **82**, 127-135 (2003)

Kuzmic, A.E., Radosevic, M., Bodganic, G., Srica, V. and Vukovic, R., "Studies on the Influence of Long Chain Acrylic Esters Polymers with Polar Monomers as Crude Oil Flow Improver Additives", *Fuel*, **87**, 2943-2950 (2008)

Leube, W., Monkenbusch, M., Schneiders, D., Richter, D., Adamson, D., Fetters, L., Dounis, P. and Lovegrove, R., "Wax-Crystal Modification for Fuel Oils by Self-Aggregating Partially Crystallizable Hydrocarbon Block Copolymers", *Energy & Fuels*, **14**, 419-430

Lorge, O., Djabourov, M. and Brucy, F., "Crystallization and Gelation of Waxy Crude Oils Under Flowing Conditions", *Reveu de L'Institut Francais de Petrole*, **52**, 235-239 (1997)

Liu, X.Y., and Bennema, P., "On the Morphology of Crystals of Triclinic Even Normal Alkanes: Theory and Observation", *J. Cryst. Growth*, **135**, 209-223 (1994)

Machado, A.L.C., Lucas, E.F. and Gonzalez, G., "Poly(ethylene-co-vinyl acetate) (EVA) as Wax Inhibitor of a Brazilian Crude Oil: Oil Viscosity, Pour Point and Phase Behavior of Organic Solutions", *J. Pet. Sci. & Engr.*, **32**, 159-165 (2001)

Mehrotra, A.K. and Bhat, N.V., "Modeling the Effect of Shear Stress on Deposition from "Waxy" Mixtures under Laminar Flow with Heat Transfer", *Energy & Fuels*, **21**, 1277-1286 (2007)

Paso, K. G., and Fogler, H. S., "Bulk Stabiliziation in Wax Deposition Systems", *Energy & Fuels*, **18**, 1005-1013 (2004)

Paso, K., Senra, M., Yi, Y., Sastry, A. M., and Fogler, H. S., "Paraffin Polydispersity Facilitates Mechanical Gelation", *Ind. Eng. Chem. Res.*, **44**, 7242-7254 (2005)

Pauly, J., Dauphine, C. and Daridon, J.L., "Liquid-Solid Equilibria in a Decane + Multi-Paraffins System", *Fluid Phase Equilibria*, **149**, 191-207 (1998)

Roberts, G.P., Barnes, H.A. and Carew, P., "Modelling the Flow Behaviour of Very Shear-Thinning Liquids", *Chem. Eng. Sci.*, **56**, 5617-5623 (2001)

Ronningsen, H.P.,Bjorndal, B., Hansen, A.B. and Pedersen, W.B., "Wax Precipitation from North Sea Crude Oils. 1. Crystallization and Dissolution Temperatures and Newtonian and Non-Newtonian Flow Properties", *Energy & Fuels*, **5**, 895-908 (1991)

Sangwal, K., "Effects of Impurities on Crystal Growth Processes", *Prog. Cryst. Growth and Proc.*, **32**, 3-43 (1996)

Singh, P., Fogler, H. S. and Nagarajan, N. R., "Prediction of the Wax Content of the Incipient Wax-Oil Gel in a Pipeline: An Application of the Controlled-Stress Rheometer," *J. Rheol.*, **43**, 1437-1459 (1999)

Singh, P., Venkatesan, R., Fogler, H. S., and Nagarajan, N., "Formation and Aging of Incipient Thin Film Wax-Oil Gels", *AIChE J.*, **46**, 1059-1074 (2000)

Singh, P., Venkatesan, R., Fogler, H.S. and Nagarajan, N.R., "Morphological Evolution of Thick Wax Deposits during Aging", *AICHE J.*, **47**, 6-18 (2001)

Soldi, R. A., Oliveira, A. R. S., Barbosa, R. V., and Cesar-Oliveira, M. A. F., "Polymethacrylates: Pour Point Depressants in Diesel Oil", *European Polymer Journal*, **43**, 3671-3678 (2007)

Soni, H.P. and Bharmbe, D.P., "Synthesis and Evaluation of Polymeric Additives as Flow Improvers for Indian Crude Oil", *Iranian Polymer Journal*, **15**, 943-954 (2006)

Svendsen, J. A., "Mathematical Modeling of Wax Deposition in Oil Pipeline Systems", *AICHE J.*, **39**, 1377-1388 (1993)

Taraneh, J. B., Rahmatollah, G., Hassan, A. and Alireza, D., "Effect of Wax Inhibitors on Pour Point and Rheological Properties of Iranian Waxy Crude Oil", *Fuel Processing Technology*, **89**, 973-977 (2008)

Tinsley, J.F., Jahnke, J.P., Dettman, H.D. and Prud'homme, R.K., "Waxy Gels with Asphaltenes 1: Characterization of Precipitation, Gelation, Yield Stress and Morpholgy", *Energy & Fuels*, **23**, 2056-2064 (2009)

Turner, W.R., "Normal Alkanes", *Ind. Eng. Chem. Prod. Res. Develop.*, **10**, 238-260 (1971)

Venkatesan, R., Singh, P. and Fogler, H.S., "Delineating the Pour Point and Gelation Temperature of Waxy Crude Oils", *SPE J.*, 349-352 (2002)

Venkatesan, R., Ostlund J.-A., Chawla, H., Wattana, P., Nyden, M. and Fogler, H.S., "The Effect of Asphaltenes on the Gelation of Waxy Oils", *Energy & Fuels*, **17**, 1630-1640 (2003)

Venkatesan, R., Nagarajan, N.R., Paso, K., Yi, Y-B., Sastry, A.M. and Fogler, H.S., "The Strength of Paraffin Gels Formed Under Static and Flow Conditions", *Chem. Eng. Sci.*, **60**, 3587-3598 (2005)

Vignati, E., Piazza, R., Visintin R.F.G., Lapasin, R., D'Antona, P. and Lockhart, T.P., "Wax Crystallization and Aggregation in a Model Crude Oil", *J. Phys. Condens. Matter*, **17**, 83651-83660 (2005)

Visintin, R.F.G., Lapasin, R., Vignati, E., D'Antona, P. and Lockhart, T.P., "Rheological Behavior and Structural Interpretation of Waxy Crude Oil Gels", *Langmuir,* **21**, 6240-6249 (2005)

Visintin, R. F. G., Lockhart, T. P., Lapasin, R. and D'Antona, P., "Structure of Waxy Crude Oil Emulsion Gels", *J. Non-Newt. Fluid Mech.*, **149**, 34-39 (2008)

Wang, K-S., Creek, J. L., Shuler, P. J. and Tang, Y, "Evaluation of Effects of Selected Wax Inhibitors on Wax Appearance and Dissolution Temperatures", *Pet. Sci. & Tech.,* **21**, 359-368 (2003)

Weispfennig, K., "Advancements in Paraffin Testing Methodology", *SPE 64997***,** 1-6 (2001)

Winter, H.H., "Can the Gel Point of a Cross-Linking Polymer Be Detected by the G' – G" Crossover?", *Polymer Eng. & Sci.*, **27**, 1698-1702 (1987)

Wu, C.-H., Wang, K.-S., Shuler, P.J., Creek, J.L., Carlson, R.M. and Cheung, S., "Measurement of Wax Deposition in Paraffin Solutions", *AIChE J.,* **48**, 2107-2110 (2002)

CHAPTER II

THE ROLE OF POLYDISPERSITY AND COCRYSTALLIZATION ON THERMODYNAMICS AND DEPOSITION

Introduction

In many industries, the ability to control crystallization is important to create crystals of a desired size, shape and/or morphology. However, the petroleum industry is greatly impacted by unwanted crystallization for it begins a sequence of events that can cause significant problems in the production, transportation and refining of crude oil (Misra et al., 1995). The crystallization of select components of crude oil in pipelines can lead to the formation of wax deposits that can restrict the flow of oil and eventually plug the process equipment and/or pipelines (Pedersen et al., 1991, Wu et al., 2002) .These wax deposits have been described as lamellar, orthorhombic wax crystals contained in a random structure that form an organic gel (Ashbaugh, et al., 2002). In spite of the fact that crude oils are extremely complex systems containing a multitude of components, it is generally accepted that the crystallizing materials which form the deposits are primarily n-alkanes (Hansen et al., 1991, Hennessy et al., 1999, Singh et al., 1999). However, this gel does not consist solely of n-paraffins, but is a spanning network of solid paraffin crystals entrapping the liquid oil (Singh et al., 1999, 2000).

In general, wax deposition in oil pipelines occurs either when oil is being transported in colder environments or has a large fraction of n-alkanes present in it (Singh

et al., 1999, Paso et al., 2005). Crystallization does not occur at the reservoir because the temperature (70-150 °C) is high enough to ensure that the paraffins remain in solution (Singh et al., 1999). However, as the crude oil passes through the colder pipelines (for example, the ocean floor is at 4 °C), the temperature of the crude oil drops, causing the higher molecular weight paraffins to precipitate out of solution and crystallize (Venkatesan et al., 2005). The United States Department of Energy estimated that remediating pipeline blockages in subsea oil pipelines at depths of around 400 m can cost $1 million/mile (Venkatesan et al., 2005). This problem is only expected to get worse as time progresses because of the necessity to drill further and further offshore in order to find more oil due to the depletion of oil reserves near the shore (Wu et al., 2002). This drilling further offshore exposes the warm oil to a cold environment for a longer period of time (Wu et al., 2002).

Greater insight on the formation of wax deposits can be gained with greater knowledge of how n-alkanes crystallize and deposit in solution. n-Alkanes (n-paraffins) are the major components of wax deposits due to their ability to crystallize easily and in an ordered structure in comparison to the other components present in crude oil and their relatively low solubility in most paraffin-based, aromatic or oil like solvents (Hennessy et al., 1999, Singh et al., 1999). Therefore, as the crude oil cools down, the solubility limit will eventually be reached and will no longer be able to support all of the n-alkanes in solution. Previous work has shown that this solubility limit decreases as the amount of n-alkane increases and as the chain length (molecular size) of the n-alkane increases (Provost et al., 1998, Dirand et al., 2002). Typical crude oils contain about 10-20% n-alkanes by weight, but can reach as high as 95% for select crudes and contain n-paraffins

with carbon numbers ranging from 10-100, with a large proportion of the deposit containing n-paraffins with carbon numbers between 20 and 50 (Srivastava et al., 1993, Coutinho et al., 1996, del Carmen Garcia, 2000, Dirand et al., 2002, Kane et al., 2003).

When n-paraffins crystallize in low chain length alkanes without the presence of any other materials, they crystallize in one of four shapes: triclinic, monoclinic, orthorhombic and hexagonal, dependent on carbon number (Turner et al., 1971, Liu et al., 1994).Dirand et al. provide an extensive literature review of the crystal morphology for a wide variety of n-alkane systems and found that (1) the solvent itself will not crystallize if the temperature is above its melting point in spite of other materials crystallizing (2) the solubility of n-alkanes in organic solvents does not vary greatly except for dilute solutions and (3) the addition of a "long" carbon number (C_n, where n represents the number of carbon atoms present in the n-alkane) alkane to a "short" C_n alkane will increase the solubility of the "short" C_n alkane (Dirand et al., 2002). Although n-alkanes in crude oil systems would be expected to crystallize in a number of different ways, it is generally accepted that the crystals formed are mostly thin, orthorhombic platelets (Dirand et al., 1998b, Singh et al., 2001). Therefore, in order for only one general shape to be observed, deviation from ideal crystallization must occur. Otherwise, deposits would consist of wax crystals of numerous shapes. The presence of impurities in a crystal growth medium has often been the explanation for such non-idealities (Kern et al., 1992, Sangwal, 1996). Impurities in crystal growth processes have been defined as any foreign substance other than the crystallizing compound (Svendsen, 1993). Therefore, any material present in the crude oil, including but not limited to asphaltenes, resins, aromatics, lower carbon number n-alkanes and inhibitors are all considered impurities.

The impact of impurities on a crystallizing system varies both in its magnitude and its focus. Previous research has shown that impurities have a marked effect on nucleation, growth and dissolution kinetics, morphology, and precipitation kinetics of paraffin systems (Kern et al., 1992, Sangwal, 1996).

An effect that has been investigated is alkane composition, particularly for systems containing two different n-alkanes in solution. In polydisperse systems, it has been shown that the composition of aggregates (crystals) that form are more commonly polydisperse than monodisperse (Srivastava et al., 1993). Further, it has been shown the presence of other n-alkanes impact the solubility of the component with the lowest solubility, which will be hereafter referred to as the chief crystallizing component (CCC) (Dirand et al., 1998a). However, the ability to form polydisperse aggregates tends to follow a few general rules. In order for mutual solubility to occur, the molecules must be similar both in form and dimension, and have symmetry with respect to pure crystal shape (Turner et al., 1971, Srivastava et al., 1993). For n-alkane systems, they are obviously of similar form and dimension if the difference in C_n is sufficiently small. However, due to the distinct shapes of n-alkane crystals, crystal symmetry does not always exist. Dirand's work discusses the work of Kravchenko, who developed predictions for the formation of solid solutions for binary n-alkane mixtures (Dirand et al., 1998a). Kravchenko predicts the degree of miscibility of two alkanes at room temperature based on two criteria: the carbon number of the longer carbon chain and the carbon difference between the two alkanes. His predictions are shown in Table 2.1.

Table 2.1: Kravchenko's predictions for miscibility of solid solutions of binary mixtures. Δn represents the difference in carbon number between the two components of the mixture (Dirand et al., 2002). [a] In order for miscibility to occur, the crystalline structures must be identical (for total miscibility) or similar (for partial miscibility)

	Miscibility of Solid Solutions		
Δn	**Total**	**Partial**	**None**
1[a]	n≥17	8<n<17	n≤7
2	n≥34	14<n<34	n≤13
4	n≥68	28<n<68	n≤27

Deposition of crude oils is becoming more of a problem because of the need to drill further offshore for oil. Svendsen showed that in order for wax deposition to occur, the following three events must occur simultaneously: (1) the temperature at the deposition location must be lower than the cloud point of the oil, (2) a radial temperature gradient must be present in the flow and (3) the deposit location must have sufficient attraction to enable wax crystals to attach to the wall (Svendsen, 1993). It is widely accepted that the major means of deposition for pipeline systems is molecular diffusion (Singh et al., 2000, 2001, Weispfennig et al., 2001, Azevedo et al., 2003). Singh et al. have provided a six step process by which deposition occurs (Singh et al., 2000). This process can be briefly described as the formation of an incipient gel layer followed by diffusion, precipitation, penetration and counter-diffusion of n-alkane molecules into and out of the gel. Although the thickness of the deposit has been analyzed, little work has been done to view the deposition characteristics from a compositional standpoint. Using model oils, Singh and Venkatesan were able to quantify aging phenomena and prove the existence of a critical carbon number, a value that indicates which n-paraffins will diffuse into and out of the solid deposit over time (Singh et al, 2000, 2001, Venkatesan et al., 2005).

The objective of this work is to develop a greater understanding on how n-alkanes impact the crystallization and deposition of other n-alkanes present in solution. To exploit Kravchenko's rules, three different n-alkanes were used: $C_{28}H_{58}$, $C_{32}H_{66}$ and $C_{36}H_{74}$ (hereafter abbreviated as C_{28}, C_{32} and C_{36}). Dodecane was utilized as a solvent for all experimental trials, a material that would not crystallize at the temperatures used for the study.

Materials

Unless otherwise specified, the mass % of the long chained n-alkanes present in the solution are 4% unless otherwise specified. Therefore, systems containing two longer chain n-alkanes had 8% wax and the systems containing three longer chain n-alkanes had 12% wax. The three n-alkanes used were hexatriacontane ($C_{36}H_{74}$, 98% purity), dotriacontane ($C_{32}H_{66}$, 97% purity) and octacosane ($C_{28}H_{58}$, 98% purity) and were purchased from Aldrich. Dodecane (99+% purity from Sigma) was used for the solvent in all trials.

Experiments

Cloud point temperature

Cloud points were determined using a constant temperature bath where a solution enclosed in a vial was slowly cooled from a starting temperature where the solution is entirely liquid. The solution was allowed to equilibrate and then removed from the temperature bath and visually inspected for any precipitation. If the system remained

homogeneous, the bath was cooled by 0.1° C and the vial was reinserted into the temperature bath. This process continues until precipitation becomes visible.

Differential scanning calorimetry (DSC)

A Perkin-Elmer DSC 10 was utilized for all DSC runs. The solutions were cooled at a rate of 0.5 °C/min. The DSC trials allowed for the determination of the onset of a liquid-solid transition and the amount of heat released in the transition from liquid to solid.

Densitometry

The densitometer used was a DMA 500 Density Meter with a measuring range of 0-3 g/mL, repeatability of $1x10^{-6}$ g/mL, a temperature accuracy of 0.001 °C and a temperature range of 0-90 °C. The solutions were cooled, starting at a temperature above the cloud point, at 2 °C/hr (0.033 °C/min) and the density was measured every 3 minutes. A change in density seen in addition to the relatively linear change in density caused by the reduction in temperature indicates a transition from liquid to solid. This phenomenon will be further discussed in the results section.

Deposition

The coldfinger apparatus is a laboratory device that is used to simulate deposition (Weispfennig, 2001, Paso et al., 2004). The apparatus consists of a steel cylinder (12.6 cm^2) that can be thermally controlled and a jacketed vessel (204 +/- 1 mL) where the fluid is located. In order for deposition to occur on the surface of the coldfinger, the bulk solution must be above the solution cloud point and the cylinder must be below the solution cloud point. For these experiments, the bulk fluid was kept at a temperature of 50 °C and the steel cylinder was maintained at 10 °C. All cloud points of the solutions

used in this work are between 10 and 50 °C, ensuring that deposition can occur. A stirbar is added to induce bulk mixing. To ensure that the fluid flow properties remain consistent from experiment to experiment, the fluid volume was held constant (+/- 1 mL) and the stirbar rotation speed was held constant at 340 rpm. This rotation speed was selected to ensure thorough mixing while preventing the formation of turbulent eddies in the system. In order to eliminate the effect of aging on the composition of the deposits, each trial was run for 6 hours. The deposit was then carefully removed from the steel cylinder and weighed.

Chromatography

To determine the deposit composition, an Agilent 6890N high temperature gas chromatography with a 0.25 μm fused silica stationary phase and an FID detector. The solutions were diluted with heptane and manually injected into the system. The samples were run through the gas chromatograph several times and an average composition (+/- 10%) was determined.

Differential Scanning Calorimetry and Cloud Point Studies

Figure 2.1 shows the DSC traces for the monodisperse experiments of 4% C_{28}, 4% C_{32} and 4% C_{36} in dodecane. Table 1.2 provides (1) the onset temperature, the temperature at which crystallization first begins to appear (hereafter referred to as the wax appearance temperature, WAT), (2) the peak temperature, the temperature at which the normalized exothermic heat is at a maximum and (3) the enthalpy of crystallization, found by integrating the area under the DSC trace. As the carbon number increases, both the cloud point temperature and enthalpy of crystallization increase. These results are

consistent with the work of Guo et al., who found that solubility of these three n-alkanes in decane decreased with increasing carbon number using visual observation and DSC (Guo et al., 2004). As expected, the location of the DSC peaks in this work is at higher temperatures (approximately 6 °C) because the solubility of an n-alkane in n-alkane solvent increases as the carbon number of the solvent decreases.

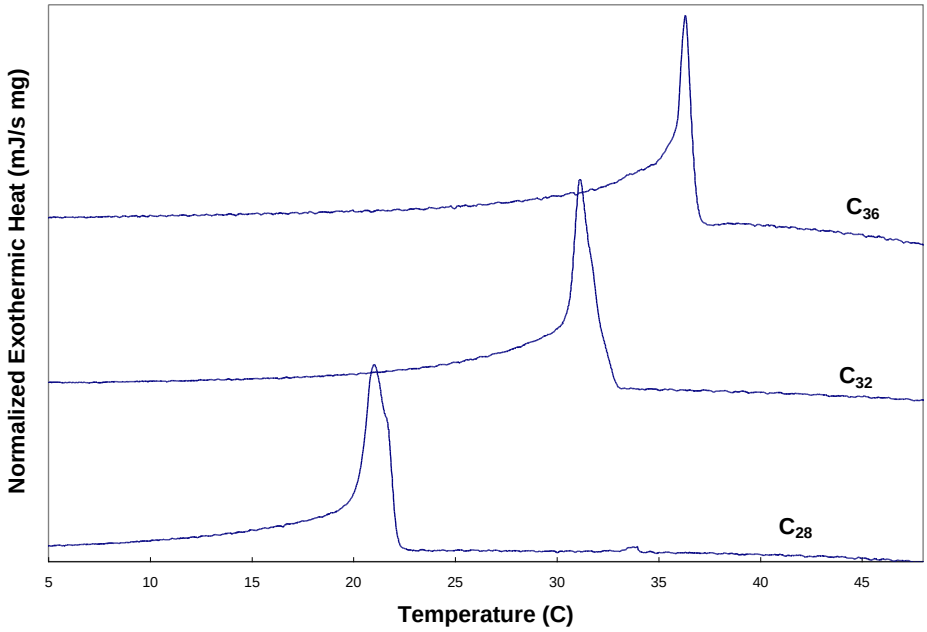

Figure 2.1: Monodisperse DSC traces: Each sample has 4 mass % of the specified n-alkane (solute) and is being cooled at a rate of 0.5 °C/min.

Table 2.2: Thermodynamic information for monodisperse trials. All temperatures are in °C.

n-Alkane	WAT	Peak T	Cloud Pt.	ΔH_{cryst} (kJ/mol)
C_{28}	22.4	20.9	23.8	107
C_{32}	33.1	31.1	33.9	151
C_{36}	38.0	36.3	39.6	174

In order to make proper comparisons between monodisperse and polydisperse (for this work, the binary and ternary systems) systems as well as between polydisperse systems, the total wax content of the chief crystallizing component (CCC, the first material to crystallize), must be kept constant. In this work, the CCC will be the largest

alkane present in the system because all n-alkanes are present in equal mass percentages. The wax content of the CCC is being held constant because many thermodynamic properties (i.e. cloud point temperature) are dependent primarily on the CCC. For dilute monodisperse systems, the van't Hoff equation has been shown to accurately relate the cloud point temperature with wax mole fraction, x_{solute}, for monodisperse solutions (Ghogomu et al., 1989, Paso et al., 2005, Guo et al., 2006).

$$\ln\left(\frac{1}{x_{solute}}\right) = \frac{\Delta H_{dissolution}}{RT} - \frac{\Delta S_{dissolution}}{R} \qquad (1)$$

Where: R = universal gas constant (J/mol K)
T = temperature (K)
x_{solute} = mole fraction of soluble (wax)
$\Delta H_{dissolution}$ = enthalpy of dissolution (kJ/mol)
$\Delta S_{dissolution}$ = entropy of dissolution (J/mol K)

Figure 2.2 confirms the validity of the van't Hoff equation for the systems used in this work. As C_n increases, the enthalpy of dissolution also increases (as shown in Table 2.3), consistent with the results seen from DSC. The results for the n-alkanes in dodecane are consistent with the work of Guo et al., who used decane as a solvent and with Paso et al. for C_{36} (Paso et al., 2005, Guo et al., 2006).

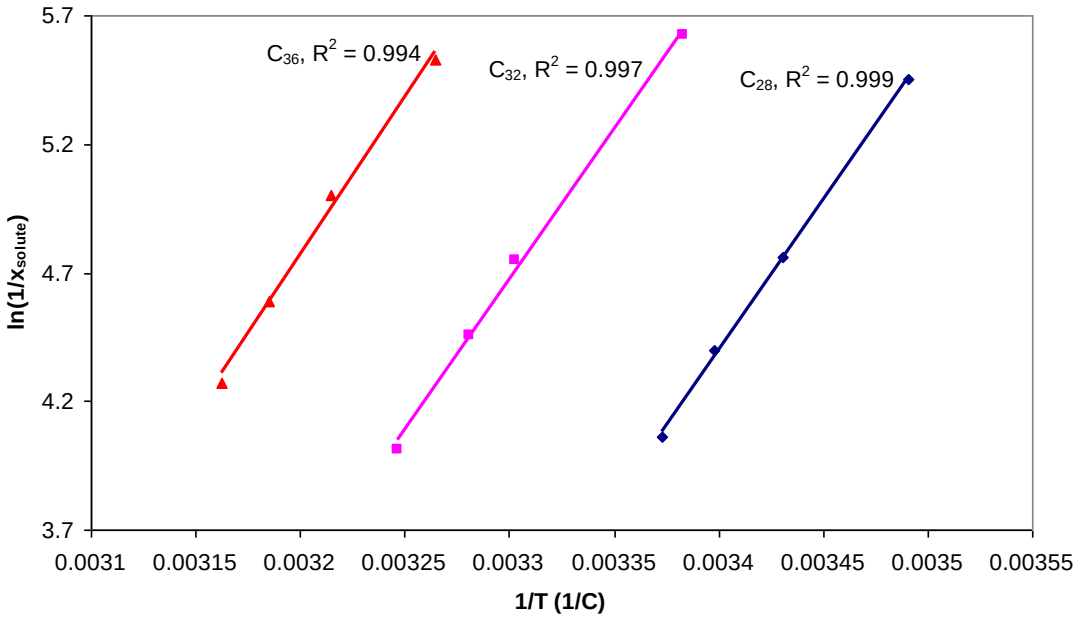

Figure 2.2: Graph of solubility vs. temperature for various n-alkanes in dodecane. (▲ represents C_{36}, ■ represents C_{32} and ♦ represents C_{28})

Table 2.3: Paraffin dissolution enthalpy and entropy values determined using the van't Hoff solubility relationship using experimental cloud points.

Alkane	ΔH_{diss} (kJ/mol)	ΔS_{diss} (J/mol K)
C_{36}	102.0	287
C_{32}	97.6	283
C_{28}	97.0	293

Figure 2.3 shows DSC traces for the entire permutation of systems where the amount of each carbon number is 4 mass % and Table 2.4 provides the relevant thermodynamic information for the polydisperse trials. From Figure 2.3 and Table 2.4, it can be seen that the wax appearance temperature, peak temperature and enthalpy of crystallization increase as the average molecular weight of the crystallizable n-alkanes increases, similar to the monodisperse systems.

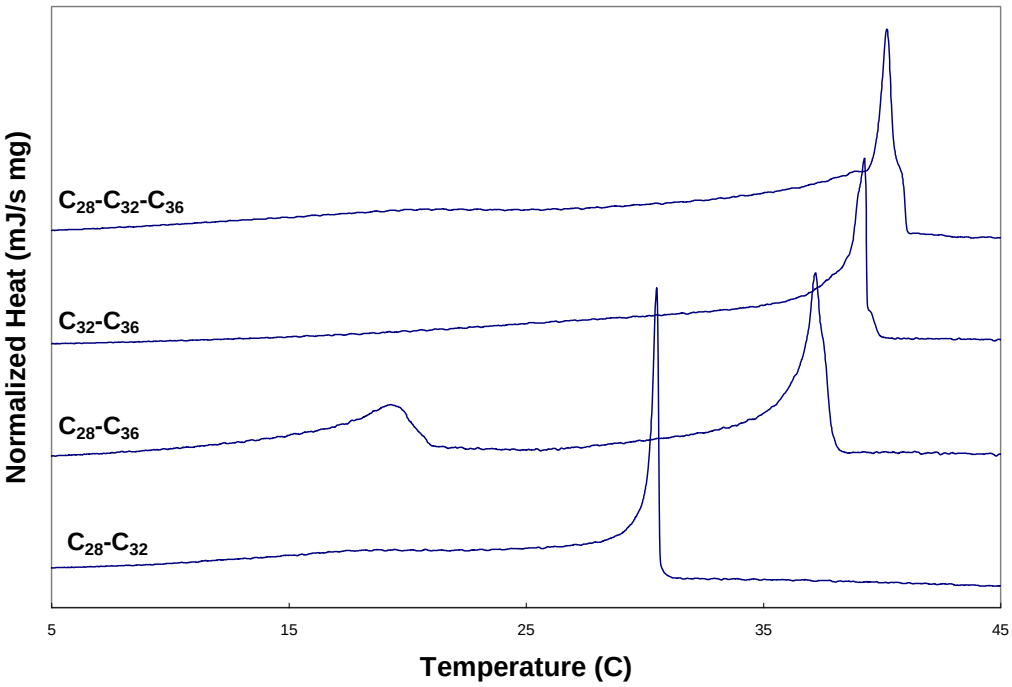

Figure 2.3: Polydisperse DSC traces: The cooling rate is 0.5 °C/min.

Table 2.4. Thermodynamic information for polydisperse trials. All temperatures are in °C.

n-Alkanes	WAT	Peak T	Cloud Pt.	ΔH_{cryst} (kJ/mol)
C_{28}-C_{32}	31.1	30.5, 18.4	32.2	105
C_{28}-C_{36}	38.4	37.1, 19.0	40.0	124
C_{32}-C_{36}	40.3	39.3	40.6	128
C_{28}-C_{32}-C_{36}	41.1	40.2, 21.1	41.7	116

Kravchenko's rules (Table 2.1) for binary mixtures suggest that the C_{36}/C_{32} and the C_{32}/C_{28} systems would be expected to exhibit partial miscibility and that the C_{36}/C_{28} system would be expected to exhibit no miscibility. However, the question arises whether or not Kravchenko's rule of thumb can be extended to simple solutions. An examination of these systems suggests that Kravchenko's rules remain relatively intact. The C_{36}/C_{32} system has one distinct peak, indicating complete cocrystallization (total miscibility) and the C_{36}/C_{28} trace contains two separate peaks indicating a lack of cocrystallization (no miscibility). Further evidence of a lack of miscibility in the C_{36}/C_{28} system will be provided later when the areas under the curve are analyzed. The C_{32}/C_{28} system also

obeys Kravchenko's rules with the presence of one major peak indicating cocrystallization. However, a minor peak around 20 °C indicates additional crystallization occurring that is distinct from the cocrystallization event. This result is an important limitation of Kravchenko's rules that will be discussed later.

The ternary system provides a means to extend the application of Kravchenko's rule. If Kravchenko's rule is evaluated simply, it could be concluded that since C_{32} will cocrystallize with C_{36} and C_{28} will cocrystallize with C_{32}, all three n-alkanes would cocrystallize together. However, this conclusion is inconsistent with the results in Figure 2.3, where complete crystallization is not occurring. This result proves that the requirement for cocrystallization is dictated by the CCC, requiring that cocrystallization is based on the CCC. The DSC trace for the ternary system shows one very distinct peak followed by a very considerable tail and the presence of an extremely broad, small peak in the vicinity of where C_{28} crystallizes by itself in dodecane. The location of the peak indicates that some C_{28} is crystallizing by itself without being integrated into the structure of either C_{32} or C_{36}. However, the relative height and width of the peak shows that the entire amount of C_{28} initially present is not crystallizing independently (approximately 20% of the total heat is under this wider peak when about 30% would be expected if C_{28} were completely crystallizing by itself in this range). A broader and shorter secondary peak is also present for the situation where no cocrystallization is occurring (C_{36}/C_{28}). This broadening occurs because although the chief crystallizing component can not integrate lower C_n alkanes into its crystal structure, it provides heterogeneous nucleation sites for the shorter alkanes, inducing crystallization at temperatures which would not be possible if the alkane were to crystallize by itself. If heterogeneous nucleation were not to occur,

then the C_{28} peak in both the C_{36}/C_{28} and the ternary trace would look similar to the one seen in the C_{28} trace. Therefore, the C_{28} in the ternary system can heterogeneously nucleate and also integrate itself into the structure of C_{32} since they can cocrystallize.

As discussed earlier, the enthalpy of crystallization for the polydisperse systems increases with increasing carbon number (molecular weight). If the n-alkanes were to crystallize independently of one another, then it would be expected that the heat required for crystallization on a molar basis would be a simple weighted molar average. (A sample calculation for the expected enthalpy of crystallization can be found in Appendix A.) However, Figure 2.3 shows the occurrence of both cocrystallization and heterogeneous nucleation, indicating the possibility that the enthalpy of crystallization will deviate from the independent situation discussed earlier. Table 2.5 shows how polydispersity and cocrystallization impact the heat of crystallization.

Table 2.5. Impact of polydispersity and cocrystallization on the heat of crystallization. ΔH_{cryst} represents the enthalpy of crystallization found using DSC. The expected ΔH_{cryst} represents the heat of crystallization expected if the various components were to crystallize independently of one another.

Sample	ΔH_{cryst} (kJ/mol)	Expected ΔH_{cryst}	% Difference	Crystallization Type Seen From DSC
C_{28}-C_{32}	105	128	18.2	Incomplete cocrystallization
C_{28}-C_{36}	124	137	9.1	Independent crystallization
C_{32}-C_{36}	128	162	21.0	Complete cocrystallization
C_{28}-C_{32}-C_{36}	116	142	22.0	Incomplete cocrystallization and independent crystallization

For each system, the heat of crystallization is less than the simple weighted average. Additionally, for the binary systems, the deviation from the expected value of the enthalpy of crystallization increases as the degree of cocrystallization increases. This result shows that both polydispersity and cocrystallization reduce the heat of crystallization for n-alkane systems crystallizing from solution. Polydispersity assists in

reducing the heat for crystallization by providing heterogeneous nucleation sites for the more soluble materials to crystallize at higher temperatures and thus lower supersaturation ratios. Crystallization at lower supersaturation ratios indicates that less material is crystallizing out initially, making it more likely that these crystals will crystallize in the most energetically favorable manner. The cocrystallization mechanism facilitates the crystallization of both alkanes, particularly the more soluble alkane, in reducing the heat of crystallization.

Figure 2.4 shows the C_{36}-C_{32} and C_{32}-C_{28} DSC traces from Figure 2.3. Figure 2.4 shows that after the primary peak for the C_{32}-C_{28} system occurs around 31 °C, the DSC trace does not monotonously decrease, contrary to what is seen for the C_{36}-C_{32} system and for all of the monodisperse trials.

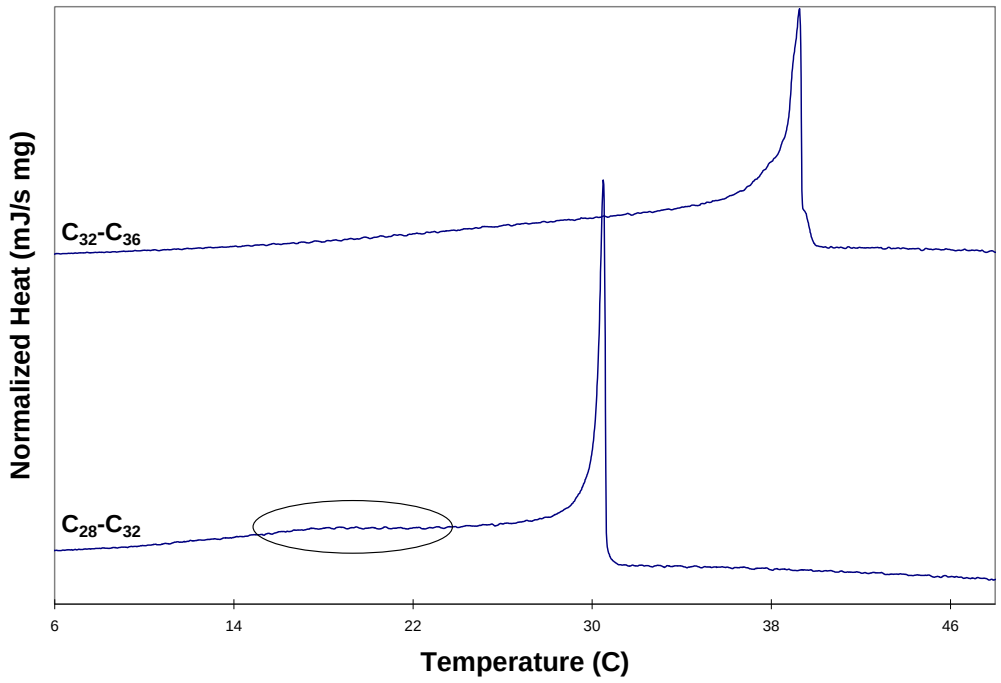

Figure 2.4: DSC traces for 4% C_{36}/4% C_{32} and 4% C_{32}/4% C_{28} from Figure 3. The oval indicates the presence of a small peak present in the 4% C_{32}/4% C_{28} trace, but absent in the 4% C_{36}/4% C_{32} trace.

For the C_{32}-C_{28} system, a second peak can be seen at around 18 °C on the DSC trace. The location of this peak is consistent with the location of the rounded peak present in the C_{28}-C_{36} trial as seen in Figure 2.3, where C_{28} is crystallizing independently of C_{36}. The trace indicates that a large majority of the C_{28} integrated into the crystal structure of the C_{32} (about 10% of the heat released is related to this independent crystallization event) but did not completely integrate as seen for the C_{36}-C_{32} system, where only one peak exists.

In order to confirm the fact that the second peak in the C_{32}-C_{28} trace was in fact excess C_{28} that independently crystallized, a solution of 2% C_{28} and 4% C_{32} with dodecane as the solvent was examined. Figure 2.5 shows that the small second peak for C_{28} seen for the 4% C_{32}/4% C_{28} system is not present for the 4% C_{32}/4% C_{28} system, in spite of the fact that a lower concentration of C_{28} has a lower cloud point (~19 °C). Figure 2.5 confirms that the peak for the 4% C_{32}/4% C_{28} is caused by some C_{28} being unable to integrate completely with C_{32}. This result adds another limitation to Kravchenko's rules in addition to carbon number difference. This limitation is that the abundance of n-alkane present in the solution is important. If an insufficient amount of the less soluble n-alkane is present to allow for the formation of co-crystals, the more soluble n-alkane that did not become a part of the crystal structure will heterogeneously nucleate at a more thermodynamically favored point (at a lower temperature).

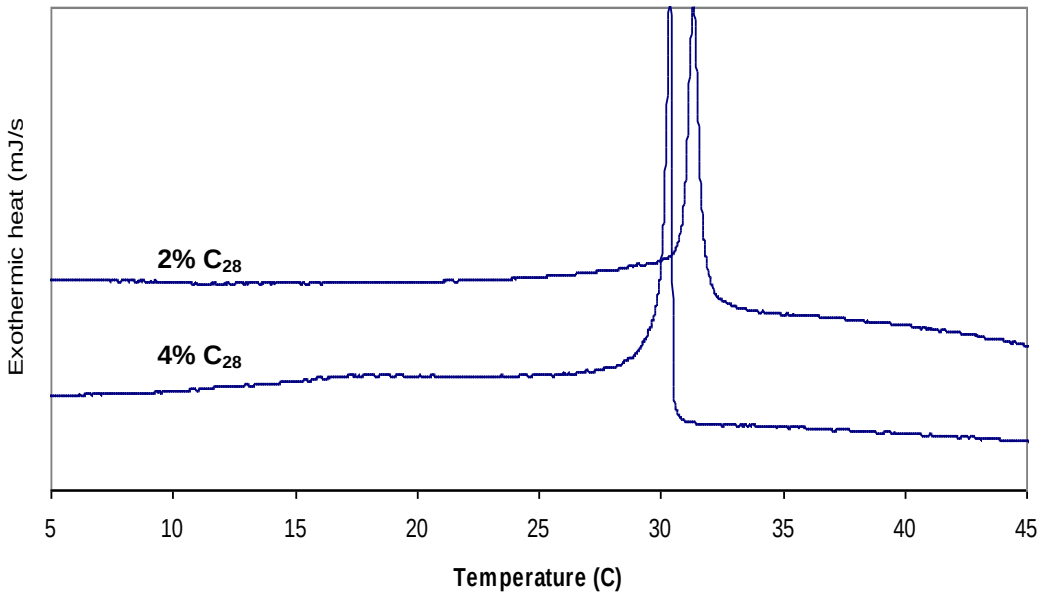

Figure 2.5: DSC traces for samples of solutions containing 4% C_{32}/4% C_{28} and 4% C_{32}/2% C_{28}

Further analysis of the C_{36}/C_{28} DSC trace can also provide insight into how these systems are crystallizing. From Kravchenko's rule, C_{36} and C_{28} should not cocrystallize. However, the C_{28} peak is much different, both in size and shape when compared to the monodisperse C_{28} system. It has been postulated earlier in this work that these differences can primarily be explained by the C_{28} molecules using the already precipitated C_{36} molecules as nucleation sites, causing the precipitation of C_{28} to be caused not only by supersaturation but also heterogeneous nucleation. Due to the fact that these events do not occur at the same time, the peak would be spread out (rounded) and lower than the peaks seen for the monodisperse DSC traces because the range over which crystallization is occurring is wider. However, the possibility exists that C_{28} is crystallizing at the same time C_{36} is crystallizing, whether by some cocrystallization mechanism or by the C_{36} molecules encapsulating some C_{28} molecules and leading to heterogeneous nucleation.

In order to determine if C_{28} is crystallizing in the same temperature range as C_{36}, the area under the curve (the enthalpy of crystallization) can be utilized. Using Table 2, it can be shown that about 56% of the heat released in an equal weight % system of C_{36}/C_{28} in dodecane would be from C_{36} crystallizing out of the solution if the two n-alkanes were to independently crystallize. The full calculation can be seen in the Appendix. Figure 2.6 shows the amount of heat released by the C_{36}/C_{28} system as a function of temperature and affirms that no C_{28} is cocrystallizing with C_{36}.

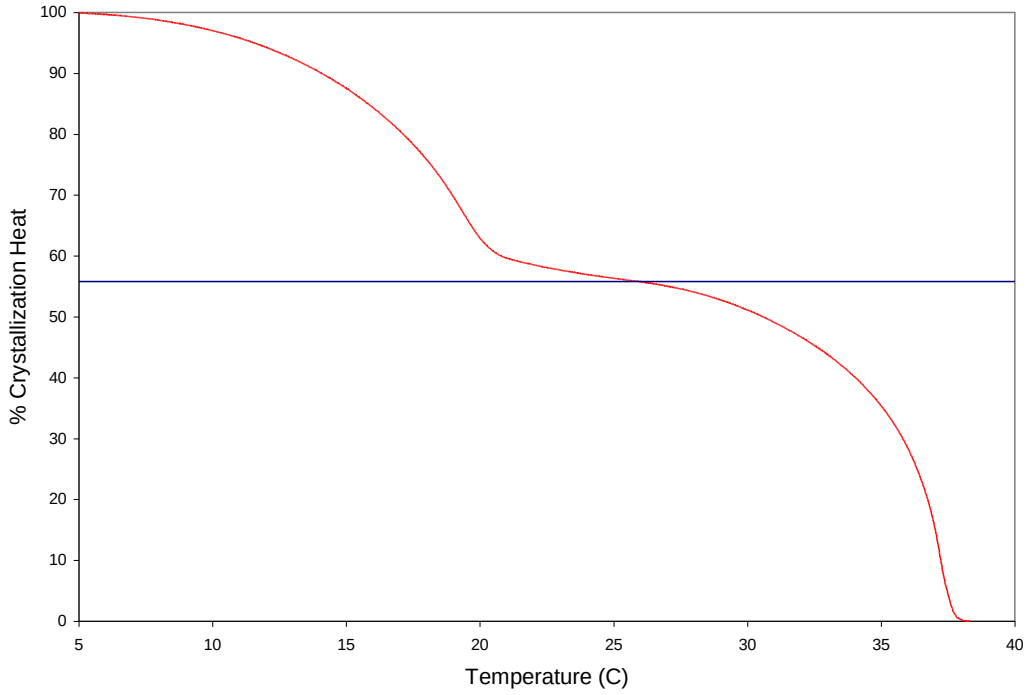

Figure 2.6: Cumulative heat released by the C_{36}/C_{28} system as a function of temperature. The thin line represents the % heat that would be devoted to C_{36} if the n-alkanes were to independently crystallize.

The first hump (between 25 and 38 °C) represents the crystallization of C_{36} and the second hump (between 5 and 20 °C) primarily represents the crystallization of $C_{28,}$ but also some equilibrium crystallization of C_{36} and C_{28} occurring. The relatively level area between 20 and 25 °C represents equilibrium crystallization and the beginning of C_{28}

heterogeneously nucleating onto C_{36}. If C_{28} were to cocrystallize with C_{36} in the regime of the first hump, it would be expected that the first hump would be higher (indicating a higher amount of crystallization occurring between 25 and 38 °C) and a lack of the level area between 20 and 25 °C.

Densitometer Studies

The densitometer measures the density as a function of temperature by varying the temperature of the solution, allowing for the measurement of density as a function of temperature. It provides a convenient means of comparison to the DSC traces using a much lower cooling rate (over 10 times slower) to see how cooling rate affects the results seen in the DSC. The slope of the density-temperature curve ($d\rho/dT$) is related to the peaks seen in the DSC trace. A change in density is caused by either two events: a reduction in temperature or a phase change, with the phase change causing a greater change on density. The change in density simply caused by a reduction in temperature seen in the densitometer is consistent with the baseline seen in the DSC, temperature regimes where no phase changes are occurring. The sharp changes in density seen in the densitometer caused by a phase change are consistent with the peaks present in the DSC, temperature regimes where a phase change is occurring. Figure 2.7 shows a typical densitometer plot as well as the slope of the density curve for the 4% C_{36} system. The sudden change in density at 39.1^0 C is indicative of a phase change and thus another estimate of the system cloud point temperature. Similar to the DSC trace, the slope of the density curves shows an area with high density change, indicating the supersaturation

crystallization regime followed by a decaying exponential-like tail, consistent with the equilibrium crystallization regime as indicated by Paso (Paso, 2005).

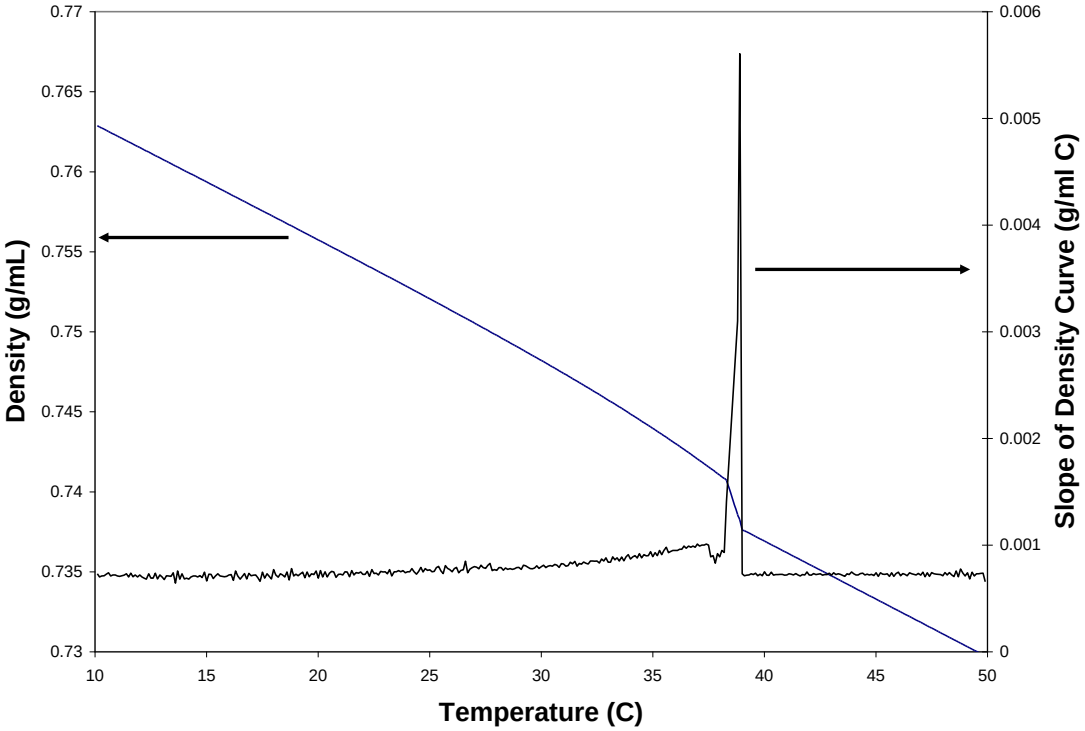

Figure 2.7: Densitometer results for 4% C_{36} in dodecane

Figure 2.8 shows the density slopes as a function of temperature for 4% C_{36} and for the 4% C_{36}/4% C_{28} system. Similar to the DSC traces, the systems crystallize at approximately the same temperature and there are two distinct events for the C_{36}/C_{28} system indicating a lack of cocrystallization between the two n-alkanes. Further, both densitometer runs decay to the same density slope curve in between 25 and 35 °C. As with the DSC traces, this temperature regime is consistent with the equilibrium crystallization regime for C_{36}. The fact that the C_{36}/C_{28} system has the same density slope curve in this temperature range provides further evidence that only C_{36} is crystallizing and that no C_{28} is heterogeneously nucleating onto the already formed C_{36} crystals in between 22 and 35 °C.

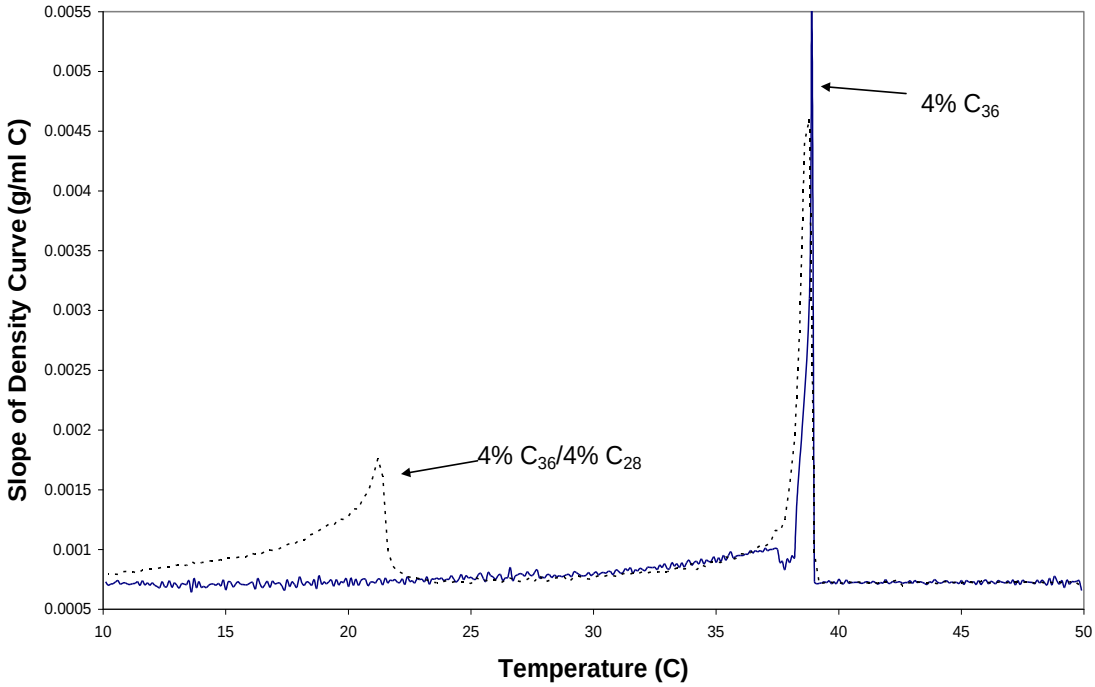

Figure 2.8: Densitometer results for 4% C_{36} (solid line) and 4% C_{36}/4% C_{28} (dashed line)

Figure 2.9 shows the densitometer results for the binary 4% C_{36}/4% C_{32} system and for the ternary 4% C_{36}/4% C_{32}/4% C_{28} system.

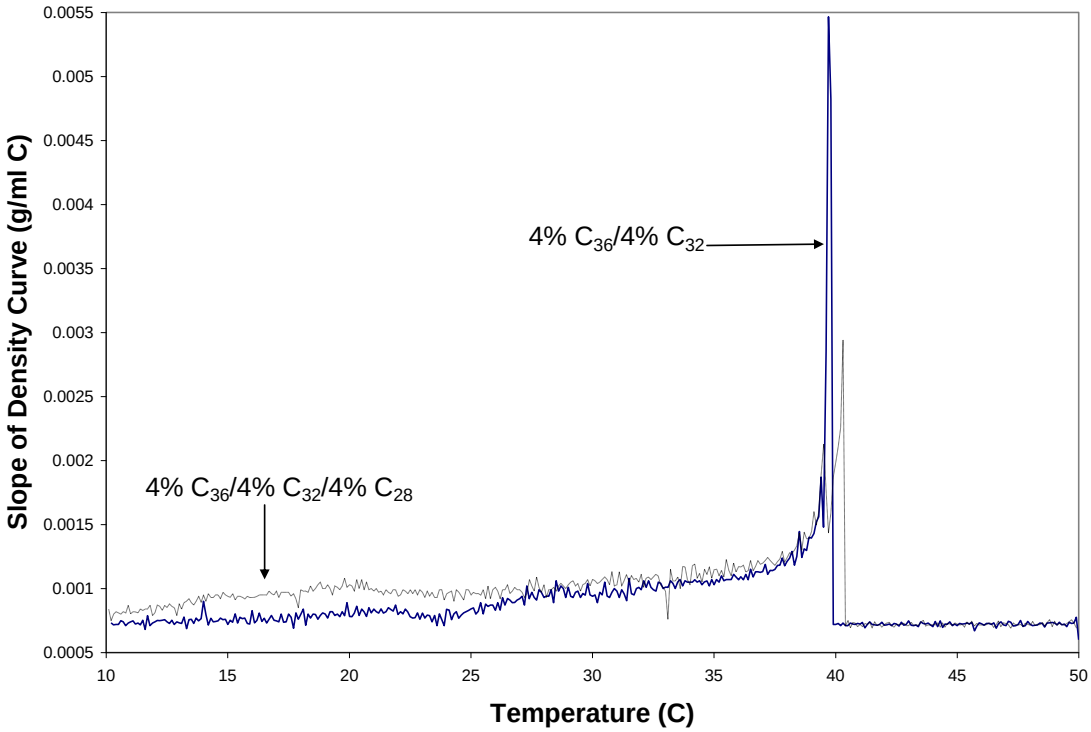

Figure 2.9: Densitometer results for 4% C_{36}/4% C_{32} (solid line) and 4% C_{36}/4% C_{32}/4% C_{28} (dashed line)

Similar to the results in Figure 2.8, both systems in Figure 2.9 exhibit a strong peak around 40 °C, indicating the crystallization of C_{36}. Further, because there is not a separate, distinct peak for C_{32} (when compared to the C_{36}/C_{28} experiment shown in Figure 8), Figure 2.9 shows that C_{36} and C_{32} are cocrystallizing at this slower cooling rate for both the C_{36}/C_{32} system and the ternary system. However, a difference between what is seen in the densitometer results in Figure 2.8 and the results in Figure 2.9 is the value of the slope of the density-temperature curve at temperatures lower than the cloud point (around 40 °C). To better visualize the difference, the results in Figures 2.8 and 2.9 have been magnified in the temperature range of 15 to 35 °C. This magnification is shown in Figure 2.10.

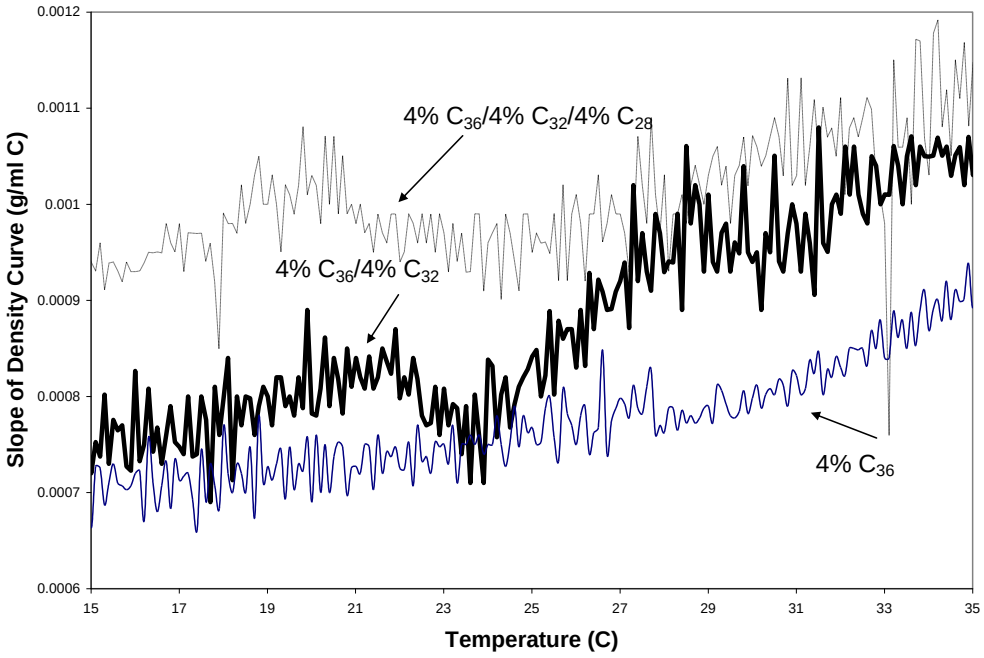

Figure 2.10: Densitometer results for 4% C_{36} (thin solid line) 4% C_{36}/4% C_{32} (thick solid line) and 4% C_{36}/4% C_{32}/4% C_{28} (thin dashed line)

It can be seen from Figure 2.10 that at lower temperatures, the slope of the density-temperature curve is greater for both the binary C_{36}/C_{32} system and the ternary system than for the C_{36} monodisperse system. This result indicates that the crystallization occurring in between 15 and 35 °C is more than just the crystallization of C_{36} because of its solubility limit in dodecane. For the C_{36}/C_{32} system, the additional crystallization occurring between approximately 27-35 °C is from the independent crystallization of C_{32}. Eventually as the temperature approaches 24 °C, the slope of the density-temperature curve for C_{36}/C_{32} becomes similar to the slope of the density-temperature curve for C_{36}, indicating that the only crystallization occurring at these lower temperatures is equilibrium crystallization of both C_{36} and C_{32}.

For the ternary system, there is additional crystallization occurring in between approximately 27-35 °C, similar to the binary C_{36}/C_{32} system, which is consistent with

C_{32} independently crystallizing. However, whereas the slope of the density-temperature curve for the binary C_{36}/C_{32} system becomes approximately equal to the slope of the density-temperature curve for C_{36} at lower temperatures, the slope of the density-temperature curve for the ternary system remains greater. This additional crystallization at temperatures below 27 °C is consistent with independent crystallization of C_{28} that is occurring at these lower temperatures as confirmed by the DSC trace in Figure 2.3.

Although the independent crystallization of C_{28} was shown in the DSC trace, the independent crystallization of C_{32} was not seen for either the C_{36}/C_{32} or the ternary system. If independent crystallization of C_{32} occurred, then the DSC trace in Figure 2.3 would have shown a secondary, less prominent peak at a temperature around where C_{32} crystallized independently. This peak would have been similar to the C_{28} peak seen in the 4% C_{32}/4% C_{28} system in Figures 2.3, 2.4 and 2.5. These results show that the degree of miscibility between two alkanes cocrystallizing in solution is also dependent on the cooling rate, an additional limitation to the rule of thumb developed by Kravchenko. A reduction in cooling rate reduces the degree of miscibility between two n-alkanes because the first crystals to precipitate out will be solely the less soluble n-alkane. At lower cooling rates, the crystals that are formed are larger, integrating more of the less soluble n-alkane molecules in the initial crystals being formed. Because these less soluble molecules are already in a crystal structure, there is an insufficient amount of the less soluble n-alkane to completely cocrystallize with the more soluble n-alkane. Therefore, an insufficient amount of the less soluble n-alkane is now present in solution to allow for complete cocrystallization with the more soluble n-alkane.

Deposition Results

A coldfinger was used to determine how polydispersity and cocrystallization impact deposition. These deposition experiments clearly show that polydispersity impacts deposition characteristics. Table 2.6 shows the results for the monodisperse systems for a six hour deposition experiment.

Table 2.6: Mass and composition information for monodisperse deposits after six hours. % wax in deposit represents the percent of the deposit constituted by the particular alkane (the remainder being the solvent, dodecane). % alkane deposited represents what percent of the alkane initially in solution deposited onto the coldfinger.

Alkane	Deposit Mass (g)	% Wax in Deposit	Mass Alkane Deposited (g)	% Alkane Deposited
C_{36}	1.17	42.2	0.49	7.9
C_{32}	0.42	26.8	0.11	1.8
C_{28}	0.19	8.0	0.015	0.24

From Table 2.6, it can be observed that the mass and wax fraction of the deposit increases with increasing carbon number. As discussed earlier, C_{36} is the least soluble of the three n-alkanes shown in Table 2.2 and it would thus follow that more C_{36} would deposit due to a higher deposition driving force. Table 2.7 shows the composition of the polydisperse deposits.

Table 2.7: Mass and composition information for polydisperse deposits after six hours. % C_n represents the percent of the deposit that is C_n. Total wax % in deposit represents the amount of the deposit that consists of C_{28}, C_{32} and/or C_{36} (with the remainder being the solvent dodecane)

System	Deposit Mass (g)	% C_{28}	% C_{32}	% C_{36}	Total Wax % in Deposit
.C_{36}-C_{32}	0.82	---	14.7	20.0	34.7
C_{36}-C_{28}	1.23	5.4	---	35.8	41.2
C_{32}-C_{28}	0.23	6.5	7.6	---	13.1
C_{36}-C_{32}-C_{28}	1.08	6.2	13.7	28.4	48.3

It would be expected that the polydisperse cases would form deposits that have a higher mass and wax fraction because these systems have double and triple the wax in solution and approximately the same cloud point (Table 2.4) when compared to the monodisperse

cases. However, this expectation is clearly not the case as can be seen in Table 2.7. Instead of an increase in deposit mass and wax fraction, the deposit mass and the total wax fraction of the deposit have actually decreased for the two binary systems where cocrystallization occurs (C_{36}/C_{32} and C_{32}/C_{28}).

For the case of the C_{36}/C_{28} binary system where independent crystallization occurs, the deposit mass for the binary (b) system (1.23g) is similar to that for the monodisperse (m) C_{36} system (1.17g). Additionally, the wax percent of C_{36} in the deposit is similar for both systems (35.8% (b) vs. 42.2% (m)). However, the deposition of C_{28} is significantly enhanced by the presence of C_{36} when compared to the monodisperse C_{28} experiment, as shown in Table 2.8, which provides the percent of the respective alkanes that precipitated out of solution and deposited onto the coldfinger.

Table 2.8: Amounts of the respective n-alkanes depositing from solution for polydisperse systems after six hours. These values represent the mass of n-alkane (in grams) that deposited and the percent of n-alkane initially in solution that deposited in the coldfinger.

	C_{28}		C_{32}		C_{36}	
System	**Mass Deposited**	**% Deposited**	**Mass Deposited**	**% Deposited**	**Mass Deposited**	**% Deposited**
C_{36}-C_{32}	---	---	0.12	1.9	0.16	2.6
C_{36}-C_{28}	0.066	1.0	---	---	0.44	6.7
C_{32}-C_{28}	0.015	0.23	0.017	0.27	---	---
C_{36}-C_{32}-C_{28}	0.067	1.0	0.15	2.2	0.31	4.5

Table 2.8 shows that about 3 times more C_{28} deposits when C_{36} is present in solution (0.066g) compared to the monodisperse C_{28} system (0.015g). This result can be explained by the fact that C_{36} forms a faster, thicker deposit than C_{28} because more C_{36} will initially deposit at the fluid/coldfinger interface. The higher initial deposit of C_{36} is caused by a higher concentration gradient because C_{36} is much less soluble than C_{28} at the lower interface temperature. The already formed C_{36} deposit allows for C_{28} to diffuse into the

deposit and precipitate, allowing for more C_{28} to interact at the liquid-wax interface, enabling more C_{28} to deposit. Additionally, when the C_{36} deposits, liquid oil (dodecane) is entrapped, which includes C_{28} that will also deposit once it reaches its solubility limit in the oil.

Two trends for the binary systems where cocrystallization occurs are seen, one for the shorter C_n alkane and one for the longer C_n. For the shorter n-alkane (C_{28} in the C_{32}/C_{28} system and C_{32} in the C_{36}/C_{32} system), the total amount of the shorter alkane deposited remains relatively unchanged when compared to the monodisperse cases for the shorter alkane (0.015g (b) vs. 0.015g (m) for C_{28} and 0.12g (b) vs 0.11g (m) for C_{32}). This result is contrary to the C_{36}/C_{28} case where much more C_{28} precipitated in the binary case in comparison to the C_{28} monodisperse system. There are two reasons why more C_{28} is found in the C_{36}/C_{28} system deposit than both the C_{32}/C_{28} system deposit and the C_{28} system deposit. For the binary system, the C_{28} can deposit onto an already formed C_{36} deposit. Further, the additional mass of the C_{36} in the C_{36}/C_{28} deposit provided more area for the C_{28} to diffuse into, allowing for further deposition of C_{28}. Although the amount of C_{32} that deposits on the coldfinger is less than the amount of C_{36} that deposits, it would still follow that more C_{28} would be present in the C_{32}/C_{28} deposit than the C_{28} deposit. This discrepancy can be explained by the fact that cocrystallization is occurring in the binary system. The impact of cocrystallization on deposition inhibition will be discussed in more detail below.

A major difference was seen in the cocrystallized systems for the longer n-alkane (C_{32} for the C_{32}/C_{28} system and C_{36} for the C_{36}/C_{32} system), when compared with the monodisperse systems. The percent composition of the longer n-alkane in the deposit

(42.2% (m) vs. 20.0% (b) for C_{36} and 26.8% (m) vs. 7.6% (b) for C_{32}) decreased by over a factor of two. Additionally, the percent of total alkane deposited decreased by over a factor of three compared to the monodisperse trials for the longer n-alkane (7.9% (m) vs. 2.6% (b) for C_{36} and 1.8% (m) vs. 0.27% (b) for C_{32}). These results show that cocrystallization significantly hinders deposition of the longer (less soluble) n-alkane. This fact is interesting because the main driving forces for deposition, a concentration gradient and a temperature gradient between the gel and the external fluid are either unchanged or increased for the binary system. This result can be explained from a morphological standpoint because when cocrystallization occurs, the larger n-alkane will bend itself and enter into the structure the size of the smaller n-alkane (Turner, 1971, Chevalier et al., 1999, Paso, 2005). This morphological change affects the ability of the n-alkanes to either continue to deposit at the interface and/or the diffuse into the deposit. These issues could also influence the nucleation and/or deposition kinetics of the system, further causing a reduction in the deposit. The idea of cocrystallization inhibiting wax deposition is consistent with simulation work done to examine the mechanisms by which wax inhibitors work, which include the wax inhibitor basically integrating into the crystal structure of the n-alkane and disrupting crystal growth (Duffy and Rodger, 2002, Duffy et al., 2004).

Similar to the DSC results, the coldfinger results for the ternary system show a combination of the cases where independent crystallization occurs and where cocrystallization occurs. The wax fraction of the deposit for the $C_{36}/C_{32}/C_{28}$ system (48.3%) is minimally higher than the monodisperse C_{36} system (42.2%). This result is caused by the occurrence of independent crystallization and a higher solution wax content

in the ternary system (12%) compared to the monodisperse C_{36} system (4%). However, the amount of C_{36} that deposited (0.31g) and the total deposit mass for the ternary system (1.08g) were both lower than that for the monodisperse C_{36} system (0.49g and 1.17g respectively). This result is consistent with what is seen for the systems where cocrystallization occurred (as shown in Table 8) because cocrystallization was shown to reduce both the deposit mass and the amount of the least soluble alkane that deposited.

A unique aspect of the ternary case occurs when comparing the relative amounts of the respective alkanes in the respective systems (as shown in Table 2.8). For the case of independent crystallization (C_{36}/C_{28}), more C_{36} deposits than C_{28} (about seven times more) because C_{36} more readily deposits than C_{28}. Due to a smaller difference in driving force and the occurrence of cocrystallization, it follows that the ratio of the longer n-alkane to the shorter n-alkane present in the deposit is much lower for the cases where cocrystallization occurs because many of the molecules are crystallizing out together. The ratios of C_{32}:C_{28} and C_{36}:C_{32} for the respective binary systems are near 1:1. However, the ratio of C_{36}:C_{32}:C_{28} in the deposit for the ternary case is about 4:2:1, indicating that this system is a combination of co-crystals of C_{36}/C_{32} and of C_{32}/C_{28} along with the independent crystallization of both C_{36} and C_{28}. This result suggests that C_{36} must be crystallizing independently in the ternary system because much more C_{36} is present in the deposit than C_{32}, which is the only material present in the system that could cocrystallize with C_{36}. Cocrystals are present in this system because the mass of the deposit is less than the monodisperse C_{36} system, consistent with the reduction in mass seen when cocrystallization occurred (as shown in Table 2.8). Finally, C_{28} must also be crystallizing independently because the amount that deposited in the ternary system is far greater than

the amount that deposited in the binary C_{32}/C_{28} trial, where cocrystallization is occurring. This result shows that the presence of C_{28} is inhibiting the cocrystallization of C_{36} and C_{32} either by interacting with C_{32} molecules while in the liquid phase or providing a physical means to limit the interactions between C_{36} and C_{32} molecules, allowing for C_{36} molecules to deposit independently.

Summary

This work elucidates various aspects of n-alkane crystallization by usage of three different types of apparatus (DSC, densitometer and coldfinger). It was found that both n-alkane polydispersity and cocrystallization play roles in how n-alkanes crystallize in solution. This work has shown that alkanes can cocrystallize in solution if their carbon numbers are sufficiently close, consistent with Kravchenko's rules for melts. Although Kravchenko's work can be extended to solutions, limitations exist because it does not account for either the relative abundance of n-alkanes in solution or the effect of cooling rate. Both of these variables impact the degree of cocrystallization, leading to cases where a more soluble alkane will cocrystallize with a less soluble alkane and by itself. The cocrystallization of two alkanes can also be affected by the presence of a third alkane, either by cocrystallization with this third alkane or by providing a physical means to prevent molecular interaction and thus cocrystallization.

Both polydispersity and cocrystallization reduce the heat released during crystallization, primarily because of the reduction of heat released by the more soluble alkanes. Additionally, polydispersity and cocrystallization reduce the mass and the wax

fraction of deposits, in spite of systems having a higher wax fraction in comparison to the monodisperse systems.

This work shows that more soluble alkanes are greatly impacted by the presence of less soluble alkanes because of the less soluble alkanes already crystallizing out of solution, providing nucleation sites for the more soluble alkanes. This homogeneous nucleation broadens the range over which the crystallization of the more soluble alkane occurs and the ability of the more soluble alkane to deposit. However, the less soluble alkanes are not impacted as much by the presence of the more soluble alkanes. The degree of the impact of the more soluble alkanes on the more soluble alkanes is directly related to cocrystallization and is primarily seen as a slight increase in the temperature which crystallization occurs and as a reduction in the amount of less soluble alkane that deposits.

References:

Ashbaugh, H. S., Radulescu, A., Prud'homme, R. K., Schwahn, D., Richter, D. and Fetters, L. J., "Interactions of Paraffin Wax Gels with Random Crystalline/Amorphous Hydrocarbon Copolymers", *Macromolecules,* **35**, 7044-7053 (2002)

Azevedo, L. F. A., and Teixeira, A. M., "A Critical Review of the Modeling of Wax Deposition Mechanisms", *Pet. Sci. & Tech.,* **21**, 393-408 (2003)

Chevalier, V., Provost, E., Bourdet, J. D., Bouroukba, M., Petitjean, D., and Dirand, M., "Mixtures of Numerous Different n-Alkanes: 1. Structural Studies by X-ray Diffraction at Room Temperature – Correlation Between the Crystallographic Long c Parameter and the Average Composition of Multi-Alkane Phases", *Polymer,* **40**, 2121-2128 (1999)

Coutinho, J. A. P., and Stenby, E. H., "Predictive Local Composition Models for Solid/Liquid Equilibrium in n-Alkane Systems: Wilson Equation for Multicomponent Systems", *Ind. Eng. Chem. Res.,* **35**, 918-925 (1996)

Dirand, M., Chevallier, V., Provost, E., Bouroukba, M., and Petitjean, M., "Multicomponent Paraffin Waxes and Petroleum Solid Deposits: Structural and Thermodynamic State", *Fuel,* **77**, 1253-1260 (1998)

Dirand, M., Bouroukba, M., Chevallier, V., Petitjean, D., Behar, E., and Ruffier-Murray, V., "Normal Alkanes, Multialkane Synthetic Model Mixtures and Real Petroleum Waxes: Crystallographic Structures, Thermodynamic Properties and Crystallization", *J. Chem. Eng. Data.,* **47**, 115-135 (2002)

Duffy, D. M., and Rodger, P. M., "Modeling the Activity of Wax Inhibitors: A Case Study of Poly(octadecylacrylate)", *J. Phys. Chen. B,* **106**, 11210-11217 (2002)

Duffy, D. M., Moon, C., and Rodger, P. M., "Computer-Assisted Design of Oil Additives", *Molec. Phys.,* **102**, 203-210 (2004)

Garcia, M.d.C., "Crude Oil Waxy Crystallization. The Effect of Heavy n-Paraffins and Flocculated Asphaltenes", *Energy & Fuels,* **14**, 1043-1048 (2000)

Ghogomu, P. M., Dellacherie, J., and Balesdent, D., "Solubility of Normal Paraffin Hydorcarbons (C_{20} to C_{24}) and Some of their Binary Mixtures (C_{22} + C_{24}) and (C_{23} + C_{24}) in Ethylbenzene", *J. Chem Thermodynamics,* **21**, 925-934 (1989)

Guo, X., Pethica, B. A., Huang, J. S., Prud'homme, R. K., Adamson, D. H., and Fetters, L. J., "Crystallization of Mixed Paraffin from Model Waxy Oils and the Influence of Micro-crystalline Poly(ethylene-butene) Random Copolymers", *Energy & Fuels,* **18**, 930-937 (2004)

Guo, X., Pethica, B. A., Huang, J. S., Adamson, D. H., and Prud'homme, R. K., "Effect of Cooling Rate on Crystallization of Model Waxy Oils with Microcrystalline Poly(ethylene butane), *Energy & Fuels,* **20**, 250-256 (2006)

Hansen, A. B., Larsen, E., and Pedersen, W. B., Nielsen, A. B., and Ronnignsen, H. P., "Wax Precipitation from North Sea Crude Oils. 3. Precipitation and Dissolution of Wax Studied by Differential Scanning Calorimetry", *Energy & Fuels,* **5**, 914-923 (1991)

Hennessy, A. J., Neville, A., and Roberts, K. J., "An Examination of Additive-Mediated Wax Nucleation in Oil Pipeline Environments", *J. Cryst. Growth,* **198/199**, 830-837 (1999)

Kane, M., Djabourov, M., Volle, J-L., Lechaire, J-P., and Frebourg, G. "Morphology of Paraffin Crystals in Waxy Crude Oils Cooled in Quiescent Conditions and Under Flow", *Fuel*, **82**, 127-135 (2003)

Kern, R., and Dassonville, R., "Growth Inhibitors and Promoters Examplified on Solution Growth of Paraffin Crystals", *J. Cryst. Growth*, **116**, 191-203, (1992)

Liu, X.Y., and Bennema, P., "On the Morphology of Crystals of Triclinic Even Normal Alkanes: Theory and Observation", *J. Cryst. Growth*, **135**, 209-223 (1994)

Misra, S., Baruah, S., and Singh, K., "Paraffin Problems in Crude Oil Production and Transportation: A Review", *SPE Prod & Facilities*, 50-60 (1995)

Paso, K. G., and Fogler, H. S. "Bulk Stabiliziation in Wax Deposition Systems", *Energy & Fuels,* **18**, 1005-1013 (2004)

Paso, K., Senra, M., Yi, Y., Sastry, A. M., and Fogler, H. S., "Paraffin Polydispersity Facilitates Mechanical Gelation", *Ind. Eng. Chem. Res.,* **44**, 7242-7254 (2005)

Paso, K., *Paraffin Gelation Kinetics*. University of Michigan Ph.D. Thesis, Ann Arbor, MI, (2005)

Pedersen, K. S., Skovborg, P., and Ronningsen, H. P., "Wax Precipitation from North Sea Crude Oils. 4. Thermodynamic Modeling", *Energy & Fuels*, **5**, 924-932 (1991)

Provost, E., Chevalier, V., Bouroukba, M., Petitjean, D., and Dirand, M., "Solubility of Some n-Alkanes (C_{23}, C_{25}, C_{26}, C_{28}) in Heptane, Methylcyclohexane, and Toluene", *J. Chem Eng Data,* **43**, 745-749 (1998)

Sangwal, K., "Effects of Impurities on Crystal Growth Processes", *Prog. Cryst. Growth and Proc.,* **32**, 3-43 (1996)

Singh, P., Fogler, H. S., and Nagarajan, N. R., “Prediction of the Wax Content of the Incipient Wax-Oil Gel in a Pipeline: An Application of the Controlled-Stress Rheometer," *J. Rheol.*, **43**, 1437-1459 (1999)

Singh, P., Venkatesan, R., Fogler, H. S., and Nagarajan, N., “Formation and Aging of Incipient Thin Film Wax-Oil Gels”, *AIChE J.*, **46**, 1059-1074 (2000)

Singh, P., Venkatesan, R, Fogler, H. S., and Nagarajan, N. R., "Morphological Evolution of Thick Wax Deposits during Aging," *AICHE J.*, **47**, 6-18 (2001)

Singh, P., Youyen, A., and Fogler, H. S., “The Existence of a Critical Carbon Number in the Aging of a Wax-Oil Gel”, *AICHE J.*, 47, 2111-2124 (2001)

Srivastava, S. P., Handoo, J., Agrawal, K. M., and Joshi, G. C., “Phase-Transition Studies in n-Alkanes and Petroleum-Related Waxes”, *J. Phys. Chem. Solids,* **34**, 639-670 (1993)

Svendsen, J. A., “Mathematical Modeling of Wax Deposition in Oil Pipeline Systems”, *AICHE J.*, **39**, 1377-1388 (1993)

Turner, W. R., “Normal Alkanes”, *Ind. Eng. Chem. Prod. Res. Develop.*, **10**, 238-260 (1971)

Venkatesan, R., Nagarajan, N. R., Paso, K., Yi, Y.-B., Sastry, A. M., and Fogler, H. S., “The Strength of Paraffin Gels Formed Under Static and Flow Conditions”, *Chem. Eng. Sci.*, **60**, 3587-3598 (2005)

Weispfennig, K., “Advancements in Paraffin Testing Methodology”, *SPE 64997***,** 1-6 (2001)

Wu, C-H., Wang K-S., Shuler, P. J., Tang, Y., Creek, J. L., Carlson, R. M., and Cheung, S., “Measurement of Wax Deposition in Paraffin Solutions”, *AICHE J.*, **48**, 2107-2110 (2002)

CHAPTER III

THE ROLE OF POLYDISPERSITY AND COCRYSTALLIZATION ON GELATION

Wax deposition is a major issue facing the petroleum industry, particularly in extremely cold environments and for highly waxy crudes. This problem has become of greater importance today as petroleum companies move further offshore to deeper and colder waters in order to find and extract crude oil (Guo, et al., 2006, Venkatesan, et al., 2002, Wu et al., 2002). Problems directly caused by wax deposition include the damaging of oil reservoir formations, the blockage of process equipment, the straining of pumping facilities, and the restarting of pipelines for a wide variety of reasons, including but not limited to maintenance, economics, weather and political strife (Carnahan and Carnahan, 1998, Mehrotra and Bhat, 2007, Soni and Bharambe, 2006). Because the crude has to travel further distances in a cold water environment, the probability of the crude cooling down sufficiently to reach its cloud point increases, increasing the likelihood that wax will deposit on the pipeline wall. Deposition can reduce production and if left untreated can leave the pipeline inoperable, a condition faced in pipelines across the world (Paso and Fogler, 2004, Venkatesan et al., 2002). While the costs of remediation, usually via mechanical pigging and/or the addition of a wide array of fluids, inhibitors and additives can be quite high, these costs are dwarfed by the production losses incurred by flow reductions and/or pipeline shutdowns and maintenance needed because of wax deposition.

Therefore, gaining a better understanding of the wax deposit would be of great utility to the petroleum industry to allow them to optimize their remediation approaches.

Crude oils can contain a large number of components, including but not limited to paraffins, aromatics, naphthenes, asphaltenes and resins (Hansen, et al., 1991, Venkatesan et al., 2003). In spite of the complexity of crude oils, it has been concluded that the primary component of wax deposits are higher molecular weight n-paraffins (interchangeably referred to as n-alkanes) (Garcia, 2000, Hennessy et al., 1999, Kane et al., 2003). n-Paraffins are straight chained hydrocarbons containing solely single bonds with the chemical formula C_nH_{2n+2}. Wax deposits can contain n-alkanes with carbon numbers (n) as low as 10 and as high as 80, but predominantly in the range of 20 to 40 (del Carmen Garcia, 2000, Ronningsen, et al., 1991). Deposits are constituted primarily of n-alkanes because of their lower solubility in organic solvents and their ability to crystallize easily in an ordered structure (Hennessy et al., 1999).

The formation of a wax deposit is a solubility based phenomenon. At reservoir conditions (temperatures ranging from 70-150 °C and pressures ranging from 8000-15000 psi), the n-paraffins will remain in solution and no solids will form (Venkatesan et al., 2005). However, as the crude oil is transported through the pipeline, both the temperature and pressure are reduced, greatly reducing n-paraffin solubility and potentially allowing for the higher carbon number n-paraffins to precipitate out of solution. Although the precipitation of n-paraffins in the bulk crude oil can cause issues in transportation and flow, the major concern is deposition on the pipeline walls. It is generally accepted that the mechanism of wax deposition is governed by molecular diffusion (Singh et al., 2001a). After the creation of an incipient gel layer, the gel

continues to change through a process called aging, where longer chained n-alkanes will continue to diffuse into the gel layer, while shorter chained n-alkanes with a carbon number less than the critical carbon number will diffuse out of the gel layer (Singh et al., 2001b). Aging causes the solid content of the wax gel to increase, leading to the formation of a harder gel, making the gel more difficult to remediate.

It is known that the gel deposits consist of lamellar crystals that form random, interlocking structures that have the ability to trap the liquid oil, forming an organic gel (Ashbaugh et al., 2002). This lamellar structure is similar to the shape seen when pure n-alkanes crystallize from either a melt or an organic solvent (Turner, 1971). The carbon atoms of the methylene groups are in an all-trans zigzag conformation where the long axes of the chains are parallel and the end methyl groups of two layers are parallel to one another (Dirand et al., 2002, Turner, 1971). A schematic of this can be seen below in Figure 3.1. More representative images have been completed by Dirand (Dirand et al., 2002).

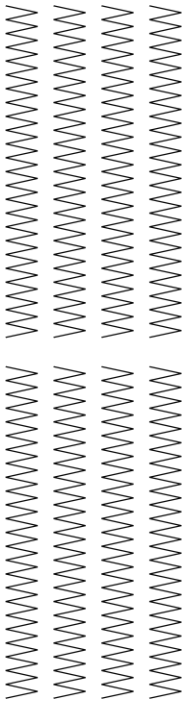

Figure 3.1: Schematic representation of a crystalline n-alkane system. Each line represents a carbon-carbon bond. The entire zigzag configuration represents a long chained n-alkane molecule. The gap between the zigzags represents the interlayer spacing between the sheets. (Adapted from Turner, 1971)

In order for a gel to form, a network needs to be formed such that the solid, interlocking crystals span the entire volume of the gel. This colloidal gel can require as little as 2% solid wax to form a gel (Singh et al., 1999). In these gels, the n-alkanes will crystallize out once their solubility limit is exceeded, a temperature known as the cloud point. As the temperature lowers further below the cloud point, further crystallization along with aggregation will occur, promoting the formation of a volume spanning network, i.e. a gel (Radinski, et al., 1996, Vignati et al., 2005). It has been shown that a polydisperse mixture will form atomically thin, flat aggregates of similar carbon length over a large temperature range (Radisnki, et al., 1996). Vignati proposed a physical mechanism in which the aggregation of the wax crystals is driven by dispersion forces into an extended fractal network (Vignati et al., 2005). While the gel is beginning to form, wax aggregation is so quick that the system becomes dynamically arrested and the gel

gains further strength as more wax enters the system because the temperature is decreasing. The system will become a true gel once it becomes strong enough to sustain the stresses from gravity and the fluid flow. This gel, particularly its thickness and its strength, is of great concern in the petroleum industry.

The major variables of interest of a gel are the yield stress, the gelation temperature (gel point) and the pour point temperature (pour point). The yield stress is the shear stress necessary to break the gel. Although the gelation temperature and the pour point temperature are similar: they are both used to represent the temperature at which a crude oil finalizes its transition from a complex fluid to a solid, their definitions ar somewhat different. A clear differentiation between the two values has been provided by Venkatesan, defining the pour point as the temperature where the fluid has stopped flowing under static conditions and a specified thermal history and the gelation temperature as the point where solid-like characteristics of the fluid dominate over the liquid-like characteristics at a particular cooling rate and applied stress (Venkatesan, et al., 2002). The definition of the gelation temperature was based upon the research of Singh, who used a controlled-stress rheometer to extend the conclusion of Winter that was developed for cross-linking polymers (Singh, et al., 1999, Winter, 1987). The gel point is the temperature where the storage modulus, (G', representing its solid-like behavior) the elastic portion showing the ability of a viscoelastic solid to store energy exceeds the loss modulus, (G", representing its liquid-like behavior), the viscous portion showing the ability of a viscoelastic solid to dissipate heat energy. They are represented as the real and imaginary portions of the complex modulus and the mathematical relationship is shown below.

$$\mathbf{G} = G' + iG'' \quad (1.1)$$

Where: **G** = complex modulus
G' = storage modulus, defined in (2)
G'' = loss modulus, defined in (3)

$$G' = \frac{\varepsilon}{\sigma}\cos(\delta), G'' = \frac{\varepsilon}{\sigma}\sin(\delta) \quad (1.2, 1.3)$$

Where: ε = strain
σ = stress
δ = phase lag between stress and strain

At temperatures above the cloud point, the loss modulus will be higher than the storage modulus. As the temperature is decreased, both G' and G'' will begin to increase and when the temperature goes below the cloud point, the solidification of wax leads to a sharp increase of G''. If the crude is capable of gelling, G' will become larger than G'', with this crossover representing the gelation temperature. Figure 3.2 shows two situations: the first represents a case where the oil has gelled and the second represents a case where the oil has not gelled.

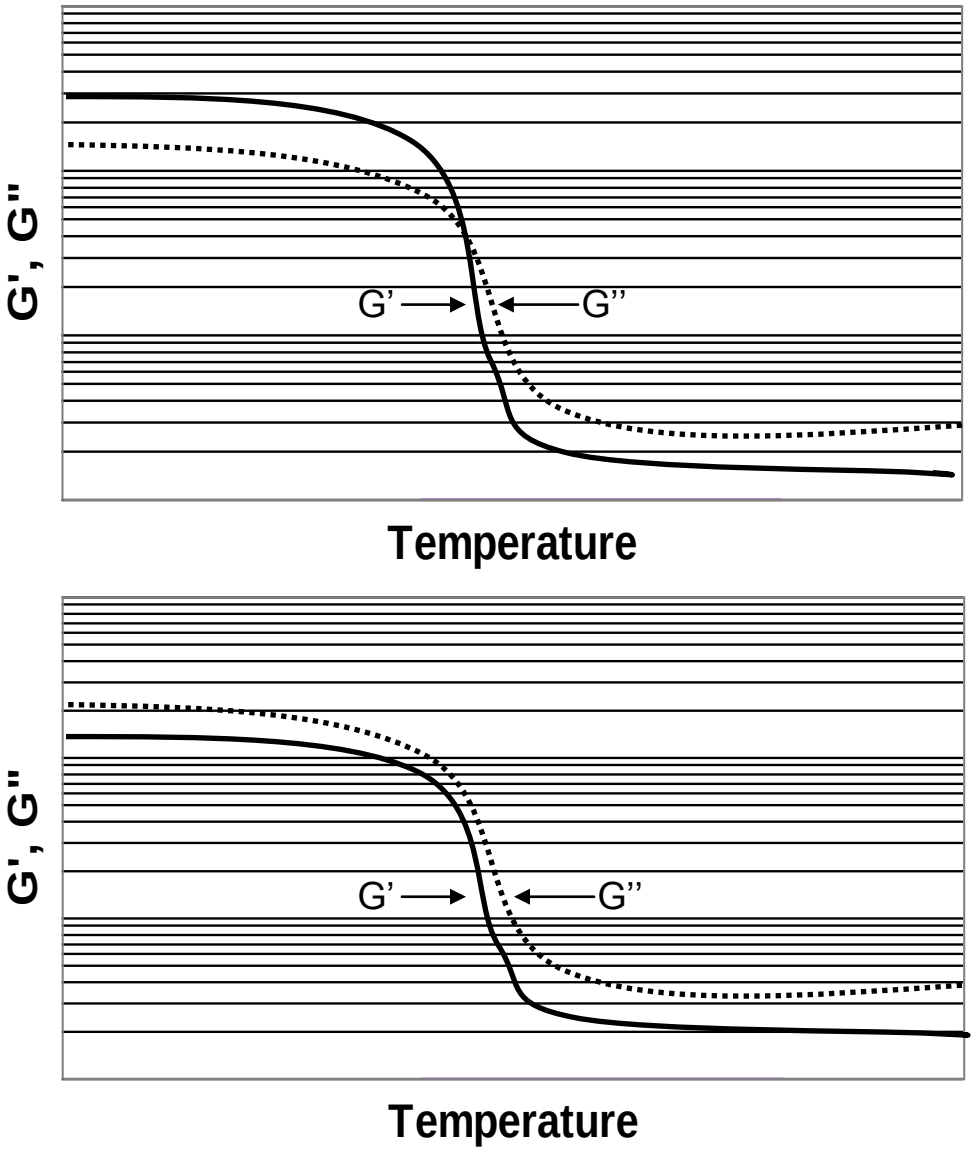

Figure 3.2: Representative rheometric results for viscoelastic fluids. In the top graph, G' and G" cross over, indicating the occurrence of the formation of a gel. In the bottom graph, G' and G" do not cross over although there has been a sharp increase in both G' and G" (indicating crystallization). The bottom graph shows a system where crystallization has occurred, but gelation has not occurred.

The properties of the gel are strong functions of the crude oil properties such as cloud point, wax solubility, wax content, and viscosity and operating conditions such as

cooling rate, applied stress, thermal history and shear history. A major reason for the multitude of properties affecting gelation is because crystallization is a required step for gelation. The larger the crystal size and the greater the number of wax crystals, the easier it is for a volume spanning network gel to form. Singh showed that faster cooling rates, lower shear stresses and higher wax fractions in the oil were conducive to forming gels at higher temperatures (Singh, et al., 1999). Faster cooling rates may lead to higher gelation temperatures, but wax-oil systems with faster cooling rates have been shown to form weaker gels (i.e. lower yield stresses) when cooled statically (Chang et al., 2000, Venkatesan, et al., 2005). Microscopic evidence was provided to show that slower cooling rates promote the formation of larger crystals that are more conducive to forming a volume spanning network gel. However, under non-quiescent conditions, Venkatesan showed that faster cooling rates will form stronger gels, primarily because the systems at lower cooling rate are exposed to shear for a longer period of time, allowing for the shear to have a greater impact in disrupting the formation of the gel (Venkatesan, et al., 2005). This conclusion was validated by Visintin, who measured the effect of stress application time on the yield stress (Visintin, et al., 2005).

Chemical additives are often introduced to crude oil to attempt to mitigate wax deposition. They have been known to reduce the temperature at which wax precipitation and/or gelation will begin, inhibit the wax from depositing onto the pipe wall and/or weaken the gel structure. Each of these effects is singularly able to reduce wax deposition. Soni and Bharambe have provided criteria for additives to be good flow improvers: a linear alkyl chain that can cocrystallize with the carbon numbers crystallizing out of solution, a polar component to limit cocrystallization and an adsorber onto the wax

crystal to sterically hinder crystal growth (Soni and Bharambe, 2006). Additionally, they highlighted properties of good pour point depressants: the number of side chains and their distance between one another, their solubility in organic solvents and their physical and chemical stability. The materials used as additives and their mechanisms by which they interact with the gel are highly varied. El-Gamal and Al-Sabbagh showed that additives containing nitrogen (amides, ester and ether with long chains) provided a dispersing effect that reduces the pour point of lighter Egyptian waxy gas-oil blends (El-Gamal and Al-Sabbagh, 1995). However, these nitrogen containing additives were not as efficient when used on Egyptian crude oils. Soni and Bharambe showed that maleic anhydride copolymers reduce the pour point of an Indian crude oil by changing the crystal morphology and reducing the viscosity by developing hydrogen bonds with asphaltenes and resins, two materials naturally present in oil that increase their viscosity (Holder and Winkler, 1965, Soni and Bharambe, 2006). In work on poly(ethylene-co-vinyl acetate (EVA) copolymers and Brazilian crude oil, Machado showed that the efficiency of EVA was a function of both the vinyl acetate composition of the copolymer and the concentration of the copolymer (Machado et al., 2001). Work using polymethacrytlates on Brazilian diesel oil emphasized that the efficiency of an additive is dependent not only on the properties of the inhibitor, but also the composition of the crude oil (Soldi, et al., 2007). This conclusion was reaffirmed by work using an acrylic ester copolymer on Croatian crude oil and in a series of works using poly(ethylene butane) copolymers on a wide variety of model oils (Ashbaugh et al., 2002a, 2002b, Guo et al., 2004a, 2006, Kuzmic et al., 2006).

Although these studies have focused on how adding materials can affect the gelation properties of oil, little work has been dedicated to seeing how the composition of oil can affect the gelation properties. n-Alkanes are of interest because they are the primary component of the waxy gels found in subsea oil pipelines. Using model waxes, Paso showed that polydispersity can assist in the formation of a strong gel (Paso, et al., 2005). Jennings and Weispfenning proved that waxes do not completely exhibit ideal solution behavior when crystallizing and that their solubility in a solvent increases as both the solvent molecular size and the solvent solubility parameter decreases (Jennings and Weispfennig, 2005). This decrease occurs because of the ability of a smaller solvent to better contact and solvate the n-alkane and the ability of a lower solubility parameter solvent to associate with other molecules instead of itself. Studies have shown that multiparaffin waxes spanning over 20 carbon numbers when cooled will crystallize in a number of different solid crystal phases at different temperatures when cooled (Briard et al., 2006, Dirand et al., 1998). These multiparaffin wax crystals are generally orthorhombic in crude systems, although n-alkanes independently crystallize in a number of shapes dependent on the carbon number and whether the carbon number is even or odd (Dirand et al., 1998, 2002). Turner proposed the existence of these groupings of solid phases and the ability of n-alkanes to form cocrystals that can include a number of n-alkanes in a particular crystal structure (Turner, 1971). His guidelines for cocrystallization were that the molecules would not only have to be similar in form and dimension, but also must have similar crystal symmetries to those when the n-alkane crystallizes out by itself. Therefore, although an even n-alkane with a carbon number of n and an odd n-alkane with a carbon number of n+1 (or n-1) are similar in form and

dimension (and typically have relatively similar solubilities in most organic solvents), they will not cocrystallize because odd and even carbon numbers have different crystal morphologies. Dirand proposed a configuration of multiple n-alkanes in one crystal structure where the length of the layer is equivalent to the layer size of the average carbon number of the n-alkanes present in the structure (Dirand, et al., 1998). A schematic of this configuration can be seen in Figure 3.3 where the dark colored molecules are bending to incorporate the two shorter light colored molecules. The average length of the cocrystal is equivalent to the length of the longer light colored molecule.

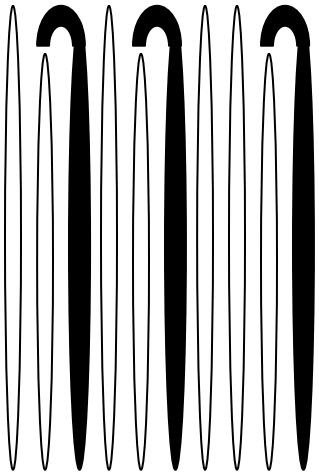

Figure 3.3: Sample molecular configuration for multiple n-alkanes cocrystallizing. The dark molecules are bending to associate with the smaller n-alkanes to form a common crystal structure. (Adapted from Dirand, et al., 1998)

Experiments using differential scanning calorimetry and densitometry were completed in Chapter 2 to help validate the conclusions by Dirand and additionally have shown that both cocrystallization and polydispersity have an impact on the thermodynamic and deposition characteristics of n-alkane systems crystallizing from n-alkane solutions.

The main objective of this work is to extend the thermodynamic analysis of n-alkane systems to gelation properties. Most of the previous gelation work on n-alkane systems focused on how inhibitors affect the gel structure. However, little work has been

dedicated to understanding how the composition of the oil itself affects the gel structure. Greater insight into how the composition of a crude oil can influence the gelation characteristics could be crucial in developing more accurate deposition models that could also incorporate such properties as the gelation temperature and the yield stress.

Materials

Dodecane (99+% purity from Sigma) was used as the solvent for all trials. Five even carbon number n-alkanes (all purchased from Aldrich) were analyzed: hexatriacontane ($C_{36}H_{74}$, hereafter abbreviated as C_{36}, 98% purity), dotriacontane ($C_{32}H_{66}$, hereafter abbreviated as C_{32}, 97% purity), triacontane ($C_{30}H_{62}$, hereafter abbreviated as C_{30}, 99% purity), octacosane ($C_{28}H_{58}$, hereafter abbreviated as C_{28}, 98% purity) and tetracosane ($C_{24}H_{50}$, hereafter abbreviated as C_{24}, 99% purity). Two odd carbon number n-alkanes (both purchased from TCI America) were used: pentatriacontane ($C_{35}H_{72}$, hereafter abbreviated as C_{35}, 95% purity) and heptacosane ($C_{27}H_{56}$, hereafter abbreviated as C_{27}, 95% purity).

Experimental Methods

Cloud point temperature

Cloud points were determined using a constant temperature bath where a solution, heated above its cloud point, is slowly cooled and allowed to equilibrate at a temperature. The solution was removed from the temperature bath and visually inspected for any precipitation. If the system remained homogeneous, the bath was cooled to a lower temperature. This process continued until precipitation became visible.

Pour point temperature

The pour point was also determined using a constant temperature bath. The bath is initially held at a temperature above the cloud point of the solution. The solution is preheated in an oven in a vial to a temperature above the cloud point of the solution and left in there for sufficient time to remove any thermal history. The heated solution is then inserted into the temperature bath. The bath is then cooled at a rate of 0.1 °C/min. At the desired sample, the solution is delicately removed from the temperature bath to prevent disruption of the gel structure and is inverted. If the solution moves upon inversion, then the solution is above the pour point. The pour point is defined as the highest temperature where the solution does not move upon inversion. Figure 3.4 shows the result of some pour point experiments.

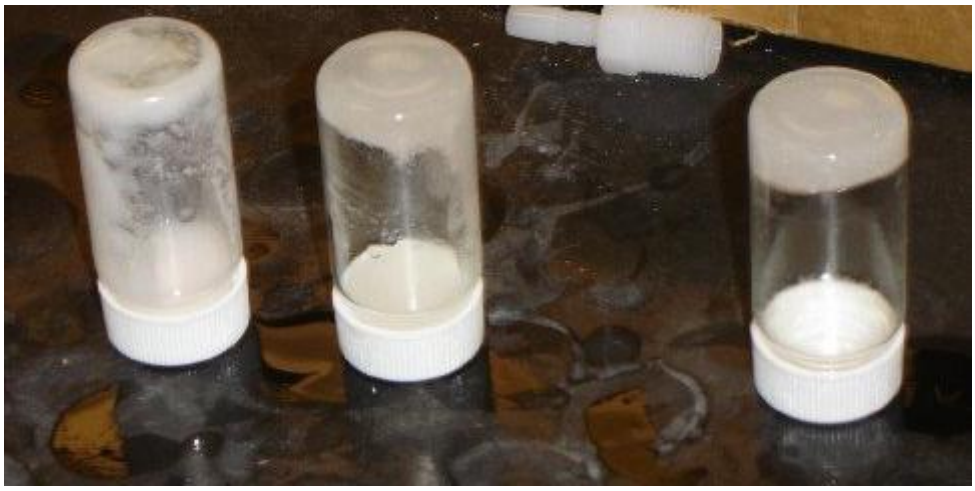

Figure 3.4: Pour point samples. The gel in the vial on the left was easily broken down upon inversion of the vial. The gel in the vial in the middle was not as easily broken down as the vial on the left but the solution was still able to flow. The gel in the vial on the right did not flow upon inversion, indicating that the solution is at or below its pour point.

Gel point temperature

The gel point was found using a TA 1000AR controlled stress rheometer. The solution is heated above the cloud point and held at this temperature to remove any thermal history. As the solution is cooled at a constant rate of 0.5 °C/min, an oscillatory stress of 0.1 Pa with a frequency of 0.1 Hz is being applied. The stress and frequency are kept relatively low in order to not disrupt the development of the gel. The storage modulus (G') and the loss modulus (G") are reported and as shown in Figure 3.2, the crossover point between G' and G" represents the gel point temperature.

Densitometer

A DMA 500 Density Meter with a measuring range of 0-3 g/mL, repeatability of $1x10^{-6}$ g/mL, a temperature accuracy of 0.001 °C and a temperature range of 0-90 °C was used to measure the density of the solutions. The solutions were cooled, starting at a temperature above the cloud point, at 2 °C/hr (0.033 °C/min) and the density was measured every 3 minutes. A change in density seen in addition to the relatively linear change in density caused by the reduction in temperature indicates a transition from liquid to solid. This phenomenon will be further discussed in the results section.

Microscopy

The solutions were examined using cross-polarized microscopy. The solutions were initially heated to a temperature far above its cloud point. The solution was held at a temperature for ten minutes and then cooled 0.5° C over one minute. An image was then taken to assess the degree of crystallization that occurred.

Pour Point and Cloud Point Studies

Before the effects of polydispersity and cocrystallization are addressed, the behavior of the gelation characteristics of single n-alkanes in solvent needs to be understood. Therefore, monodisperse systems of C_{28}, C_{32} and C_{36} were prepared in wax percents ranging from 2.5% to 12.5% and both the cloud point and pour point were prepared for each system. Systems below approximately 2 wax % did not form gels at temperatures below 0° C, indicating insufficient wax present for the crystals to interlock and form a volume spanning network needed to form a gel. Figure 3.5 shows the relationship between the pour point and the cloud point for these monodisperse systems.

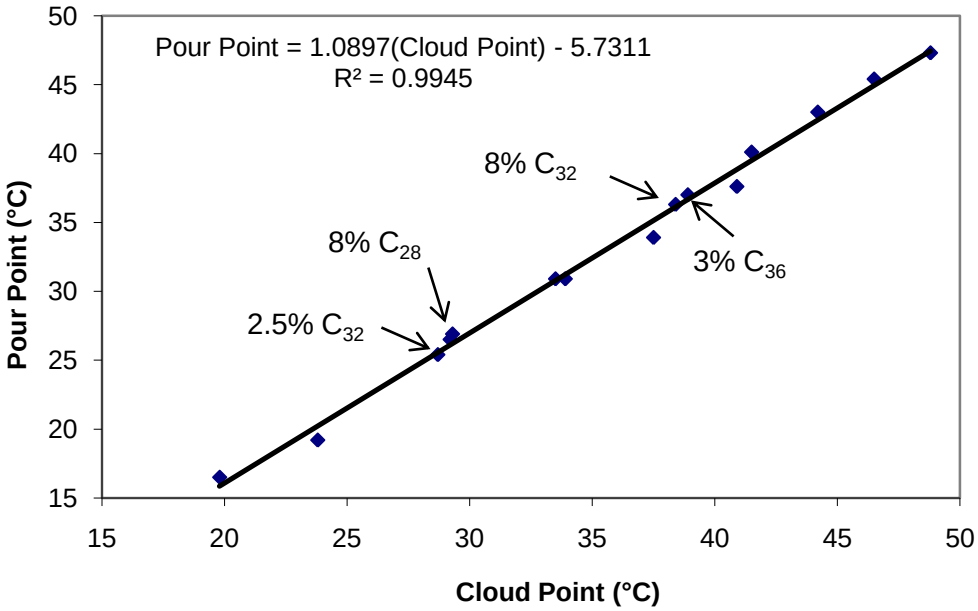

Figure 3.5: Relationship between the pour point and cloud point for monodisperse solutions of C_{28}, C_{32} and C_{36} in dodecane. Wax percents ranged from 2.5 to 12%.

Figure 3.5 shows that the pour point of the system of a monodisperse system can be predicted simply by knowing the cloud point of the system. Highlighted on the graph are systems that have much different wax percents, but have similar cloud points. In spite

of the wax content difference, the systems have similar pour points, further confirming the concept that only a fraction of the wax is necessary to form a gel. An interesting point to note here is that the slope is greater than one, indicating that the gap between the cloud point and pour point decreases as the cloud point is increases. Therefore, the difference between the pour point and the cloud point decreases when (1) the carbon number increases for a fixed wax percentage and (2) the wax percent increases for a given n-alkane. The first point can be explained by the fact that higher carbon numbers are longer molecules that will form longer, larger crystals and the larger the crystals are, the easier it is to form a volume spanning network. The second point can be explained by the fact that although only a portion of wax is needed to form a gel, more wax would facilitate in forming of a gel by more solid wax crystals being present to form a volume spanning network. Paso's work has shown that a supersaturation growth regime exists because of a crystallization lag caused by nucleation, causing a burst of crystals to be released once the nucleation lag has been overcome (Paso et al, 2005). Therefore, the higher the wax content, the more wax that is able to precipitate as the solution is cooling. A higher solid wax present in the solution makes it easier is to form a volume spanning network gel.

To determine if this linear relationship between cloud point and pour point would hold for polydisperse solutions, various solutions were prepared using a combination of C_{28}, C_{32} and C_{36}. All of the solutions were made such that the least soluble component was the highest carbon number alkane. These results can be seen on the left hand side of Figure 3.6.

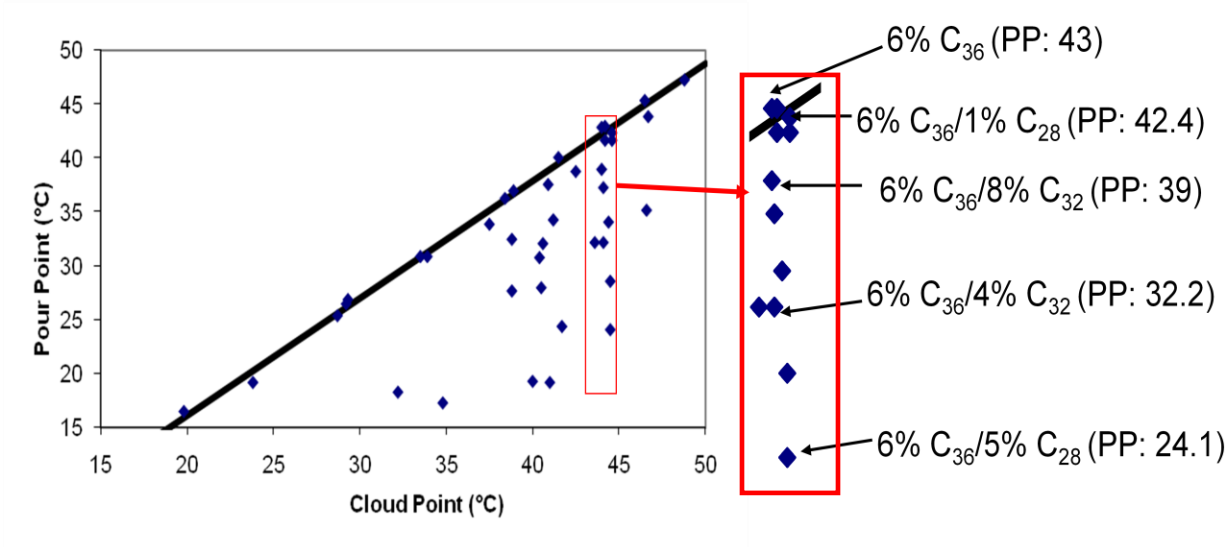

Figure 3.6: (left) Relationship between the pour point and cloud point for monodisperse and polydisperse systems. The line is the trendline from the monodisperse samples shown in Figure 5. (right) A blown-up portion of the graph on the left corresponding to a cloud point of about 44°C.

Figure 3.6 shows that the trendline created from the monodisperse results in Figure 3.5 represents an upper bound for a pour point at a particular cloud point. Additionally, the pour point of the solution can vary as much as 20°C for a given cloud point. The data points that fall on a relatively vertical line represent solutions that have the same percentage of the least soluble component present in the solution. Although adding a more soluble n-alkane will alter the solubility of the longer n-alkane by changing the mass ratio of the less soluble n-alkane to dodecane, the solvent, this change has little effect on the cloud point. Greater insight can be gained by analyzing the vertical columns, because the same amount of the less soluble n-alkane is present, but their pour points vary drastically by *adding* crystallizable n-alkanes Initially, this result appears counterintuitive because by adding more crystallizable components to a system, the amount of potential wax crystals that could form a volume spanning network has increased.

The right hand side of Figure 3.6 shows a vertical column corresponding to a cloud point of 44°C, which represents the cloud point for the family of solutions containing 6% C_{36}. As the data points are assessed, a peculiar trend is seen: the pour points for many of the solutions containing C_{36} and C_{32} are surrounded by the pour points of the solutions containing C_{36} and C_{28}. Additionally, it appears that there is no direct correlation between the wax percent of the shorter n-alkane and the pour point: from the data points explicitly shown on the right hand side of Figure 3.6, an increase in C_{28} concentration led to a sharp decrease in the pour point while an increase in C_{32} concentration led to an increase in the pour point. An important difference between C_{32} and C_{28} is how they crystallize with C_{36}. Chapter 2 showed that C_{32} cocrystallizes with C_{36} while C_{28} does not cocrystallize with C_{36}, primarily due to difference in molecular size. Figure 3.6 shows that both polydispersity and cocrystallization impact the gelation characteristics of a solution, but their impacts are vastly different.

Rheometric Studies

To gain greater insight into these impacts, two of the vertical lines in Figure 3.6 were further analyzed: the line at a cloud point of approximately 39° C corresponding to solutions containing 4% C_{36} and the vertical line shown in Figure 3.6 for 6% C_{36}, solutions with a cloud point around 44° C. For both cases, the C_{36} wax percent was held constant while the C_{28} and C_{32} were varied from 0 to 10% and both the pour point and gel point were measured. The results for the 4% C_{36} systems can be seen in Figure 3.7.

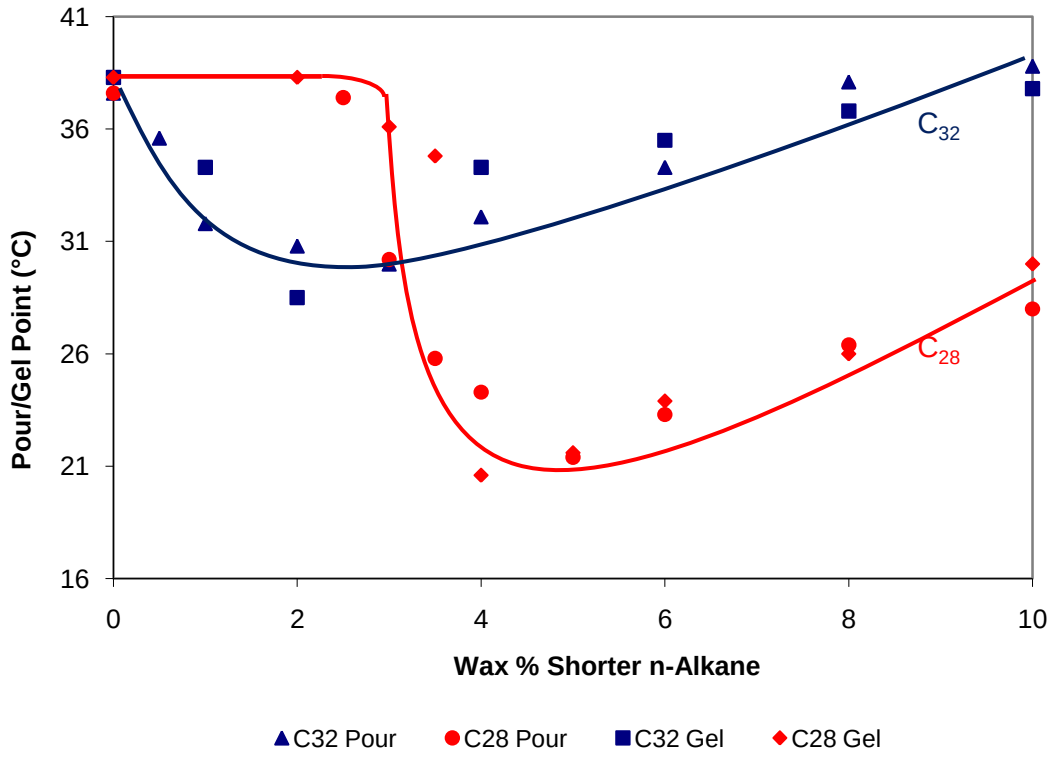

Figure 3.7: The effect of varying the wax percent of C_{28} and C_{32} on the gelation properties of 4% C_{36} solutions in dodecane. ▲and ● represent the pour points of the solutions containing C_{32} and C_{28} respectively and ■ and ♦ represent the gel points of the solutions containing C_{32} and C_{28} respectively.

Figure 3.7 shows that similar trends are seen for both the gel point and the pour point and that the temperatures for the gel points and the pour points for a particular solution are relatively similar. However, it must be noted that this occurrence is purely coincidental: if different cooling were used and/or if a different oscillatory stress were used for the gel point experiments, the values of the gel point and the pour point would change.

From Figure 5, it is clear that two distinct trends exist. First considering the C_{36}/C_{32} systems where cocrystallization occurs, it can be observed that adding a small amount of C_{32} causes a noticeable decrease in the pour point and gelation temperature. This decrease continues until around 3% C_{32}, wherea minimum is reached. As more C_{32}

is added, the pour point and gelation temperature both increase. However, it takes 10% of C_{32} in the system for the gel and pour points to reach the temperatures obtained for the monodisperse 4% C_{36} system. The trajectory of the curve can be explained by the fact that C_{36} and C_{32} cocrystallize. When two (or more) materials cocrystallize together, the crystal formation will not be as perfect as a single material forming a crystal structure because of the different size of the components as seen in Figure 3.3. The different chain lengths provide defects and weaknesses in the crystal structure, making it harder to form the large crystals that are more conducive to forming volume spanning network gels. Because cocrystallization reduces crystal size, a decrease in the ability of a gel to form is seen, even when a small amount of the cocrystallizable material is added. However, as the concentration of C_{32} is increased, the amount of material crystallizing out of solution will increase because more C_{32} will be available to cocrystallize with the C_{36}. At low C_{32} concentrations, a competing effect between the adding more wax crystals (more conducive to forming a gel) with the decrease in crystal size seen because of cocrystallization (less conducive to forming a gel) occurs. However, once the wax crystal size is unaffected by adding more C_{32} (at higher concentrations), the gel point and pour point will increase monotonically.

When the C_{36}/C_{28} systems are considered, a completely different trend is seen. At low concentrations (less than about 3%), the pour point and gel point are unaffected by the addition of C_{28}. However, when slightly more C_{28} is added, a sharp decrease in the pour point and gelation temperature is seen with an approximately 15 °C change when the C_{28} concentration is raised 3% to 5%. Once more C_{28} is added, an increase in the pour point and gel point of the system similar to the trajectory for the C_{32} system is seen. To

explain this trend, recall that C_{36} and C_{28} do not cocrystallize together and that the solubility of 4% C_{36} and the mass percents of C_{28} examined in Figure 3.7 are drastically different. Therefore, most of the C_{36} will precipitate before any C_{28} will crystallize out of solution. At low concentrations, insufficient C_{28} is present to disrupt the C_{36} crystallization so C_{36} is crystallizing without recognizing the presence of C_{28} and thus the gel point and the pour point are unchanged. However, once C_{28} is added in sufficient amounts, it disrupts the formation of the C_{36} gel even though C_{28} has not crystallized. This fact that the gelation is dependent on C_{28} is accentuated when the pour points of monodisperse C_{28} solution are compared to the pour and gel points of the C_{36}/C_{28} systems as shown in Figure 3.8. Figure 3.8 shows that the pour points of the C_{36}/C_{28} systems for higher wax percents of C_{28} are the same as the pour points for the corresponding monodisperse C_{28} systems. This result shows that these systems will not gel until the shorter chained, more soluble n-alkane has sufficiently crystallized. From this result, it appears that the C_{28} molecules are disrupting the formation of the gel structure by getting in between the C_{36} crystals and preventing them from aggregating with one another and inhibiting their ability to form a volume spanning network. In other words, the C_{36} molecules are associating with the C_{28} molecules via van der Waal forces, preventing the C_{36} molecules from forming large crystals.

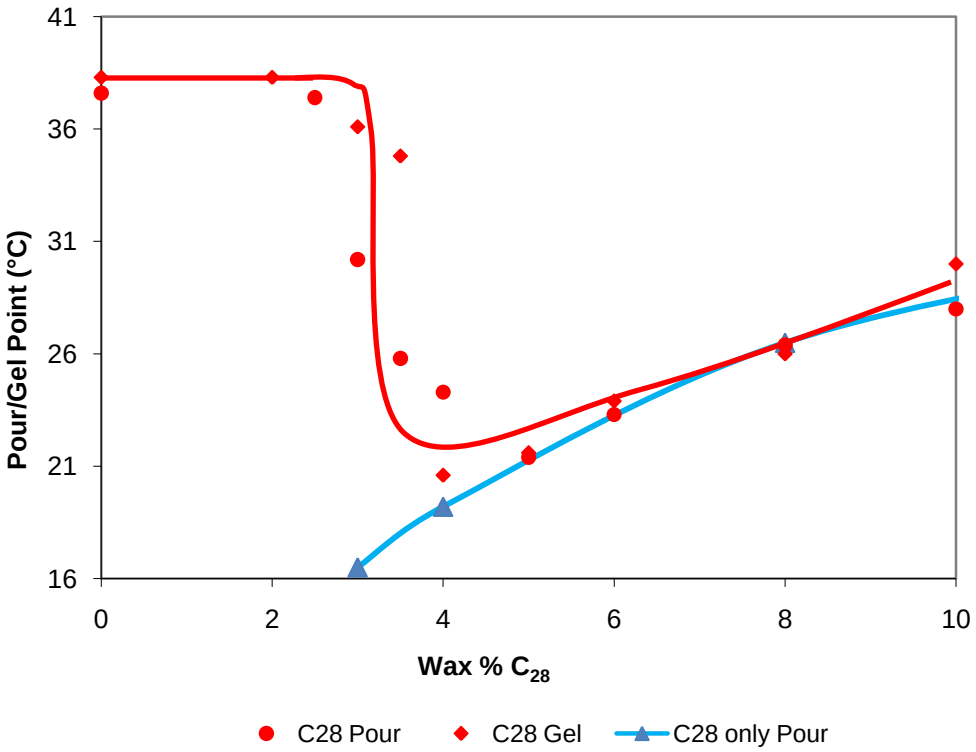

Figure 3.8: A comparison of the gelation properties of 4% C_{36}/ x% C_{28} solutions in dodecane and x% C_{28} solutions. ● and ♦ are unchanged from Figure 3.7. ▲ represents the pour points for the monodisperse C_{28} solutions in dodecane.

Cross-Polarized Microscopy Studies

To assess this conclusion, cross-polarized microscopy experiments were carried out and images were taken as the temperature was lowered. Figure 3.9 shows the microscope images for the monodisperse 4% C_{36} base case. At temperatures above the cloud point (Figure 3.9a)), the microscopy image will not show anything. However, when the cloud point is reached (Figure 3.9b)), the formation of very large crystals in a lamellar sheet formation can be seen, conducive to forming a gel. These lamellar sheets are consistent with what is seen in systems of n-alkanes crystallizing in n-alkane or many other organic solvents. Therefore, the cloud point and the gel point for this system would be close together, a result seen in Figures 3.5 and 3.6. As the temperature is cooled

(Figure 3.9c)), the crystal images remain virtually unchanged except for some crystal growth because small amounts of C_{36} that will crystallize out of solution as the solution is further cooled because the solubility of C_{36} is reduced as the temperature is lowered.

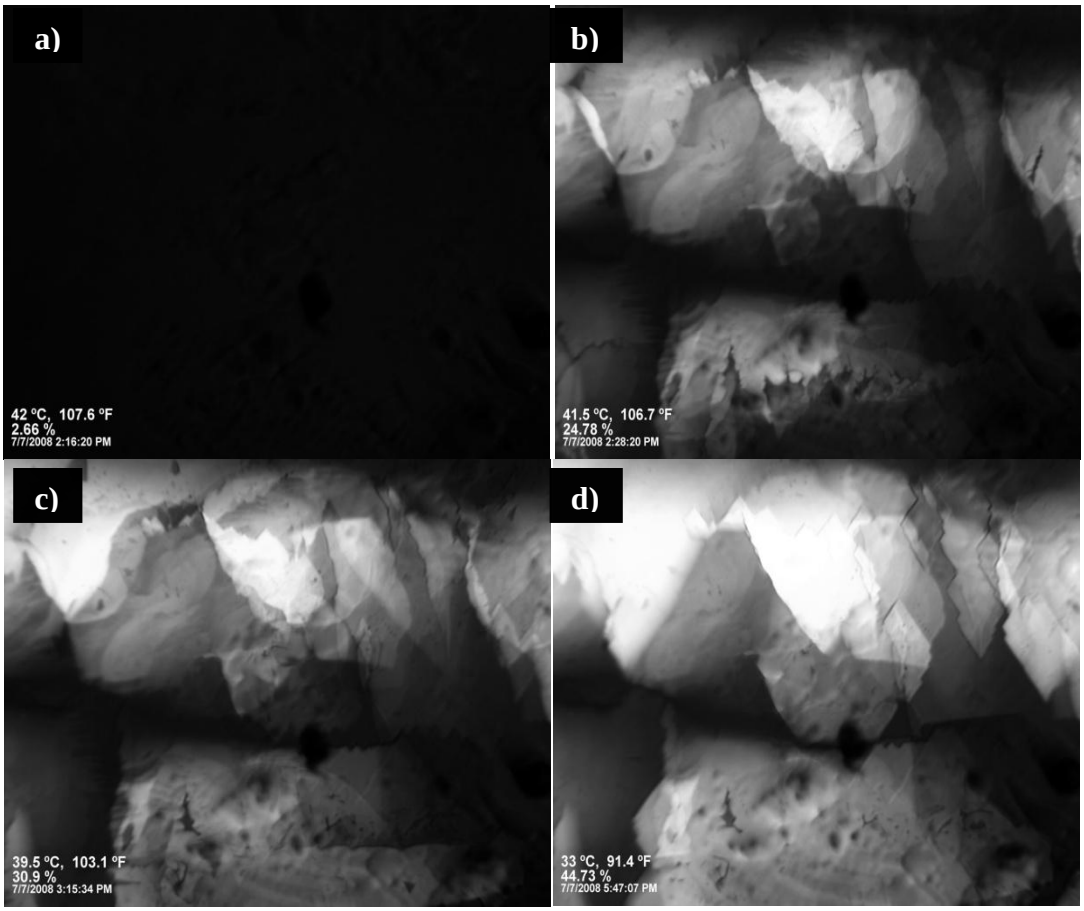

Figure 3.9: Cross-polarized microscopy images for a slowly cooled 4% C_{36} solution. The temperatures of the respective micrographs are 42° C for a), 41.5° C for b), 39.5° C for c) and 33° C for d).

Figure 3.10 shows microscopy images from the systems where 2% C_{28} is added to the 4% C_{36} system, which is on the level part of the 4% C_{36}/C_{28} gelation curve in Figure 3.7. The images (Figures 3.10a) and 3.10b)) are relatively unchanged in comparison with the images seen in Figure 3.9. This result confirms the results in Figure 3.7 that the gelation characteristics of the 4% C_{36} and the 4% C_{36}/2% C_{28} systems are very similar. The only difference seen in the micrographs occurs at a much lower

temperature (16.5° C, Figure 3.10c)), where C_{28} will begin to crystallize out because of its solubility in dodecane. As the solution is further cooled, an increase in the number and particularly the size of crystals occurs (Figure 3.10d)). These events occur primarily on the lamellar C_{36} sheets because of heterogeneous nucleation.

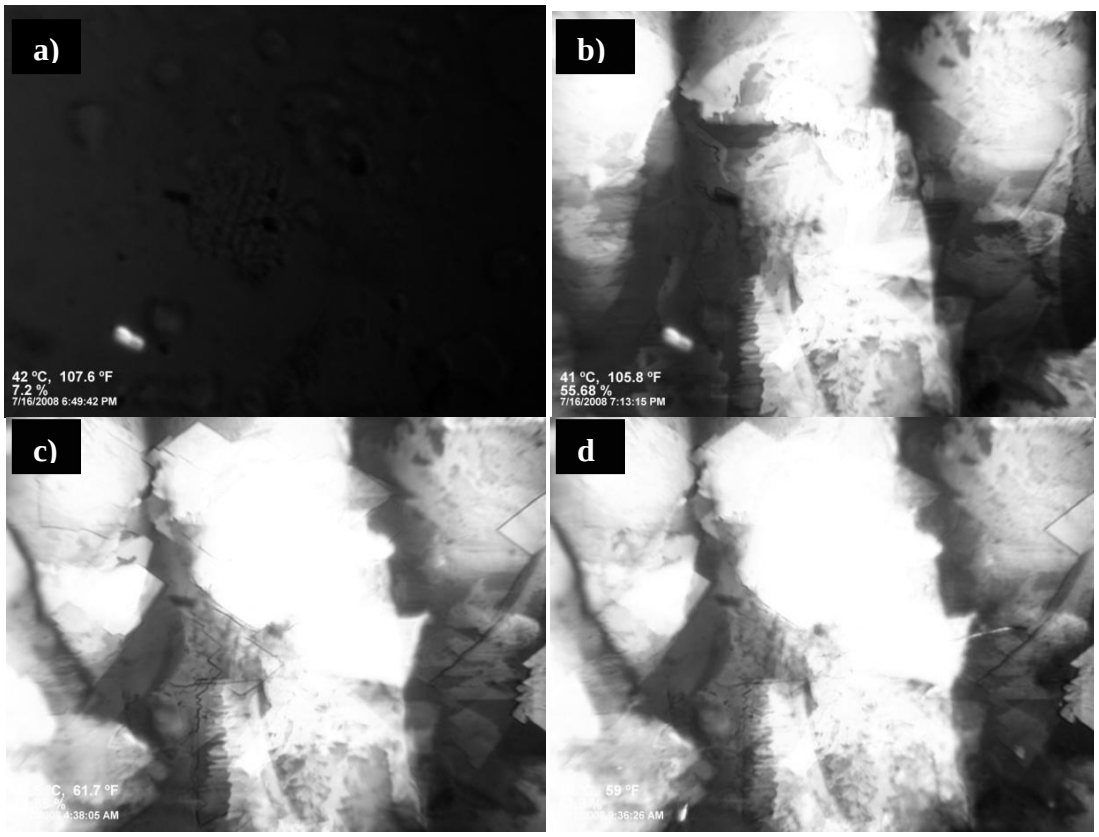

Figure 3.10: Cross-polarized microscopy images for a slowly cooled 4% C_{36}/2% C_{28} solution. The temperatures of the respective micrographs are 42° C for a), 41° C for b), 16.5° C for c) and 15° C for d). (Note: the white speck seen in the bottom left corner of the two images on the top are not wax and do not affect crystal formation.)

Figure 3.11 shows the microscopic images for the 4% C_{36}/5% C_{28} solution, the bottom of the valley in the C_{36}/C_{28} curve developed in Figure 3.7. It is evident that the images shown in Figure 3.11 are far different from the ones seen in Figures 3.9 and 3.10. Instead of the lamellar sheets at temperatures right around the cloud point (see Figures 3.8b) and 3.9b)), the 4% C_{36}/5% C_{28} solution (Figure 3.11b)) has fewer, smaller crystals present, insufficient for a gel to from. This image is continuously seen (intermediate

images shown in the Appendices) under the microscope for temperatures between 41° C and 25° C. At 25° C (Figure 3.11c)), a sudden burst of crystals can be seen, representing C_{28} crystals that have reached their solubility limit and are ready to precipitate. Once the C_{28} crystals precipitate (Figure 3.11c)), the crystals begin to agglomerate together. As the solution is further cooled (Figure 3.11d)), a few more crystals appear and there is some crystal growth, indicating an overall strengthening of the gel. Figure 3.11 confirms the result presented in Figure 3.8 that the gelation properties of the system become dependent on C_{28} once sufficient C_{28} has been added to the system.

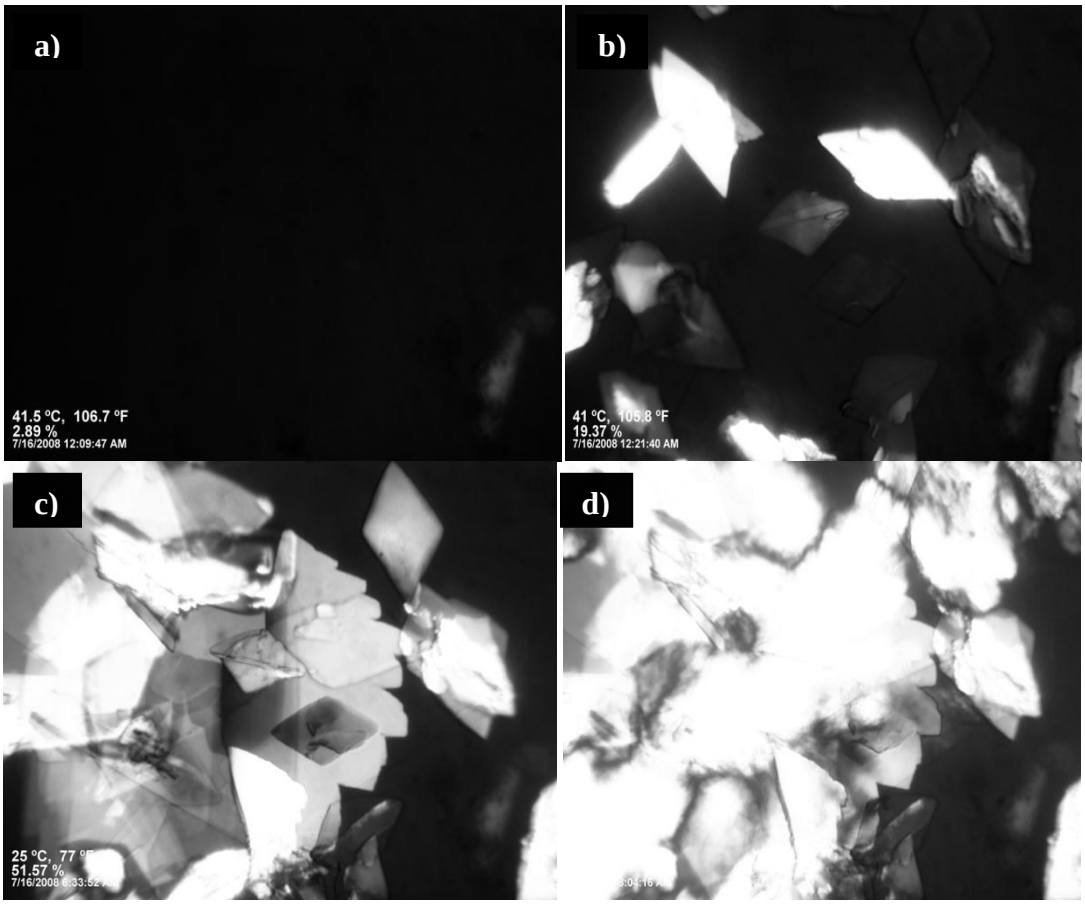

Figure 3.11: Cross-polarized microscopy images for a slowly cooled 4% C_{36}/5% C_{28} solution. The temperatures of the respective micrographs are 41.5° C for a), 41° C for b), 25° C for c) and 21° C for d).

Figure 3.12 shows the microscopic images for the 4% C_{36}/8% C_{28} systems. The images in Figure 3.12 are similar to the ones seen in Figure 3.11. The only major difference is the temperature where the burst of crystals is first visible shifts from 25° C for the system containing 5% C_{28}, (Figure 3.11c)) to 29° C for the system containing 8% C_{28} (Figure 3.12c)). This difference occurs because the solubility limit of C_{28} is lower for the system containing 8% C_{28} than the system containing 5% C_{28}. Figure 3.12 further confirms the results seen in Figure 3.8 showing that the gelation characteristics become dependent on C_{28} concentration, causing an increase in the gel and pour points will increase with increasing C_{28} concentration at sufficiently high C_{28} concentrations.

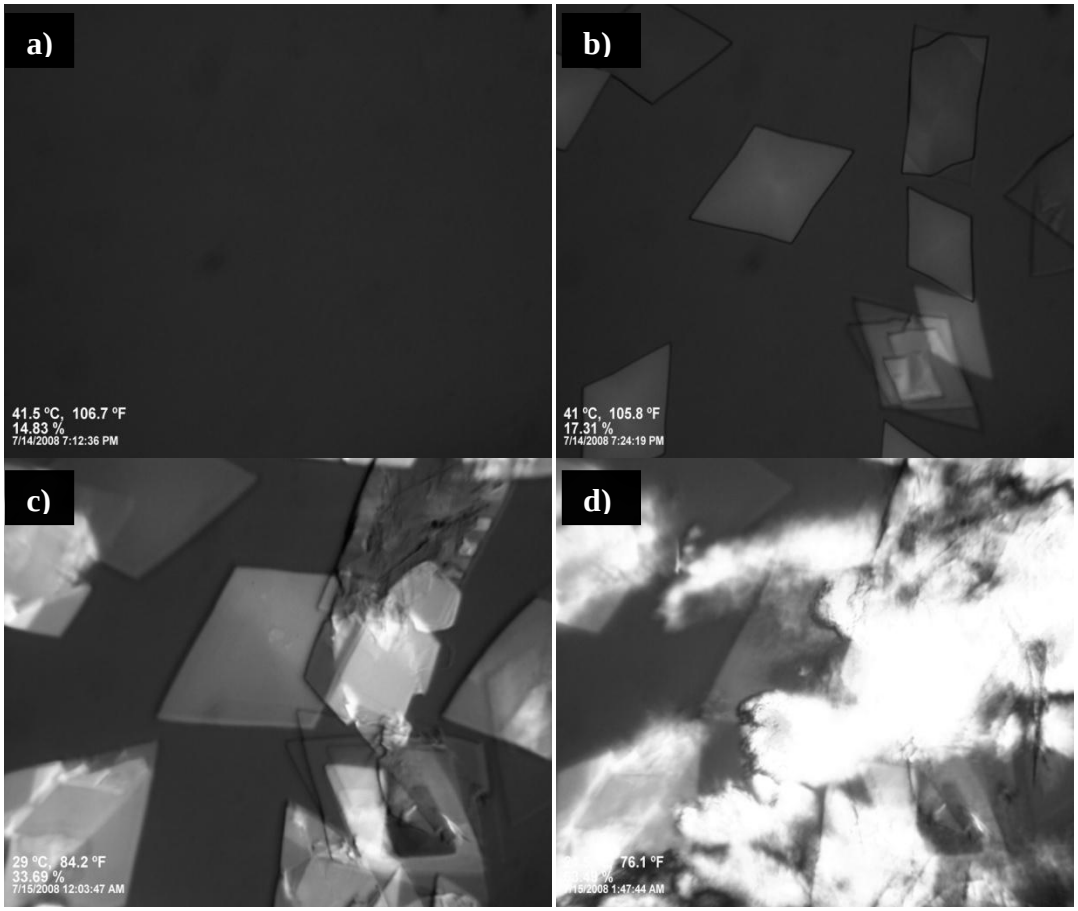

Figure 3.12: Cross-polarized microscopy images for a slowly cooled 4% C_{36}/8% C_{28} solution. The temperatures of the respective micrographs are 41.5° C for a), 41° C for b), 29° C for c) and 25° C for d).

Figure 3.13 shows the results for three C_{36}/C_{28} systems using the densitometer. As the system is cooled, the density of the system will increase. However, when a phase change occurs, the density will increase at a larger rate. Therefore, the slope of the density curve will be greater at temperatures when part of the solution is changing from liquid to solid. Figure 3.13 confirms that (a) C_{36} and C_{28} independently crystallize because of the presence of two densitometer peaks, (b) the location of the C_{28} peak shifts to higher temperatures as the wax % of C_{36} increases and (c) the temperatures at which the bursts of C_{28} crystallization were seen using microscopy were reasonable taking into account the facts that different methods will vary based on the methodology used and that the cooling rates used were different.

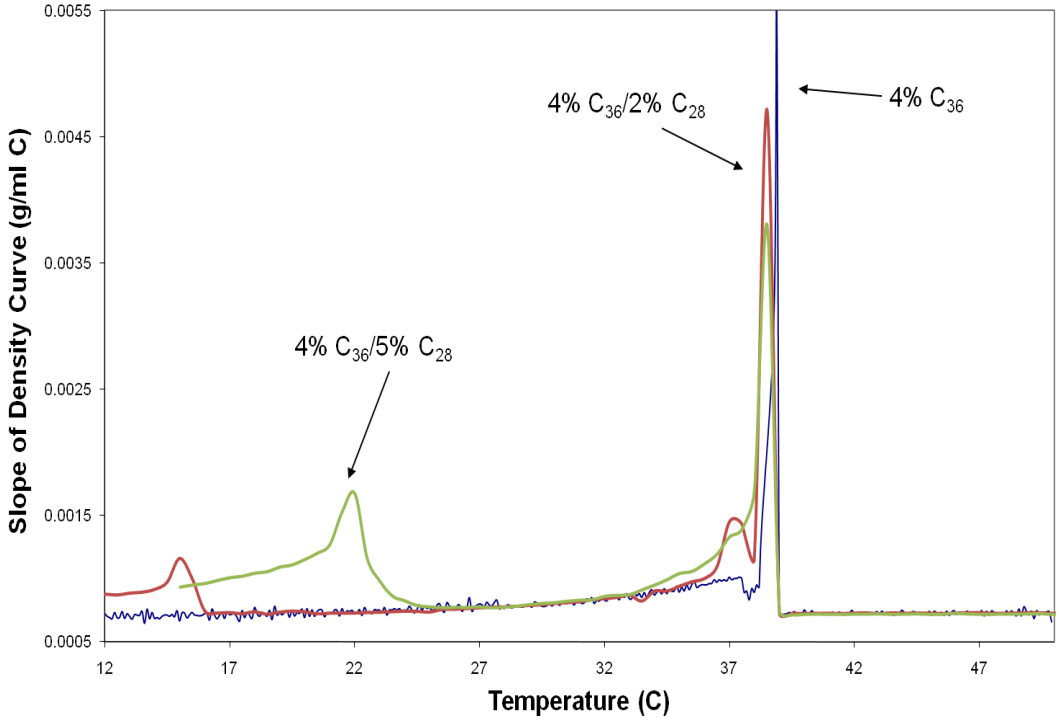

Figure 3.13: Densitometer results for varying C_{28} concentrations in 4% C_{36} in dodecane solutions.

A similar analysis for the C_{36}/C_{32} systems can be completed. Figure 3.14 provides microscopic images for the 4% C_{32}/3% C_{32} system. Unlike the 4% C_{32}/2% C_{28} system (Figure 3.10b)), the crystal morphology at the cloud point is significantly modified and lamellar sheets are not seen (Figure 3.14b)). Instead, large crystals that lack a well defined shape are seen, contrary to the C_{36}/high mass % C_{28} systems that contain smaller crystals with a well defined shape (Figures 3.11b) and 3.12b)). As the solution is further cooled (Figures 3.14c) and 3.14d)), more large crystals begin to appear, making it possible for a gel to form. The presence of C_{32} interferes with the ability of 4% C_{32} to form a gel by cocrystallizing and hampering the ability to form long crystals.

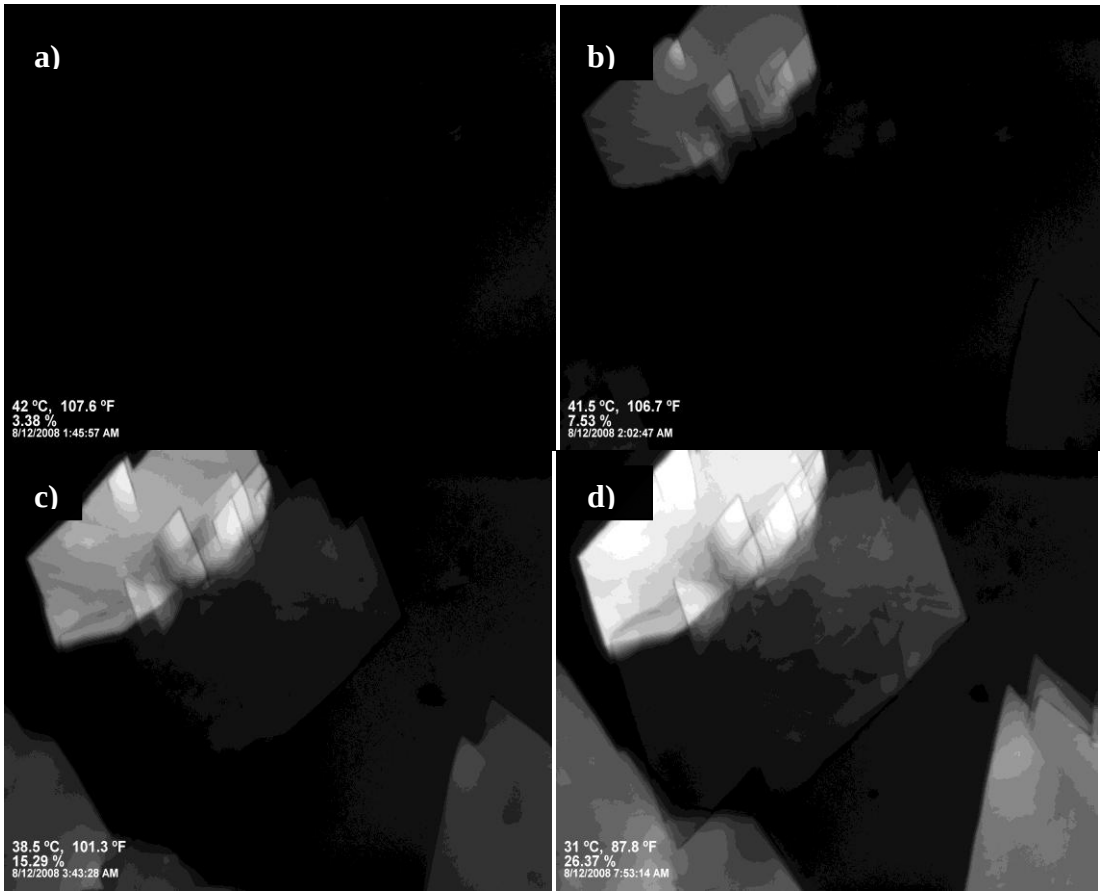

Figure 3.14: Cross-polarized microscopy images for a slowly cooled 4% C_{36}/3% C_{32} solution. The temperatures of the respective micrographs are 42° C for a), 41.5° C for b), 38.5° C for c) and 31° C for d).

Figure 3.15 shows microscopic images for the 4% C_{36}/6% C_{32} system. As the amount of C_{32} is increased, that the crystal size has decreased but the number of crystals present has increased. Although the crystals are initially too small and separated to form a volume spanning network, the crystals will grow and more crystals will form, enabling the formation of the gel at a temperature higher than the one for the system containing 3% C_{32}.

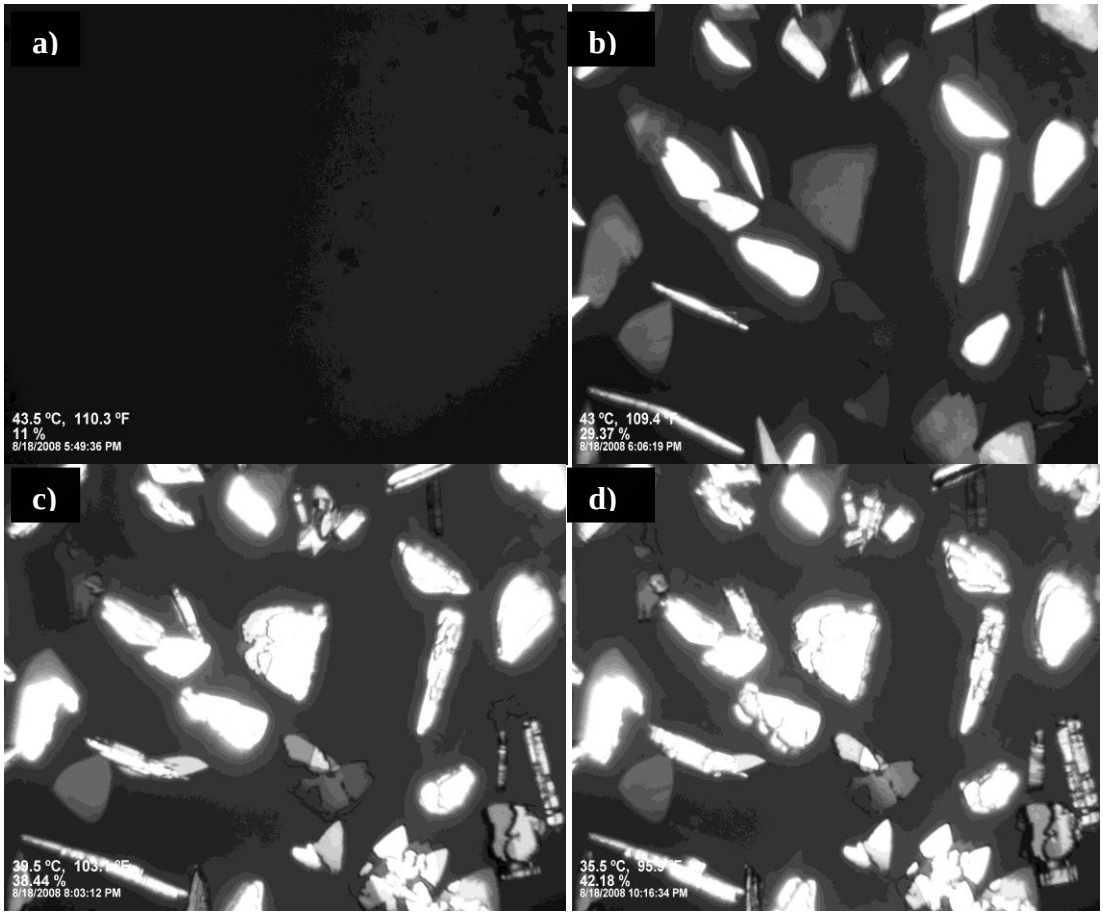

Figure 3.15: Cross-polarized microscopy images for a slowly cooled 4% C_{36}/6% C_{32} solution. The temperatures of the respective micrographs are 43.5° C for a), 43° C for b), 39.5° C for c) and 35.5° C for d).

Figure 3.16 shows the densitometer results for the 4% C_{36}/C_{32} solutions analyzed using microscopy along with the base case of 4% C_{36}. The densitometer results confirm that cocrystallization is occurring in these systems by the presence of one sharp

densitometer peak. If cocrystallization were not occurring, C_{32} would precipitate by itself at a temperature approximately 5 degrees lower than C_{36}. Additionally, the increase in C_{32} leads to an increase in the slope of the density curve at intermediate temperatures (between 20 and 38° C), which indicates that although a large amount of C_{32} will cocrystallize with C_{36}, all of it will not cocrystallize.

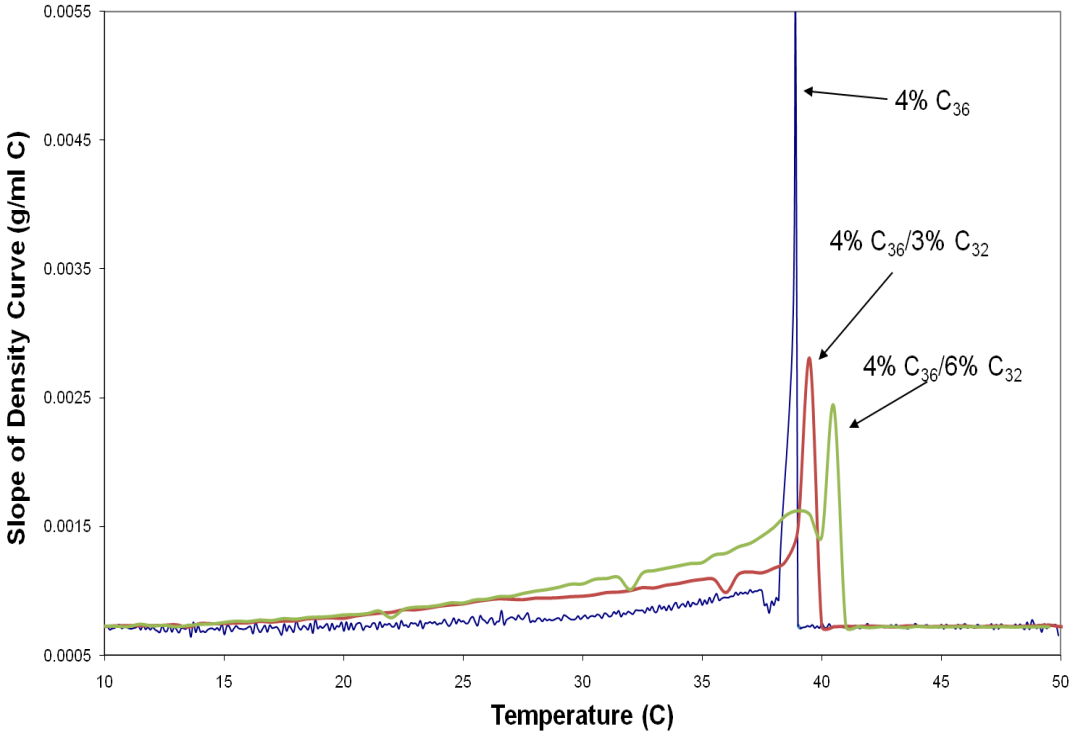

Figure 3.16: Densitometer results for varying C_{32} concentrations in 4% C_{36} in dodecane solutions.

Extensions to Other n-Alkane Systems

Although these results show that cocrystallization and polydispersity greatly influence the properties the gelation properties of the system, it is important to determine the universality of these results. Consequently, the effect of wax percent of C_{36} was analyzed with the wax percent of C_{36} increased from 4% to 6%. Figure 3.17 shows the

gel point and pour point results for systems containing 6% C_{36} and various amounts of C_{32} and C_{28}. Comparing Figure 3.17 (6% C_{36}) to Figure 3.7 (4% C_{36}), similar trends are observed, but a few differences do exist. One difference is that although the difference between the minimum and maximum pour/gel point temperature for the C_{32} containing systems is about 8° C, the location of the minimum has shifted to a higher C_{32} concentration. This result can be explained by the fact that more C_{32} is needed to cocrystallize with 6% C_{36} than 4% C_{36} to see the same effects on the crystal structure.

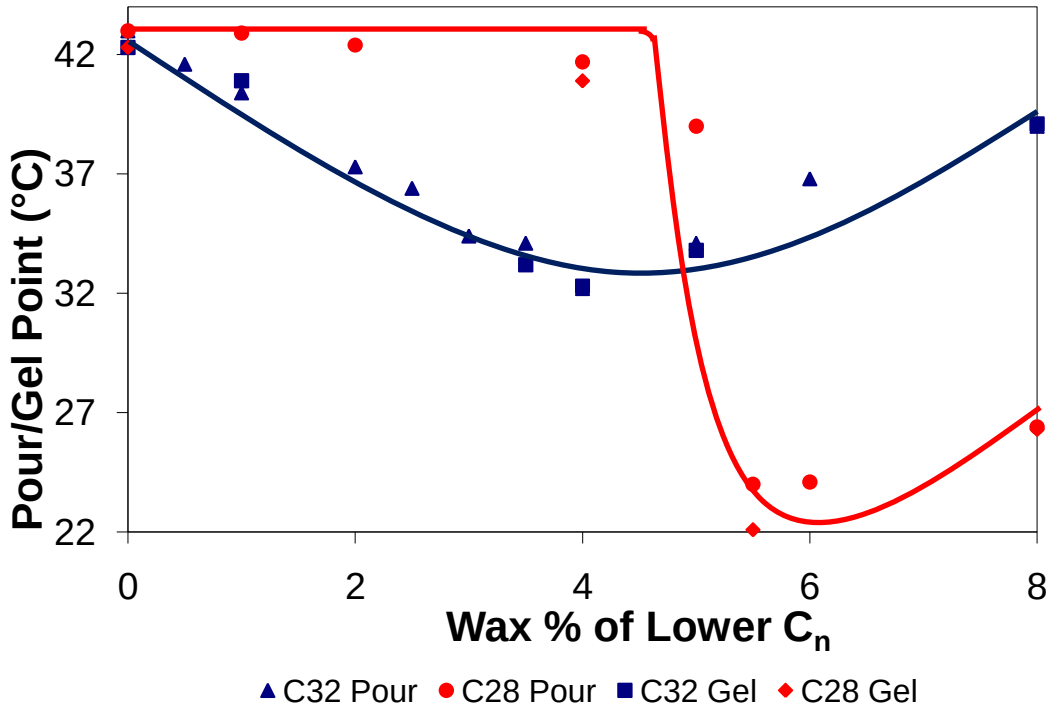

Figure 3.17: The effect of varying the wax percent of C_{28} and C_{32} on the gelation properties of 6% C_{36} solutions in dodecane. ▲and ● represent the pour points of the solutions containing C_{32} and C_{28} respectively and ■ and ♦ represent the gel points of the solutions containing C_{32} and C_{28} respectively.

Similarly, the shifting C_{28} curve occurs because more C_{28} is needed to prevent the larger amount of C_{36} molecules in the 6% C_{36} trials from interacting with one another to form a gel. This shift creates a longer plateau region for the 6% C_{36} systems (approximately

4.5%) than the 4% C_{36} systems (approximately 2.5%). Therefore, the amount of the less soluble n-alkane only shifts the concentration at which the phenomena occur, but does not change the phenomena, namely (1) that the addition of a small amount of C_{32} causes a decrease in the pour point, (2) a threshold concentration of C_{28} is needed before it impacts the gel and (3) once the threshold concentration has been reached, a drastic decrease in the gel and pour points can be seen and these temperatures are dependent on C_{28} and not C_{36}.

Another way to explore the universality of the results is to change the most soluble n-alkane in the system by using C_{32} as the longest n-alkane. Experiments were carried out using C_{28} (a carbon number difference of four, same as C_{36}/C_{32}), C_{24} (a carbon number difference of eight, same as C_{36}/C_{28}) and C_{30} (a carbon number difference of two). C_{32} cocrystallizes with both C_{30} and C_{28}, but not with C_{24}. Figure 3.18 shows the results of the experiments where cocrystallization occurs. The trend for the C_{32}/C_{28} system matches well with its corollary, the C_{36}/C_{32} system (see Figure 5) where adding a small amount of the shorter alkane will cause a decrease in the gel point and pour point. Further, both curves reach a minimum and then increase because of the changing of solubility limits and an increase in the number of crystals present as the wax percent of the shorter chained n-alkane increases.

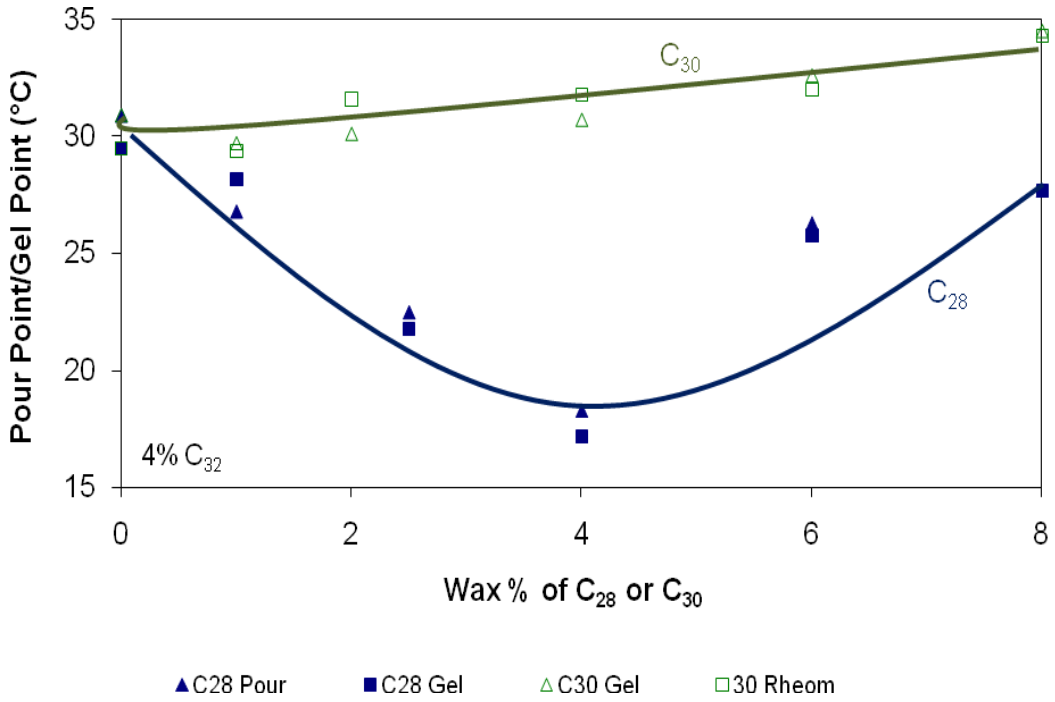

Figure 3.18: The effect of varying the wax percent of C_{28} and C_{30} on the gelation properties of 4% C_{32} solutions in dodecane. ▲ and Δ represent the pour points of the solutions containing C_{28} and C_{30} while ■ and □ represent the gel points of the solutions containing C_{28} and C_{30}.

Although the C_{32}/C_{28} and C_{36}/C_{32} systems have similar gelation curves, the C_{32}/C_{30} gelation curve is drastically different with the C_{32}/C_{30} systems having an increase in the pour and gel points as the wax percent of C_{30} is increased. This result can be explained by considering the differences in molecular size and solubility between C_{30} and C_{28}. Because the size of C_{30} is closer to C_{32} than C_{28} is, a smaller amount of the C_{32} molecule will need to bend to accommodate C_{30} than C_{28}. The sizes of C_{32} and C_{30} could be sufficiently close enough such that the C_{32} crystal would not need to bend in order to accommodate C_{30}, reducing the vulnerable points of the crystal structure, making it easier for sustained crystal aggregation to occur, conducive to the formation of a gel.

The solubility difference is important mainly because the carbon number difference between C_{30} and C_{32} is very small, they have similar solubility characteristics in dodecane.

In the C_{36}/C_{32} and C_{32}/C_{28} systems, a mass percent of around 8 to 10% is needed before the solubility limit is affected. However, with a smaller carbon number difference, much less C_{30} is needed to alter the system solubility. The effect of C_{30} concentration on the solubility limit is shown in Figure 3.19, which shows that the cloud point increases by a few degrees as the C_{30} concentration increases. However, the pour point initially decreases slightly at low wax percents of C_{30} as a result of the formation of cocrystals. As the wax percent of C_{30} increases, the slight changes in crystal structure that would lead to a reduction in the pour point temperature is overwhelmed by a decrease in solubility, which allows for the gelation process to begin at a higher temperature. Because the cocrystals sufficiently resemble the C_{32} crystal structure, the C_{32}/C_{30} results will act similarly to a monodisperse system with the gap between the pour point and the cloud point decreasing as the cloud point increases, a trend previously shown in Figure 3.5.

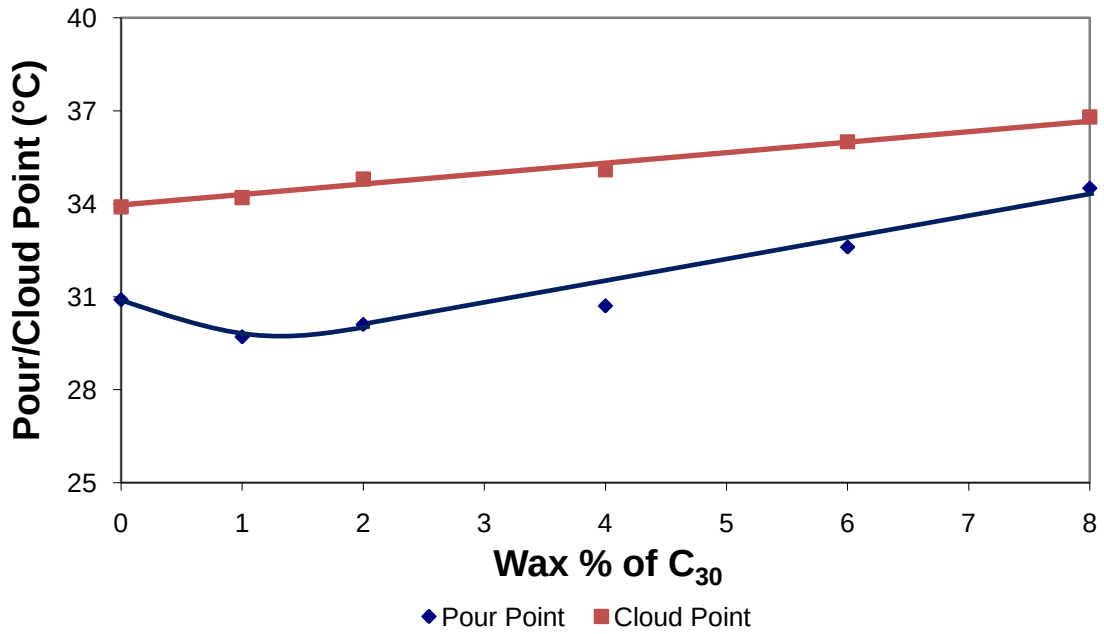

Figure 3.19: The effect of varying the wax percent of C_{30} on the pour point and the cloud point of 4% C_{32} solutions in dodecane. ♦ and ■ represent the pour point and cloud point of the 4% C_{32}/C_{30} solutions respectively.

Figure 3.20 shows the results for the C_{32}/C_{24} system where cocrystallization does not occur. These results are drastically different from its corollary, the C_{36}/C_{28} system. Instead of a plateau at low concentrations followed by a sharp decrease where the gelation properties become dependent on the shorter n-alkane at higher concentrations, a relatively flat trend is seen with a slight decrease in the gel and pour point temperatures. Although there appears to be a difference, a major reason why C_{28} influences the gelation of C_{36} is because of its molecular size, large enough to disrupt the C_{36}. For example, the solvent (dodecane) is insufficiently large enough to disrupt the crystal structure. If C_{24} is also too small, it will not influence the crystal structure and not impact C_{36} gelation. To test this hypothesis, systems of 4% C_{36}/C_{24} were analyzed and these results are also shown in Figure 3.20.

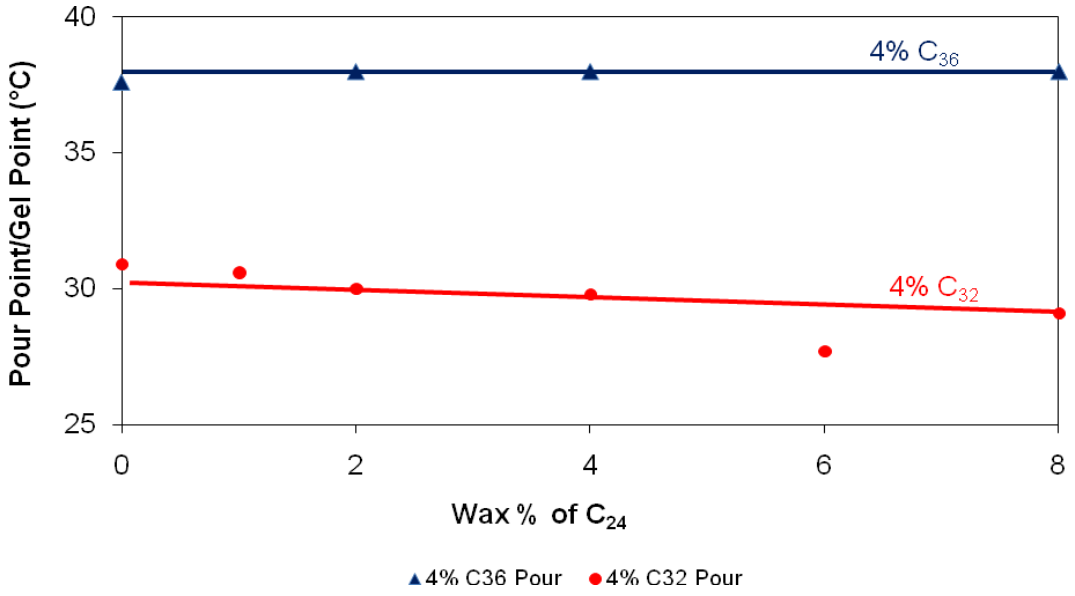

Figure 3.20: The effect of varying the wax percent of C_{24} on the pour point of 4% C_{36} and 4% C_{32} solutions in dodecane. ▲and ● represent the pour points of the solutions containing C_{36} and C_{32} respectively.

Figure 3.20 shows that C_{24} has no effect on the gelation properties of C_{36}, showing that C_{24} is too small to affect the crystallization of C_{36} and instead acts like the solvent. This

result confirms that in order for a non-crystallizable n-alkane to impact the crystallization of an n-alkane, a steric requirement exists.

The exploration of role of odd carbon numbers on gelation was also conducted. The systems where no cocrystallization occurred will initially be analyzed. Four systems were studied: C_{36}/C_{28}, C_{36}/C_{27}, C_{35}/C_{27} and C_{35}/C_{28}. The results of these experiments are presented in Figure 3.21, which shows that the trends are not greatly impacted by whether the carbon number is even or odd. An initial difference of about 1° C is seen between the C_{36} systems and the C_{35} systems because C_{36} is less soluble than C_{35} in dodecane. Once the wax concentration of the lower carbon number is sufficiently high, the large drop in the pour point is seen and the two graphs collapse onto one another, an expected result because at higher concentrations of C_{28}, the pour point is dictated by C_{28} and not the longer n-alkane. A point to note is that the minimum for the C_{27} systems is shifted to higher concentrations when compared to the C_{28} systems, a result that can be explained by the fact that C_{28} is a larger molecule so less is required to interfere with the formation of a gel.

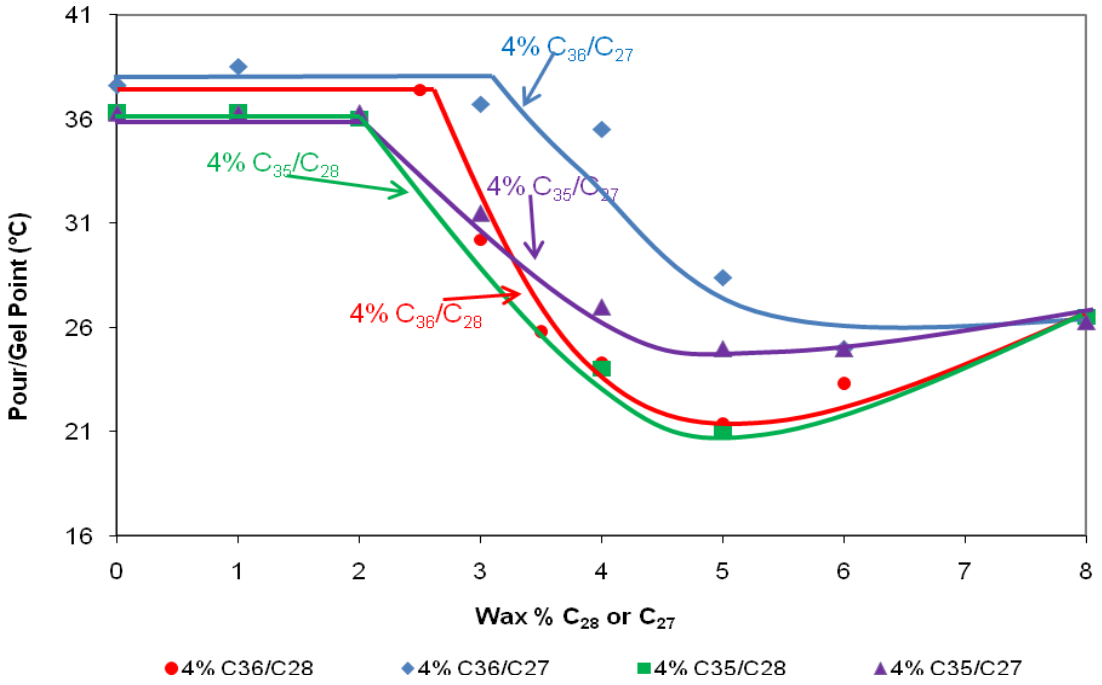

Figure 3.21: The effect of varying the wax percent of C_{28} and C_{27} on the pour point of 4% C_{36} and 4% C_{35} solutions in dodecane. ●, ♦, ■ and ▲ represent the pour points of the solutions containing 4% C_{36}/C_{28}, 4% C_{36}/C_{27}, 4% C_{35}/C_{28} and 4% C_{35}/C_{27} respectively.

Figure 3.21 shows that the gelation properties are not impacted by whether the carbon number is even or odd. For the systems containing C_{28} as the shorter n-alkane, there is an initial difference of about 1° C solely based on the fact that C_{36} is less soluble than C_{35} in dodecane. However, once the C_{28} wax concentration is sufficiently high, the drastic difference in the pour point is seen and the two graphs collapse onto one another, which is expected because at the higher concentrations of C_{28}, the pour point is dictated by C_{28} and not the longer n-alkane. A similar result is seen when comparing the two systems that both contain C_{27} at the more soluble n-alkane. A point to note is that the minimum for the C_{27} systems are shifted to higher concentrations when compared to the C_{28} systems, a result that can be explained by the fact that C_{28} is a larger molecule so therefore less of it would be required to interfere with the formation of a gel.

Finally, the effect of odd/even carbon will be looked at for systems where cocrystallization occurs. To observe this effect, 4% C_{36} and 4% C_{35} systems with a range of C_{32} concentrations were analyzed. It is important to note that C_{35} and C_{32} will not cocrystallize because odd carbon number n-alkanes and even carbon number n-alkanes will not crystallize out for these molecular sizes because odd and even carbon number alkanes crystallize in different morphologies (Turner, 1971). The results of this work are seen in Figure 18, which confirms that C_{35} and C_{32} will not cocrystallize with one another because no reduction in the pour point is seen. C_{32} will thus act as a non cocrystallizable material and affect the C_{35} crystallization if present in sufficient amounts.

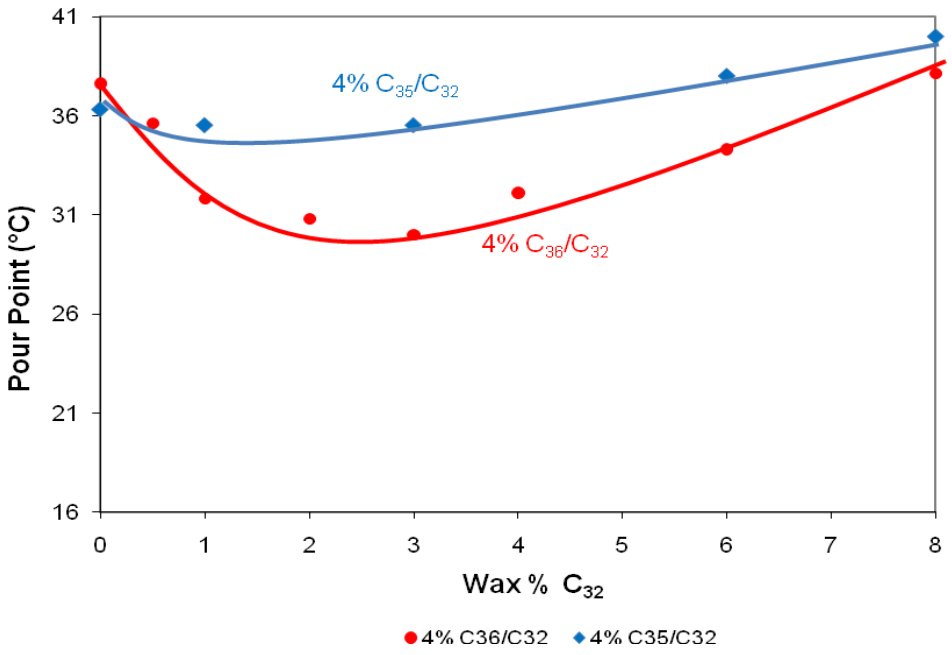

Figure 3.22: The effect of varying the wax percent of C_{32} on the pour point of 4% C_{36} and 4% C_{35} solutions in dodecane. ●, ♦ represent the pour points of the solutions containing 4% C_{36}/C_{32} and 4% C_{35}/C_{32} respectively.

However, because the solubility of C_{35} and C_{32} are not extremely different from one another, a significant drop is not seen. C_{35} and C_{32} will instead crystallize independently and precipitate out of solution. Although C_{35} and C_{32} are unable to cocrystallize, the

crystals from C_{35} and C_{32} interlock with one another to form a gel. Therefore, the presence of both materials will not hinder but in fact accelerate the formation of a gel.

Summary

This work has provided a thorough examination of how cocrystallization and polydispersity can greatly impact the gelation characteristics of an n-alkane crystallizing out in an n-alkane solvent. For a given wax percent of a long chained n-alkane, both polydispersity and cocrystallization actually *weaken* the gel in spite of the fact that more crystallizable wax is present in solution. Decreases in the pour point and gel point of as much as 20° C were seen for the solutions analyzed.

For systems where cocrystallization occurs, the addition of only a small amount (0.5 mass %) of a more soluble n-alkane reduces the gel and pour points. This reduction is caused by the more soluble n-alkane joining the crystal structure of the less soluble n-alkane, causing the formation of weak points in the crystal structure. These weak points are a result of the longer n-alkane must contort to allow for the shorter n-alkane to be incorporated the crystal structure. These defects result in smaller crystal aggregates being formed, thereby inhibiting the formation of a gel, a result shown in microscopy. The magnitude of this effect is lowered as the carbon number difference between the materials entering the cocrystal decreases because these form a more "ideal" cocrystal that contains less of these defects.

For systems where cocrystallization does not occur, a threshold concentration of the shorter n-alkane is required before the gelation characteristics are affected. For amounts below this threshold concentration, the longer n-alkane will crystallize without

recognizing the presence of the shorter crystallizable n-alkane. In other words, the shorter n-alkane is no different from the solvent. However, as the concentration of the shorter n-alkane is increased, the shorter n-alkane molecules still in the liquid phase associate near the longer n-alkane molecules and provide a steric barricade for the crystals to crystallize out together and form very large aggregates. This result has been confirmed by microscopy, where the crystal system changes from lamellar sheets to single crystals that are incapable of forming a volume spanning network gel initially. This hindrance is so strong that these systems are unable to form a gel until the shorter n-alkane is capable of forming a volume spanning network, causing a dramatic drop in the pour and gel point at the threshold concentration . However, because this mechanism is driven in part by molecular size, the molecules need to be a sufficient size in order for a severe drop in the gelation properties of the system. This work has also shown that C_{28} and C_{27} are large enough to affect the crystal structure of C_{32}, C_{35} and C_{36}, but that C_{24} is not large enough affect the crystal structure of C_{32} and C_{36}. This effect was not impacted by whether or not the longer or shorter carbon number was even or odd.

References:

Ashbaugh, H.S., Radulescu, A., Prud'homme, R.K., Schwahn, D., Richter, D., and Fetters, L.J., "Interaction of Paraffin Wax Gels with Random Crystalline/Amorphous Hydrocarbon Polymers", *Macromolecules*, **35**, 7044-7053 (2002)

Briard, A.-J., Bouroukba, M., Petitjean, D., Hubert, N., Moise, J.-C., and Dirand, M., "Thermodynamic and Structural Analyses and Mechanisms of the Crystallisation of Multi-Alkane Model Mixtures Similar to Petroleum Cuts", *Fuel*, **85**, 764-777 (2006)

Carnahan, N.F. and Carnahan, L.Q., "Transportation Systems for Waxy Crude Oils", Proceedings of the 20th ASME Energy Sources Technology Conference & Exhibition (1998)

Chang, C., Boger, D.V. and Nguyen, Q.D., "Influence of Thermal History on the Waxy Structure of Statically Cooled Waxy Crude Oil", *SPE J.*, 5, 148-157 (2000)

Dirand, M., Bouroukba, M., Chevallier, V., Petitjean D., Behar, E. and Ruffier-Meray, V., "Normal Alkanes, Multialkane Synthetic Model Mixtures and Real Petroleum Waxes: Crystallographic Structures, Thermodynamic Properties and Crystallization", *J. Chem. Eng. Data*, **47**, 115-143 (2002)

El-Gamal, I.M. and Al-Sabbagh, A.M., "Polymeric Additives for Improving the Flow Properties of Waxy Distillate Fuels and Crudes", *Fuel*, **75**, 743-750 (1995)

Garcia, M.d.C., "Crude Oil Wax Crystallization. The Effect of Heavy n-Paraffins and Flocculated Asphaltenes", *Energy & Fuels*, **14**, 1043-1048 (2000)

Guo, X., Pethica, B.A., Huang, J.S., Prud'homme, R.K., Adamson, D.H. and Fetters, L.J., "Crystallization of Mixed Paraffin from Model Waxy Oils and the Influence of Micro-crystalline Poly(ethylene-butene) Random Copolymers", *Energy & Fuels*, **18**, 930-947 (2004)

Guo, X., Pethica, B.A., Huang, J.S., and Prud'homme, R.K., "Crystallization of Long Chain n-Paraffins from Solutions and Melts as Observed by Differential Scanning Calorimetry", Macromolecules, **15**, 5638-5645 (2004)

Guo, X., Pethica, B.A., Huang, J.S., Adamson, D.H. and Prud'homme, R.K., "Effect of Cooling Rate on Crystallization of Model Waxy Oils with Microcrystalline Poly(ethylene butane)", *Energy & Fuels*, **20**, 250-256 (2006)

Hansen, A.B., Larsen, E., Pedersen, W.B. and Neilsen, A.B., "Wax Precipitation from North Sea Crude Oils. 3. Precipitation and Dissolution of Wax Studied by Differential Scanning Calorimetry", *Energy & Fuels*, **5**, 914-923 (1991)

Hennessy, A.J., Neville, A. and Roberts, K.J., "An Examination of Additive-Mediated Wax Nucleation in Oil Pipeline Environments", *J. Cryst. Growth*, **198/199**, 830-837

(1999)

Holder, G.A. and Winkler, J., "Wax Crystallization from Distillate Fuels, II: Mechanism of Pour Depression", *J. Inst. Petrol.,* **51**, 235-252 (1965)

Jennings, D.W. and Weispfennig, K. "Experimental Solubility Data of Various n-Alkane Waxes: Effects of Alkane Chain Length, Alkane Odd Versus Even Carbon Number Structures and Solvent Chemistry on Solubility", *Fluid Phase Equlibria*, **227**, 27-35 (2005)

Kane, M., Djabourov, M., Volle, J.-L., Lechaire, J-P. and Frebourg, G., "Morphology of Paraffin Crystals in Waxy Crude Oils Cooled in Quiescent Conditions and Under Flow", *Fuel*, **82**, 127-135 (2003)

Kuzmic, A.E., Radosevic, M., Bodganic, G., Srica, V. and Vukovic, R., "Studies on the Influence of Long Chain Acrylic Esters Polymers with Polar Monomers as Crude Oil Flow Improver Additives", *Fuel*, **87**, 2943-2950 (2008)

Machado, A.L.C., Lucas, E.F. and Gonzalez, G., "Poly(ethylene-co-vinyl acetate) (EVA) as Wax Inhibitor of a Brazilian Crude Oil: Oil Viscosity, Pour Point and Phase Behavior of Organic Solutions", *J. Pet. Sci. & Engr.,* **32**, 159-165 (2001)

Mehrotra, A.K. and Bhat, N.V., "Modeling the Effect of Shear Stress on Deposition from "Waxy" Mixtures under Laminar Flow with Heat Transfer", *Energy & Fuels*, **21**, 1277-1286 (2007)

Paso, K., Senra, M., Yi, Y., Sastry, A.M., and Fogler, H.S., "Paraffin Polydispersity Facilitates Mechanical Gelation", *Ind. Eng. Chem. Res.*, **44**, 7242-7254 (2005)

Paso, K.G. and Fogler, H.S., "Bulk Stabilization in Wax Deposition Systems", *Energy & Fuels,* **18**, 1005-1013 (2004)

Radinski, A.P., Barre, L. and Espinat, D., "Aggregation of n-Alkanes in Organic Solvents", *J. Molec. Struct.*, **383**, 51-56 (1996)

Ronningsen, H.P. and Bjorndal, B., "Wax Precipitation from North Sea Crude Oils. 1. Crystallization and Dissolution Temperatures and Newtonian and Non-Newtonian Flow Properties", *Energy & Fuels,* **5**, 895-908 (1991)

Senra, M., Panacharoensawad, E. Kraiwattanawong, K., Singh, P. and Fogler, H.S., "Role of n-Alkane Polydispersity on the Crystallization of n-Alkanes from Solution", *Energy & Fuels*, **22**, 545-555 (2008)

Singh, P., Fogler, H.S. and Nagarajan, N.R., "Prediction of the Wax Content of the Incipient Wax-Oil Gel in a Pipeline: An Application of the Controlled-Stress Rheometer",

J. Rheol., **43**, 1437-1459 (1999)

Singh, P., Venkatesan, R., Fogler, H.S. and Nagarajan, N.R., "Morphological Evolution of Thick Wax Deposits during Aging", *AICHE J.*, **47**, 6-18 (2001)

Singh, P., Youyen, A. and Fogler, H.S., "Existence of a Critical Carbon Number in the Aging of a Wax-Oil Gel", *AIChE J.*, **9**, 2111-2121 (2001)

Soldi, R.A., Oliveira, A.R.S., Barbosa, R.V. and Cesar-Oliveira, M.A.F., "Polymethacrylates: Pour Point Depressants in Diesel Oil", *European Polymer J.*, **43**, 3671-3678 (2007)

Soni, H.P. and Bharambe, D.P., "Synthesis and Evaluation of Polymeric Additives as Flow Improvers for Indian Crude Oil", *Iranian Polymer Journal*, **15**, 943-954 (2006)

Turner, W.R., "Normal Alkanes", *Ind. Eng. Chem. Prod. Res. Develop.*, **10**, 238-260 (1971)

Wu, C.-H., Wang, K.-S., Shuler, P.J., Creek, J.L., Carlson, R.M. and Cheung, S., "Measurement of Wax Deposition in Paraffin Solutions", *AIChE J.*, **48**, 2107-2110 (2002)

Venkatesan, R., Singh, P. and Fogler, H.S., "Delineating the Pour Point and Gelation Temperature of Waxy Crude Oils", *SPE J.*, 349-352 (2002)

Venkatesan, R., Nagarajan, N.R., Paso, K., Yi, Y-B., Sastry, A.M. and Fogler, H.S., "The Strength of Paraffin Gels Formed Under Static and Flow Conditions", *Chem. Eng. Sci.*, **60**, 3587-3598 (2005)

Vignati, E., Piazza, R., Visintin R.F.G., Lapasin, R., D'Antona, P. and Lockhart, T.P., "Wax Crystallization and Aggregation in a Model Crude Oil", *J. Phys. Condens. Matter*, **17**, 83651-83660 (2005)

Visintin, R.F.G., Lapasin, R., Vignati, E., D'Antona, P. and Lockhart, T.P., "Rheological Behavior and Structural Interpretation of Waxy Crude Oil Gels", *Langmuir*, **21**, 6240-6249

Winter, H.H., "Can the Gel Point of a Cross-Linking Polymer Be Detected by the G' – G" Crossover?", *Polymer Eng. & Sci.*, **27**, 1698-1702 (1987)

CHAPTER IV

THE ROLE OF A CARBOXYLIC ACID ON THE CRYSTALLIZATION, DEPOSTION AND GELATION OF LONG CHAINED N-ALKANES IN SOLUTION

Introduction

The deposition of select components of crude oil in petroleum transport pipelines and process equipment is a major problem in the oil industry. Crude oil is a complex mixture containing a wide variety of organic compounds including paraffins, aromatics, resins, asphaltenes and napthenes (Paso and Fogler, 2003, Venkatesan, et al., 2005. Although crude oils contain hundreds or even thousands of individual components, the primary constituents of the deposits are n-paraffins (Hansen et al., 1988, Hansen et al., 1991, Hennessy et al., 1999, Singh et al., 1999, Garcia, 2000). Crude oils contain n-paraffins with carbon numbers ranging from 5 to 160, but deposits generally contain n-paraffins with carbon numbers ranging from 20 to 50 (Hennessy et al., 1999, Singh et al., 1999). Paraffins are the chief components of deposits because of their ability to crystallize easily and in an ordered structure and their relatively low solubility in most paraffin-based, aromatic or oil like solvents (Hennessy et al., 1999, Singh et al., 1999, Venkatesan, et al., 2005). As crude oil is transported from the reservoir (temperatures of 70-150 °C and pressures of 8,000-15,000 psi) through subsea pipelines with external temperatures as low as 4° C, the heavier n-paraffins originally soluble in the crude oil can

become insoluble (Venkatesan, et al., 2005). This loss of solubility can lead to precipitation and deposition onto the pipe walls, forming a gel containing orthorhombic wax crystals trapping liquid oil (Singh et al., 1999, Venkatesan et al., 2002). This deposit restricts the flow of oil through the pipeline and becomes harder and massier as time progresses by the process of aging, which can lead to the complete obstruction of flow pipes or production lines (Singh et al., 2000, Machado et al., 2001, Paso and Fogler, 2004).

In order to gain insight into the deposition seen in crude oil pipelines, a better understanding of the crystallization of alkanes is needed. n-Paraffins crystallize in one of four general shapes when allowed to self-crystallize in short chain n-alkane solvents. The shapes are triclinic, monoclinic, orthorhombic and hexagonal and the shape is largely dependent on the molecular size and whether the carbon number is even or odd (Turner et al., 1971, Liu and Bennema, 1994, Dirand et al., 2002). However, it is generally accepted that wax crystals found in the deposits are primarily orthorhombic in shape (Singh et al., 1999, 2000, Dirand et al., 2002). Therefore, deviations from the expected crystallization must be occurring. These deviations are caused by the presence of other components present in the crystal growth medium, even the solvent (Kern et al., 1992, Singh et al, 2000). Therefore, materials such as aromatics, asphaltenes, resins, water, additives, inhibitors, pour point depressants and shorter chained n-paraffins can influence how the long chain n-paraffins crystallize out of solution. These components can impact a number of factors: crystal morphology, crystal growth rate, nucleation kinetics, crystallization thermodynamics, precipitation kinetics and dissolution kinetics (Kern et al., 1992, Singh et al, 2000).

The ability of other materials present in crude oils to impact the crystallization of n-alkanes is an issue of great interest to the oil industry as it attempts to minimize or eradicate wax deposition. Substantial work has been completed to find additives that can reduce the wax appearance temperature, modify the wax crystal morphology, decrease the yield stress of the deposited gel and inhibit crystallization kinetics, all of which can reduce the problem of wax deposition in subsea oil pipelines. Of particular interest have been polymers, copolymers and block copolymers containing components such as alkyl chains, methacrylates, anhydrides, esters, polyethylenes and vinyl acetates (Qian et al., 1996, Garcia et al., 2000, Machado et al., 2001, Ashbaugh et al., 2002a, 2002b, Wang et al., 2002).

The mechanisms by which additives work to prevent deposition and/or weaken the resultant gel vary. In their study of ethylene vinyl acetate copolymer (EVA), Qian showed that the ability for EVA to reduce the viscosity and depress the pour point of the crude oil was directly related to the compactness of the copolymer in solution (Qian et al., 1996). As the EVA copolymer coil dimension decreased, the reduction in both the viscosity and pour point increased. Machado showed that the ability of an EVA copolymer to reduce the viscosity and pour point for a particular crude oil was based on the concentration of the additive added and percent of vinyl acetate in the copolymer (Machado et al, 2001). Ashbaugh showed that poly(ethylene-butene) (PEB) random copolymers reduce the yield stress of the resulting gels by aggregating and cocrystallzing with the paraffins and its efficacy is dependent on the size of the alkane, and the microcrystallinity and concentration of the copolymer (Ashbaugh et al., 2002a). Further work on PEB by Guo, et al. showed that aggregation and cocrystallization caused the

formation of much smaller crystals, which in turn led to decreases in the yield stress (Guo et al., 2004). Additionally, PEB can impact the nucleation of particular alkanes, further impacting the flow properties of the crude. Although the mechanisms of wax inhibitors are varied, it is generally accepted that these mechanisms are only able to act on particular n-alkanes (Garcia et al., 2000, Machado et al., 2001, Ashbaugh et al., 2002a, 2002b, Wang et al., 2002). Stearic acid is a long chain, saturated carboxylic (fatty) acid containing 18 carbons and a carboxyl group on an edge carbon that can bind with a wide range of molecules (Schmidt et al, 2006). It crystallizes in a monoclinic structure in n-alkane solutions, similar to some long chain n-alkanes (Beckmann et al., 1986). Additionally, stearic acid is known to dimerize in n-alkane solutions and the basic growth unit of stearic acid is the dimer, which occurs because of hydrogen bonding between the carboxyl groups of the respective stearic acid molecules. A schematic of the dimerization can be seen in Figure 4.1.

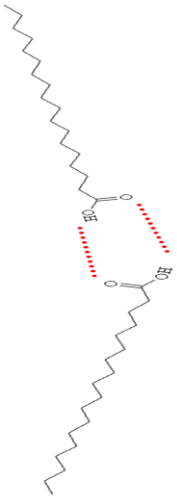

Figure 4.1: Schematic of the dimerization of stearic acid. The dashed lines indicates the hydrogen bonding between the two stearic acid molecules.

The objective of this paper is to determine how a long, straight chained non n-alkane can have on the crystallization, deposition and gelation characteristics of n-alkanes in n-alkane solutions. Work in Chapter 2 showed that shorter n-alkanes can impact the thermodynamic and deposition characteristics of longer n-alkanes and vice versa. The impact of stearic acid concentration on these characteristics will also be explored. The dimerization of stearic acid allows it to be dimensionally similar to n-alkanes $C_{32}H_{66}$ and $C_{36}H_{74}$ (hereafter abbreviated as C_{32} and C_{36} respectively). Additionally, if the solubility characteristics of stearic acid are similar to both C_{36} and C_{32}, it may be possible for these materials to cocrystallize together according to the criterion set by Turner (Turner, 1971).

Materials

For all solutions prepared (unless otherwise noted), the mass % of any alkane present in the solution was 4%. Dodecane was used for the solvent for all trials. The amount of stearic acid present in solution with C_{36} and C_{32} was varied from 1% to 4%. Hexatriacontane (98% purity), dotriacontane (97% purity), stearic acid (95% purity) and dodecane (99% purity) were all obtained from Sigma-Aldrich.

Experimental Methods

Cloud Point Determination

Cloud points were determined using a constant temperature bath where a solution, heated above its cloud point, is slowly cooled and allowed to equilibrate at a temperature. The solution was removed from the temperature bath and visually inspected for any

precipitation. If the system remained homogeneous, the bath was cooled to a lower temperature. This process continued until precipitation became visible.

Differential scanning calorimetry (DSC)

A Perkin-Elmer DSC 10 was utilized for all DSC runs. The solutions were heated initially above their cloud point and then cooled at a rate of 1.0 °C/min. The DSC trials allowed for the onset of a liquid-solid transition and the amount of heat released in the transition to be determined.

Coldfinger

The coldfinger apparatus is a laboratory device that is used to simulate deposition (Paso et al., 2005). An image of the coldfinger apparatus can be seen in Figure 4.2.

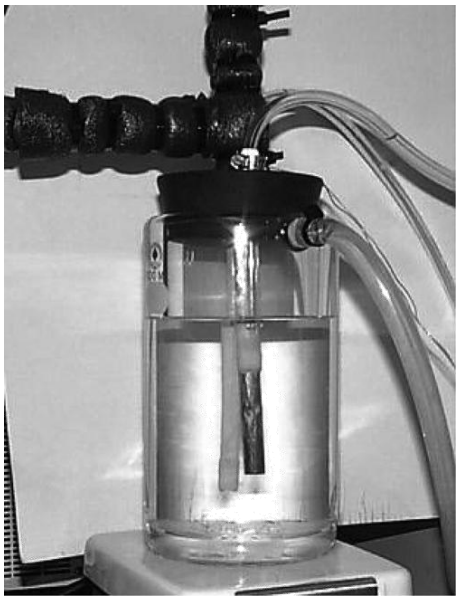

Figure 4.2 The coldfinger apparatus

The apparatus consists of a steel cylinder (12.6 cm^2) that can be thermally controlled and a jacketed vessel (204 +/- 1 mL) where the fluid is located. In order for

deposition to occur on the surface of the coldfinger, the bulk solution must be above the solution cloud point and the cylinder must be below the solution cloud point. For these experiments, the bulk fluid was kept at a temperature of 50 °C and the steel cylinder was maintained at 10 °C. All cloud points of the solutions used in this work are between 10 and 50 °C, ensuring that deposition can occur. A stirbar was added to induce bulk mixing. To ensure that the fluid flow properties remain consistent from experiment to experiment, the fluid volume was held constant (+/- 1 mL) and the stirbar rotation speed was held constant at 340 rpm. This rotation speed was selected to ensure thorough mixing while preventing the formation of turbulent eddies in the system. In order to eliminate the effect of aging on the composition of the deposits, each trial was run for 6 hours. The deposit was then carefully removed from the steel cylinder and weighed.

Chromatography

To determine the deposit composition, an Agilent 6890N high temperature gas chromatography with a 0.25 μm fused silica stationary phase and an FID detector was used. The solutions were diluted with heptane and manually injected into the system. The samples were run through the gas chromatograph several times and an average composition (+/- 10%) was determined.

Pour point determination

The pour point was also determined using a constant temperature bath. The pour point is defined as the highest temperature where a solution can pour when cooled under static conditions (Venkatesan, et al., 2002). The bath is initially held at a temperature above the cloud point of the solution. The solution is preheated in an oven in a vial to a temperature above the cloud point of the solution and kept there for sufficient time to

remove any thermal history. The heated solution is then inserted into the temperature bath. The bath is then cooled at a rate of 0.1 °C/min. At the desired temperature, the solution is delicately removed from the temperature bath to prevent disruption of the gel structure and is inverted. If the solution moves upon inversion, then the solution is above the pour point. The pour point is defined as the highest temperature where the solution does not move upon inversion.

Gel point determination

The gel point was found using a TA 1000AR controlled stress rheometer. The gel point is defined as the point where the solid-like behavior of a solution is stronger than the liquid-like behavior of a solution. The solution is heated above the cloud point and held at this temperature to remove any thermal history. As the solution is cooled at a constant rate of 0.5 °C/min, an oscillatory stress of 0.1 Pa with a frequency of 0.1 Hz is being applied. The stress and frequency are kept relatively low in order to not disrupt the development of the gel. The storage modulus (G') and the loss modulus (G") are found and the crossover point between G' and G" represents the gel point temperature.

Solubility Studies

In order to assess the solubility of stearic acid in dodecane in comparison to both C_{36} and C_{32}, solutions with varying concentrations were prepared and their cloud points were measured. The results of these cloud point experiments can be seen in Figure 4.3, which shows that the solubility of stearic acid in dodecane is very similar to the solubility of C_{32} in dodecane.

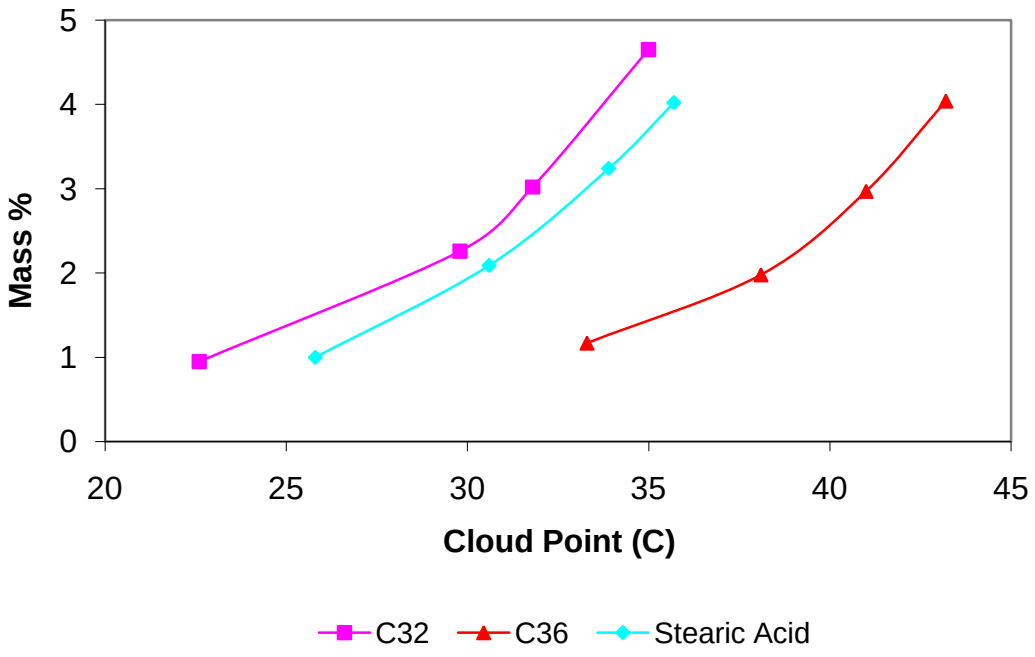

Figure 4.3: Graph of solubility vs. temperature for C_{36}, C_{32} and stearic acid in dodecane. (▲ represents C_{36}, ■ represents C_{32} and ♦ represents stearic acid)

This result shows that stearic acid, a straight chain carboxylic acid containing 18 carbon atoms and the straight chain n-alkane C_{32}, a molecule containing almost double the number of carbons, have similar solubilities in dodecane, a pure straight chain solvent. Stearic acid dimerizes in solution, meaning that stearic acid exists as a thirty six carbon atom molecule when in dodecane. However, it will be more soluble than C_{36} because of the presence of the carboxylic acid, which helps stabilize the molecule in solution because of the energy provided by the hydrogen bonding.

Figure 4.3 can be replotted to determine if stearic acid obeys the van't Hoff solubility theory, a relationship seen for n-paraffins in organic solvents (Ashbaugh et al, 2002a, Chapter 2). The van't Hoff relationship shown below assumes ideal solubility and that the crystallization does not cause a change in the heat capacity of the solution.

$$\ln\left(\frac{1}{x_{solute}}\right) = \frac{\Delta H_{dissolution}}{RT} - \frac{\Delta S_{dissolution}}{R} \qquad (1)$$

Where: x_{solute} = mole fraction of soluble material
$\Delta H_{dissolution}$ = enthalpy of dissolution (kJ/mol)
$\Delta S_{dissolution}$ = entropy of dissolution (J/mol K)
R = universal gas constant (J/mol K)
T = temperature (K)

As can be seen in Figure 4.4, stearic acid also obeys the van't Hoff equation. It is important to note that although the van't Hoff equation was derived for infinitely dilute solutions, it can be extended to solutions that have relatively low solute concentrations (at least 4 mass % or approximately 3 mol %), that are not considered dilute. From the slope and intercept, estimates of the enthalpy and entropy of dissolution can be obtained, results shown in Table 4.1. The results show that stearic acid has similar values of $\Delta H_{dissolution}$ and $\Delta S_{dissolution}$ when compared to the two n-alkanes.

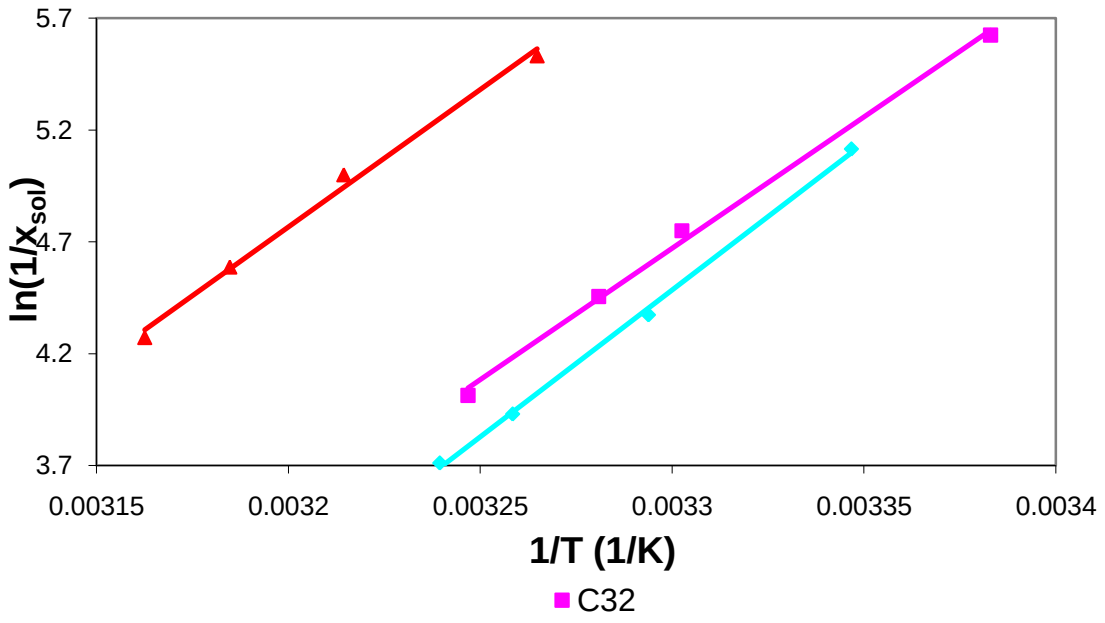

Figure 4.4: Graph of solubility vs. temperature for various organic materials in dodecane. (▲ represents C_{36}, ■ represents C_{32} and ♦ represents stearic acid)

Table 4.1: Paraffin dissolution enthalpy and entropy values determined using the van't Hoff solubility relationship using experimental cloud points.

Component	ΔH_{diss} (kJ/mol)	ΔS_{diss} (J/mol K)
C_{36}	102.0	287
C_{32}	97.6	283
Stearic Acid	109.1	323

Differential scanning calorimetry was used to obtain a better understanding of the difference in the thermodynamic solubility between the n-alkane systems and the stearic acid systems. Figure 4.5 shows the results when 4% solutions of C_{36}, C_{32} and stearic acid were analyzed using DSC. Thesee results are consistent with Figure 4.3 that at 4% concentration, the solubility of C_{36} in dodecane is much lower than both C_{32} and stearic acid and that the solubilities of C_{32} and stearic acid are very similar. In addition, the solubilities of C_{32} and stearic acid are very similar as indicated by Figure 4.3. This result can be explained by the work of Paso, who showed crystallization at low cooling rates was defined in three regimes: (1) a nucleation lag regime where the saturation limit has been reached but no crystallization has occurred, (2) a supersaturation growth regime where crystallization begins and (3) an equilibrium growth regime where crystallization obeys thermodynamic solubility. The peak represents a large portion of the supersaturation growth regime (Paso et al., 2005). The temperature range of the supersaturation growth regime is related to the nucleation lag. The larger the nucleation lag, more time (greater temperature range) is necessary for the solution to return to thermodynamic equilibrium. The peak for stearic acid is much broader than for either of the n-alkanes, indicating that the nucleation lag for stearic acid is larger than for the n-alkanes. This result means that the nucleation kinetics of stearic acid are slower than the nucleation kinetics for the n-alkanes.

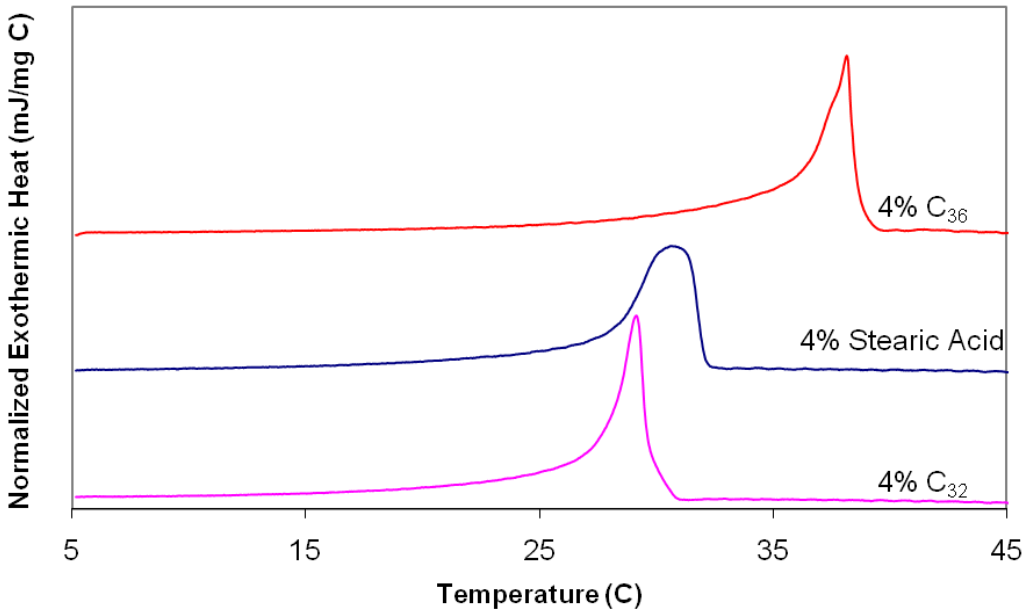

Figure 4.5: Monodisperse DSC traces: Each sample has 4 mass % of the specified solute and is being cooled at a rate of 1.0 °C/min.

Table 4.2 shows the relevant thermodynamic values that can be obtained from the DSC trace. The wax appearance temperature (WAT) represents the temperature where the trace begins to deviate from the relatively flat heat capacity baseline, indicating that a phase transition is occurring. The peak temperature represents the temperature where the exothermic heat (directly correlated to the rate of crystallization) is at a maximum. The enthalpy of crystallization is proportional to the area in between the curve and the heat capacity baseline, which is formed by connecting the flat parts of the DSC trace.

Table 4.2: Thermodynamic information for monodisperse trials. All temperatures are in °C. All materials are present in 4% mass abundance in dodecane.

Material	WAT (°C)	Peak T (°C)	ΔH_{cryst} (kJ/mol)
C_{36}	39.4	38.2	165
C_{32}	31.4	29.2	132
Stearic Acid	32.7	31.1	80

Figure 4.6 shows the DSC traces where 4% C_{32} and 4% stearic acid are

independently added to 4% C_{36} in dodecane. The two graphs are distinctly different with the 4% C_{36}/4% C_{32} trace showing the presence of only one peak with a lengthy tail and the 4% C_{36}/4% stearic acid trace showing two separate peaks.

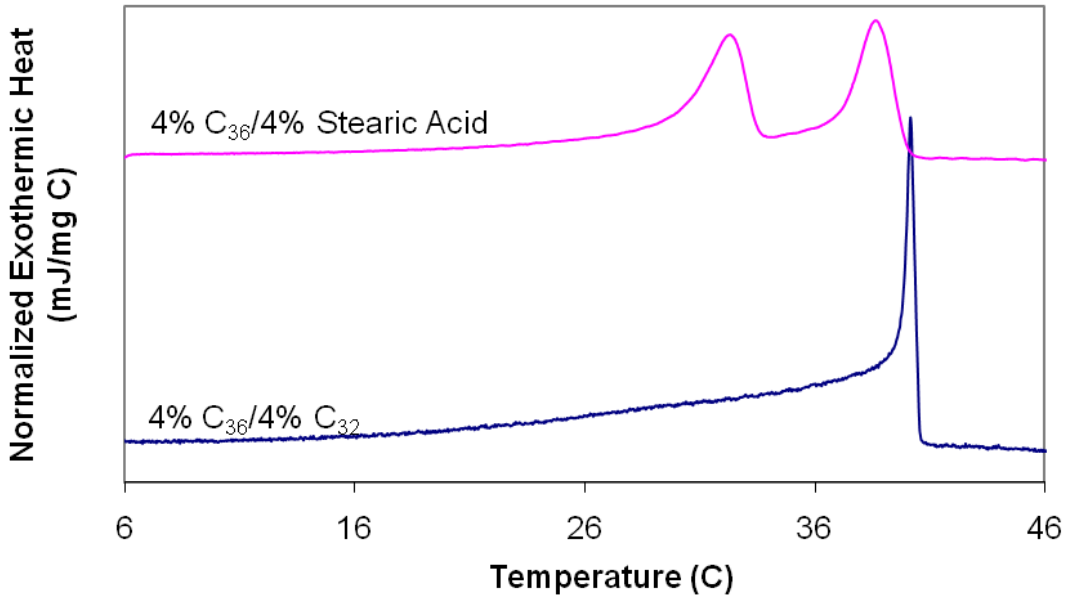

Figure 4.6: Polydisperse DSC traces: Each sample has 4 mass % of the specified solute and is being cooled at a rate of 1.0 °C/min.

Previous work has shown that C_{36} and C_{32} cocrystallize together, causing C_{32} to crystallize out at the solubility limit of C_{36} (Guo et al., 2004, Chapter 2). This effect is not solubility driven as it is seen for any concentration of C_{32}. The presence of two peaks in the C_{36}/stearic acid DSC trace indicates that C_{36} and stearic acid have not cocrystallized together. Using Turner's criteria for cocrystallization, it appears that the two molecules are sufficiently structurally different (the carboxylic acid groups in the dimerized stearic acid) and their pure crystal shapes are dissimilar enough to prevent the two materials from cocrystallizing together. This lack of cocrystallization occurs even though C_{36} and stearic acid consist primarily of straight chained carbons and the solubility characteristics of stearic acid are similar to C_{32}, a material that cocrystallizes with C_{36}.

Beyond the difference in the number of peaks, further information can be obtained by analyzing both the peaks and the relevant thermodynamic information, provided in Table 4.3. In the 4% C_{36}/stearic acid system, the peak location of C_{36} has shifted about 1 °C higher from the monodisperse C_{36} system because the ratio of solute to solvent has increased. The shapes of the C_{36} and stearic acid peaks remain relatively unchanged compared to the monodisperse systems, indicating that the presence of stearic acid does not affect the crystallization of C_{36} and vice versa. However, the peak for the C_{36}/C_{32} system has drastically changed when compared to the monodisperse trials. The decrease in the peak width and the increase in the slope right below the wax appearance temperature show that the presence of C_{32} is accelerating the crystallization kinetics of C_{36}.

Table 4.3: Thermodynamic information for polydisperse trials in Figure 6. All temperatures are in °C. All materials are present in 4% mass abundance in dodecane.

Material	WAT (°C)	Peak T (°C)	ΔH_{cryst} (kJ/mol)
4% C_{36}/4% C_{32}	41.0	39.8	131
4% C_{36}/4% Stearic Acid	40.7, 34.4	38.9, 32.6	112

A review of the literature on chemical inhibitors has shown that adding too much inhibitor may reduce its efficacy for a number of reasons including the fact that the inhibitor can self-associate with itself and not the n-alkane (Guo et al., 2004). To determine if this effect is being seen with stearic acid, the concentration was reduced to 1% and 2%. Additionally, monodisperse systems containing 1% and 2% of stearic acid were prepared and analyzed using DSC to determine if the crystallization of smaller amount of stearic acid is influenced by the presence of an excess of C_{36}. The DSC traces for all the monodisperse stearic acid trials are presented in Figure 4.7 and the DSC traces for all the binary 4% C_{36}/x% stearic acid trials are displayed in Figure 4.8.

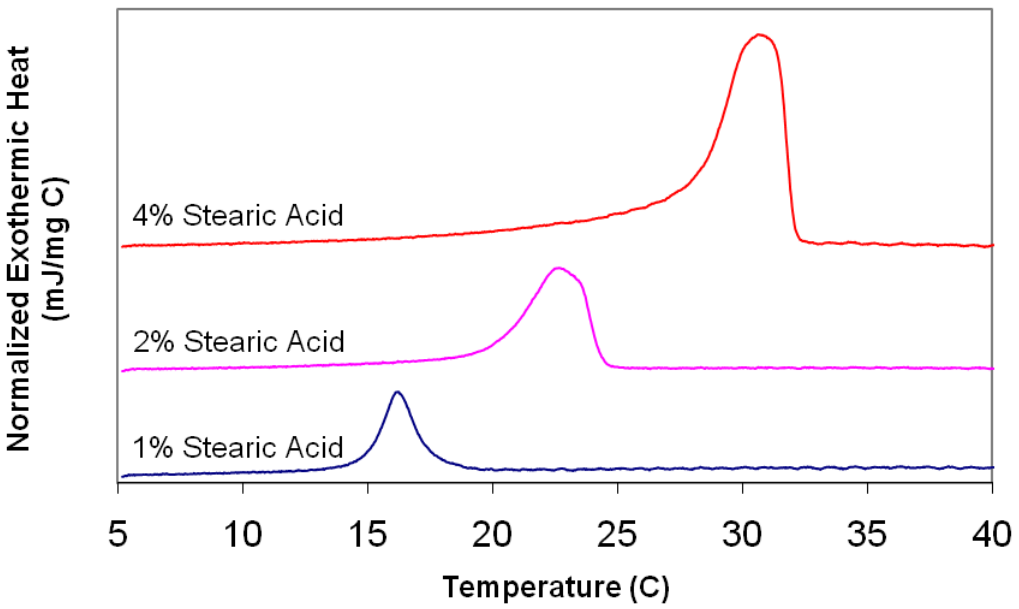

Figure 4.7: Monodisperse stearic acid DSC traces: The cooling rate is 1.0 °C/min.

Comparing Figures 7 and 8, it can be observed that stearic acid has virtually no effect on the precipitation of C_{36}. The C_{36} peaks are reasonably similar to one another in both size and shape and occur at approximately the same temperature. However, it appears that the precipitation of stearic acid is influenced by the presence of C_{36}. When comparing the stearic acid curves, a noticeable shift in the temperature where the peaks occur is present.

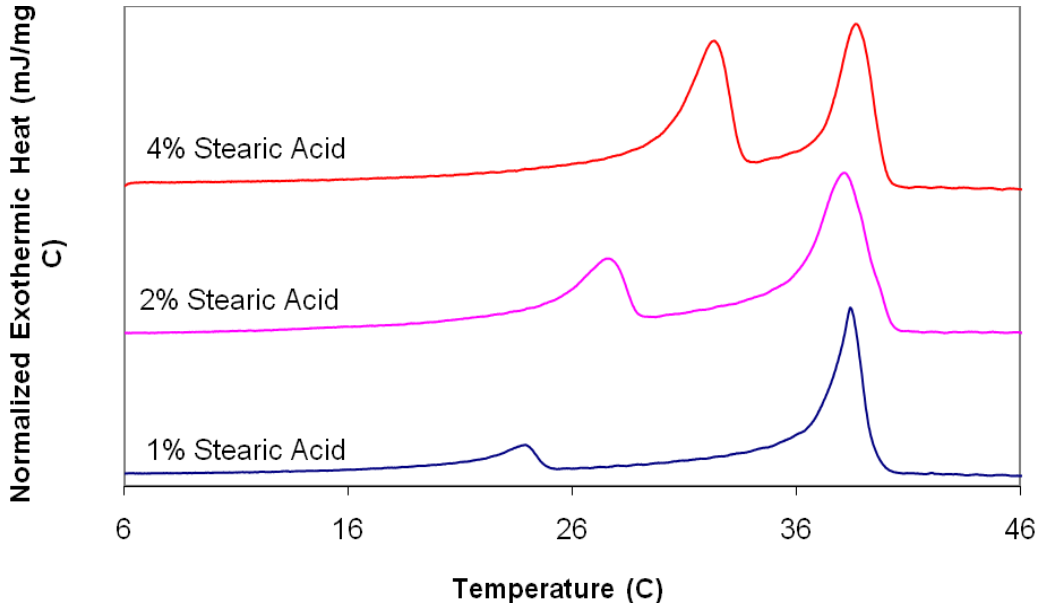

Figure 4.8: Binary C_{36}/stearic acid DSC traces: All systems contain 4% C_{36} and the cooling rate is 1.0 °C/min.

Table 4.4 provides the WAT and peak temperatures for the monodisperse stearic acid trials as well as for the stearic acid peaks for the binary systems. The magnitude of the shift increases as the amount of stearic acid decreases with approximately a two degree shift for the 4% sample and an approximately seven degree shift for the 1% sample.

Table 4.4. Peak information for monodisperse stearic acid trials and binary trials with stearic acid and 4% C_{36}.

	Monodisperse		Binary (with 4% C_{36})	
% Stearic Acid	**WAT (°C)**	**Peak T (°C)**	**WAT (°C)**	**Peak T (°C)**
1%	19.8	16.5	25.3	24.2
2%	25.1	23.3	29.6	28.1
4%	32.7	31.1	34.4	32.6

Previous work and Chapter 2 have shown that a more soluble material can experience a reduction in solubility with the presence of a less soluble material even if cocrystallization does not occur (Dirand et al., 2002). The precipitated crystals provide nucleation sites that allow the more soluble components to crystallize out before reaching

their solubility limit. However, this heterogeneous nucleation generally leads to a broadening of the temperature regime over which crystallization can occur, which is not seen for the stearic acid in these trials. Instead, the entire peak has shifted and the peak has undergone little to no broadening. This result can best be explained by recalling the strong hydrogen bonding that exists between the stearic acid monomers, a result that has been discussed elsewhere (Jennings and Weispfennig, 2005). This strong association indicates that the stearic acid molecules are likely to cluster together in various locations throughout the solution. Therefore, if a small amount of the stearic acid heterogeneously nucleates, there will be a cluster of molecules nearby that will be capable of crystallizing.

To determine if the trends seen for stearic acid are valid for other long carbon number n-alkanes, solutions of 4% C_{32} and 1, 2 and 4% stearic acid were prepared. C_{32} is the least soluble component for the 1% and 2% stearic acid experiments, but stearic acid is the least soluble component for the 4% stearic acid experiment. The DSC traces are shown for the 4% C_{32}/stearic acid experiments in Figure 4.9.

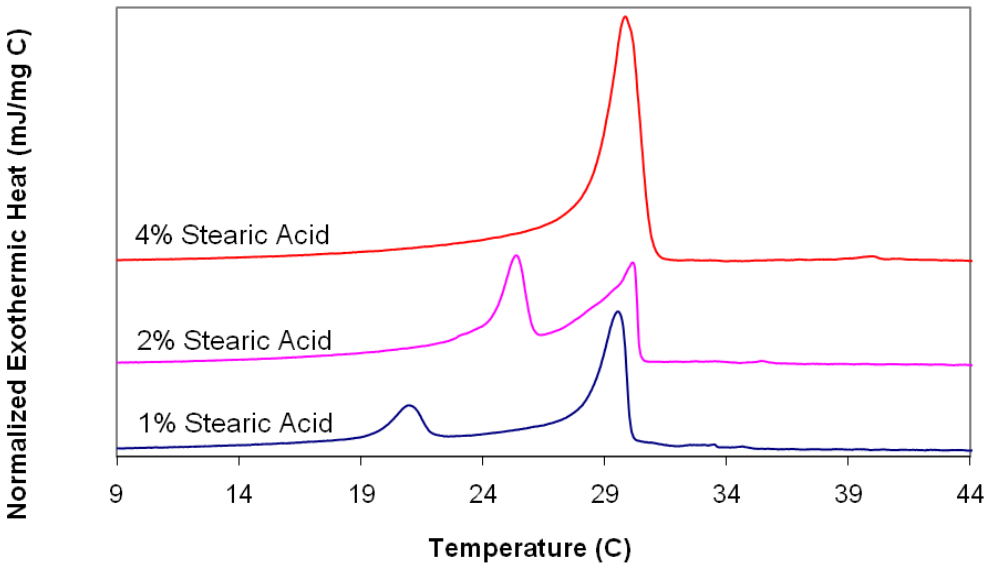

Figure 4.9. Binary C_{32}/stearic acid DSC traces: All systems contain 4% C_{32} and the cooling rate is 1.0 °C/min.

A major difference can be seen for the 4% C_{32}/4% stearic acid trace where only one peak is present. Initially, the one peak indicates that it is possible for stearic acid and C_{32} to cocrystallize together. However, the other two traces in Figure 4.9 show two distinct peaks. If the two materials did cocrystallize, then the second peak would not be present or severely minimized because the less soluble component would enter the crystal structure of the more soluble component independent of its solubility limit or concentration. Therefore, the 4% C_{32}/4% stearic acid result is best explained as simultaneous crystallization without cocrystallization with stearic acid (the slightly less soluble component, see Figure 4.5) influencing the solubility of C_{32}. The precipitation of stearic acid allows for heterogeneous nucleation sites for C_{32}, which shortens the nucleation lag regime for C_{32} by providing an easier means for C_{32} to precipitate. This heterogeneous nucleation allows for stearic acid and C_{32} to enter the supersaturation regime almost simultaneously.

A comparison of the stearic acid peak locations for the C_{32}/stearic acid experiments is displayed in Table 5. Similar to the C_{36} systems, the precipatiting n-alkane decreases the solubility of stearic acid in dodecane. The shifts in the peak locations for the C_{32} solutions are smaller than the shifts for the C_{36} solutions, indicating the existence of a nucleation time lag between the formation of solid n-alkane crystals and the heterogeneous nucleation of stearic acid on the n-alkane. The shift is larger for C_{36} than C_{32} because C_{36} precipitates at a higher temperature than C_{32}.

Table 4.5: Peak information for monodisperse stearic acid trials and binary trials with stearic acid and 4% C_{32}.

	Monodisperse		**Binary (with 4% C_{32})**	
% Stearic Acid	**WAT (°C)**	**Peak T (°C)**	**WAT (°C)**	**Peak T (°C)**
1%	19.8	16.5	22.5	21.3
2%	25.1	23.3	26.9	25.5
4%	32.7	31.1	32.1	30.0

Finally, the area under the curve, the amount of heat released during crystallization can be analyzed to assess how the combination of stearic acid and an n-alkane affects the heat requirements of the system. Chapter 2 showed that for multicomponent n-alkane systems, both polydispersity and cocrystallization lower the enthalpy of crystallization with cocrystallization having a greater effect. Table 4.6 compares the enthalpy of crystallization found for the binary systems to the enthalpy of crystallization that would be expected if the components were to crystallize independently. This value was found by taking a weighted mass average of the crystallizable components and multiplying by the respective enthalpies of crystallization found in the monodisperse systems shown in Table 2 (see Appendix A). These results are shown in Table 4.6.

Table 4.6: Impact of stearic acid on heat of crystallization. ΔH_{cryst} represents the enthalpy of crystallization found using DSC. The expected ΔH_{cryst} represents the heat of crystallization expected if the various components were to crystallize independently of one another.

Sample	ΔH_{cryst} (kJ/mol)	Expected ΔH_{cryst}	% Difference
4% C_{36}-4% C_{32}	132	148	-10.8
4% C_{36}-1% Stearic Acid	149	139	7.2
4% C_{36}-2% Stearic Acid	129	125	3.2
4% C_{36}-4% Stearic Acid	112	111	0.9
4% C_{32}-1% Stearic Acid	128	117	9.4
4% C_{32}-2% Stearic Acid	118	109	8.3
4% C_{32}-4% Stearic Acid	105	100	5.0

The most interesting result from Table 4.6 is that although the 4% C_{36}/4% C_{32} system has a lower actual enthalpy of crystallization than what would be expected, all of the stearic acid trials have a higher actual enthalpy of crystallization than what would be

expected if the enthalpy of crystallization was taken as a weighted average. Because the C_{32} and C_{36} are basically unaffected by the presence of stearic acid, the increase in ΔH is caused by stearic acid. As discussed earlier, the presence of the long chained n-alkane allows stearic acid to crystallize out of solution at higher temperatures than if stearic acid were to precipitate out of dodecane by itself. This fact, along with the energy needed for stearic acid to come out of solution at temperatures above its solubility limit causes the enthalpy of crystallization to be higher than expected.

Deposition Studies

Table 4.7 shows the deposition results for the monodisperese systems in dodecane. When completing a deposition run, there are two variables of interest: the amount of the deposit and the composition of the deposit.

Table 4.7. Mass and composition information for monodisperse deposits after six hours. % in deposit represents the percent of the deposit constituted by the crystallizable material (the remainder being the solvent, dodecane). % component deposited represents what percent of the alkane initially in solution deposited onto the coldfinger. All components are present in dodecane at a concentration of 4 mass %.

Component	WAT (°C)	Deposit Mass (g)	% in Deposit	Mass Deposited of Component (g)	% Component Deposited
C_{36}	39.4	1.17	42.2	0.49	7.9
C_{32}	31.4	0.42	26.8	0.11	1.8
Stearic Acid	32.7	0.54	29.4	0.16	2.5

The driving force for deposition is a concentration gradient between the concentration in the bulk liquid and the equilibrium concentration at the interface between the bulk and the deposit (initially, the temperature of the coldfinger apparatus) (Singh et al., 2001). Because the initial mass concentration of the three solutions were the same and the coldfinger apparatus was held at the same temperature for all trials, the rate

of deposition and the mass of the deposit was expected to be related to the solubility of the crystallizable component. This hypothesis is confirmed by the results in Table 4.7 where the deposit mass, the solid percent of the deposit and the amount of the material deposited were directly correlated to the solubility limit of the three components. The deposit containing C_{36} had the greatest mass and largest solid percent followed by stearic acid and then C_{32}, with the latter two having similar deposits because of their similar solubility limits in dodecane at 4% concentration.

Table 4.8 presents the results for the binary deposition trials. For the 4% C_{36} experiments, C_{32} greatly influences the ability of C_{36} to deposit whereas stearic acid has no effect.

Table 4.8. Mass and composition information for polydisperse deposits after six hours. % in deposit represents the percent of the deposit constituted by the crystallizable material (the remainder being the solvent, dodecane). % component deposited represents what percent of the component initially in solution deposited onto the coldfinger.

		% in Deposit			% Component Deposited		
Solution	**Deposit Mass (g)**	**C_{36}**	**C_{32}**	**SA**	**C_{36}**	**C_{32}**	**SA**
4% C_{36}/4% C_{32}	0.82	20.0	14.7	---	2.6	1.9	---
4% C_{36}/4% Stearic Acid (SA)	1.39	36.7	---	6.5	7.8	---	1.2
4% C_{36}/2% Stearic Acid	1.13	41.0	---	3.3	7.0	---	1.1
4% C_{36}/1% Stearic Acid	1.17	41.4	---	1.6	7.4	---	1.1
4% C_{32}/4% Stearic Acid	0.72	---	8.3	10.2	---	0.9	1.2
4% C_{32}/2% Stearic Acid	0.47	---	10.0	3.0	---	0.7	0.4
4% C_{32}/1% Stearic Acid	0.40	---	10.7	1.1	---	0.7	0.3

This result is even true for the sample containing 4% stearic acid, which is less soluble in dodecane and thus has higher thermodynamic driving force than 4% C_{32}. The ability of C_{32} to form cocrystals with C_{36} limits the ability of C_{36} to deposit onto the coldfinger. Although the wax percent of C_{36} in the 4% C_{36}/4% stearic acid deposit is slightly lower

than in the monodisperse 4% C_{36} deposit, this reduction can be explained by the presence of another crystallizable material in the deposit. However, the amount of C_{36} that deposited remains relatively the same.

Although C_{36} is unaffected by the presence of stearic acid, the ability of stearic acid to deposit is hindered by the presence of C_{36}. The percentage of stearic acid in the deposit and the percentage of stearic acid in solution that actually deposits are much lower than the monodisperse stearic acid system. This result can also be explained by the strong self-association of stearic acid. When the solution consists of only stearic acid and dodecane, the solid part of the deposit contains of stearic acid molecules, providing a large area (the entire deposit) for the stearic acid molecules to precipitate and deposit. However, when C_{36} is present, the ability of stearic acid to deposit onto the coldfinger is limited because C_{36} has a stronger driving force. Stearic acid's strong self-association will allow it to primarily and rapidly deposit only where stearic acid has deposited. These limitations to where stearic acid can easily deposit subsequently reduces the presence of stearic acid in the deposit.

As the concentration of stearic acid is decreased in the 4% C_{36}/stearic acid trials, the absolute amount of stearic acid present in the deposit is also decreased. . This result is expected because less stearic acid is present in the fluid, which alters the solubility limit and reduces the driving force for stearic acid to precipitate. However, the percent of stearic acid in solution that becomes part of the deposit is independent of the concentration of stearic acid, but is half the amount seen for the monodisperse stearic acid solution.

The 4% C_{32}/stearic acid deposition results show distinctly different results for the 4% stearic acid system from the 1% and 2% stearic acid system. When the stearic acid concentration is 4%, it has a larger driving force than $C_{32,}$ allowing for stearic acid to constitute a larger portion of the deposit than C_{32}. Because the solubility limits for 4% stearic acid and 4% C_{32} in dodecane are similar, their relative amounts in the deposit are similar to one another because a competition between the molecules ensues for nucleation sites both on the coldfinger and on the gel layer. This competition reduces the amount of C_{32} and stearic acid that deposits out of solution when compared to their respective monodisperse solutions. However, when the stearic acid concentration is reduced to values where C_{32} is the least soluble component, the results resemble those seen for the 4% C_{36}/ stearic acid systems. In the C_{32}/lower concentration stearic acid deposits, the solid percent of C_{32} remains relatively the same along with the percent of C_{32} in the initial solution that becomes part of the deposit. These amounts are higher than the values seen for the 4% C_{32}/4% stearic acid trials because stearic acid becomes a weaker competitor for nucleation sites now that it is no longer the least soluble crystallizable material in solution. Similar to the C_{36} trials, the percent of the deposit containing stearic acid is reduced as the amount of stearic acid in the solution is reduced, but the percent of stearic acid in solution that deposits remains constant. However, this percentage is lower than the one seen for the C_{36} trials. This result can be explained by the fact that C_{36} forms larger deposits than C_{32} because it is less soluble in dodecane. The larger deposit allowed for a larger surface area and volume for the stearic acid to diffuse into the gel layer and then precipitate.

Gelation Studies

Experiments were carried out on binary solutions containing either 4% C_{36} or 4% C_{32} and stearic acid in concentrations ranging from 0% to 8%. The results of these experiments can be seen in Figure 4.10. The results show that the pour point and gel point results fall on the exact same curves. However, it must be noted that this phenopmenon is purely coincidental: the cooling rates for the two experiments were different and the pour points are found statically while an oscillatory stress is applied in order to find the gel point. If the cooling rates were different and/or the applied oscillatory stress was different, the values would be different and not relatively identical. The most important point to note is that two separate methods used to measure the gelation properties of a system both had similar trends.

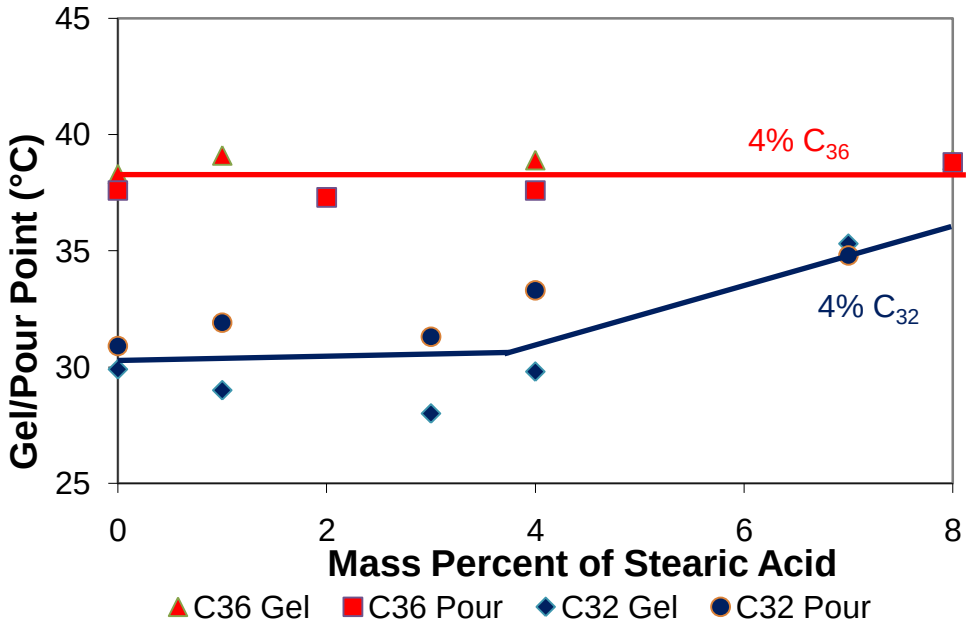

Figure 4.10: The effect of varying the mass percent of stearic acid on the gelation properties of 4% C_{36} and 4% C_{32} solutions in dodecane. ▲and ♦ represent the gel points of the solutions containing C_{36} and C_{32} respectively and ■ and ● represent the pour points of the solutions containing C_{36} and C_{32} respectively.

The trends shown for C_{36} and for C_{32} are quite similar from 0 to 4%, but deviate at concentrations higher than 4% where the C_{36} curve remains flat, but the C_{32} curve increases as the stearic acid concentration increases. At stearic acid concentrations below 4%, C_{36} and C_{32} are both less soluble than stearic acid. Chapter 3 showed that more soluble components can greatly inhibit the ability of an n-alkane to form a gel if the component can associate with the crystallizing n-alkane and is sufficiently large enough to act as a blockade between the C_{36} crystals from interacting with one another. Preventing this interaction inhibits the formation of a volume spanning network of solid crystals, which is the definition of a gel. Because stearic acid undergoes dimerization in solution, the molecule would be large enough to impact the gelation properties of the system. The strong hydrogen bonding that exists between stearic acid molecules prevents them from associating with the n-alkane. Therefore, the n-alkanes will crystallize and form a gel independently of stearic acid until sufficient stearic acid is present so that it will crystallize out at a similar temperature as the n-alkane. The difference in solubility between stearic acid and C_{36} is large enough such that even at 8% stearic acid, 4% C_{36} is still less soluble and therefore the gel point and pour point remain relatively independent of stearic acid concentration. However, for the 4% C_{32}/x% stearic acid systems, stearic acid will become less soluble than C_{32} at a stearic acid concentration of around 4%. Therefore, as the stearic acid concentration is increased, an increase in the cloud point will be seen because more of stearic acid, the least soluble material, is present. An increase in the wax appearance temperature causes the gel point and pour point to increase.

Summary

This work has analyzed how an organic non n-alkane can influence a wide range of thermodynamic, deposition and gelation properties of a crystallizing n-alkane in an n-alkane solute. Although stearic acid, a straight chained carboxylic acid, dimerizes in solution such that its size and its solubility in an n-alkane solvent resembles a long chained n-alkane, it behaves much differently than the long chained n-alkane. Differential scanning calorimetry results show that C_{32} is capable of cocrystallizing with C_{36}, but stearic acid at any concentration is unable to cocrystallize with either C_{32} or C_{36}. Deposition experiments carried out using a coldfinger apparatus showed that while adding C_{32} to a C_{36} solution inhibits the formation of a deposit, adding stearic acid to a C_{36} solution does not slow deposition and at high concentrations of stearic acid can actually increase the amount of deposit that forms. Further, the deposition of C_{32} was influenced by stearic acid only when stearic acid was present in sufficient concentration such that it was less soluble than C_{32}. Rheometric experiments showed that adding C_{32} to C_{36} caused a decrease in the pour point for a wide range of concentration whereas adding stearic acid to C_{36} did not affect the gelation characteristics. Similar to the deposition results, stearic acid only influenced C_{32} when stearic acid was the least soluble component.

The major reason for the differences seen between C_{32} and stearic acid is the hydrogen bonding that exists between the carboxylic acid groups of stearic acid molecules. This strong hydrogen bonding causes strong self-association between the stearic acid molecules, causing a minimization of association between the stearic acid molecules and the crystallizing n-alkane molecules. Because the stearic acid molecules

are not interacting with the n-alkanes, the ability of the n-alkane to crystallize, deposit and gel are not greatly influenced by stearic acid unless stearic acid is present in sufficient quantities such that its solubility is similar to or less than its n-alkane counterpart.

References:

Ashbaugh, H.S., Fetters, L.J., Adamson, D.H., and Prud'homme, R.K., "Flow Improvement of Waxy Oils Mediated by Self-Aggregating Partially Crystallizable Diblock Copolymers", *J. Rheol*, **46**, 763-776 (2002)

Ashbaugh, H.S., Radulescu, A., Prud'homme, R.K., Schwahn, D., Richter, D. and Fetters, L.J., "Interaction of Paraffin Wax Gels with Random Crystalline/Amorphous Hydrocarbon Copolymers", *Macromolecules*, **35**, 7044-7053 (2002)

Beckmann, W., "Growth Kinetics of the (001) and (110) Faces of the B Modification of Stearic Acid Growing From n-Alkanes", *J. Cryst. Growth*, **79**, 797-800 (1986)

Dirand, M., Bouroubka, M., Chevalier, V., Petitjean, D., Behar, E. and Ruffier-Murray, V., "Normal Alkanes, Multialkane Synthetic Model Mixtures and Real Petroleum Waxes: Crystallographic Structures, Thermodynamic Properties and Crystallization", *J. Chem. Eng. Data*, **47**, 115-143 (2002)

Garcia, M.d.C., "Crude Oil Wax Crystallization. The Effect of Heavy n-Paraffins and Flocculated Asphaltenes", *Energy & Fuels*, **14**, 1043-1048 (2000)

Garcia, M.d.C., Carbognani, L., Orea, M., Urbina, A., "The Influence of Alkane Class-Types on Crude Oil Wax Crystallization and Inhibitors Efficiency", *J. Pet. Sci & Engr.*, **25**, 99-105 (2000)

Guo, X., Pethica, B.A., Huang, J.S., Prud'homme, R.K., Adamson, D.H. and Fetters, L.J., "Crystallization of Mixed Paraffin from Model Waxy Oils and the Influence of Micro-Crystalline Poly(ethylene-butene) Random Copolymers", *Energy & Fuels*, **18**, 930-937 (2004)

Hansen, A.B., Larsen, E.W., Pedersen, B. and Nielsen, A.B., "Wax Precipitation from North Sea Crude Oils. 3. Precipitation and Dissolution of Wax Studied by Differential Scanning Calorimetry", *Energy & Fuels*, **5**, 914-923 (1991)

Hansen, J.H., Pedersen, K.S. and Ronningsen, H.P., "A Thermodynamic Model for Predicting Wax Formation in Crude Oils", *AICHE J.*, **34**, 1937-1942 (1988)

Hennessy, A.J., Neville, A. and Roberts, K.J., "An Examination of Additive-Mediated Wax Nucleation in Oil Pipeline Environments", *J. Cryst. Growth*, **198/199**, 830-837 (1999)

Jennings, D.W. and Weispfennig, K., "Experimental Solubility Data of Various n-Alkane Waxes: Effects of Alkane Chain Length, Alkane Odd versus Even Carbon Number Structures and Solvent Chemistry on Solubility", *Fluid Phase Equlibria.* **227**, 27-35 (2005)

Kern, R. and Dassonville, R., "Growth Inhibitors and Promoters Exemplified on Solution Growth of Paraffin Crystals", *J. Cryst. Growth*, **116**, 191-203 (1992)

Liu, X.-Y. and Bennema, P., "On the Morphology of Crystals of Triclinic Even Normal Alkanes: Theory and Observation", *J. Cryst. Growth*, **135**, 209-223 (1994)

Machado, A.L.C., Lucas, E.F. and Gonzalez, G., "Poly(ethylene-co-vinyl acetate) (EVA) as Wax Inhibitor of a Brazilian Crude Oil: Oil Viscosity, Pour Point and Phase Behavior of Organic Solutions," *J. Pet. Sci. & Engr.*, **32**, 159-165 (2001)

Paso, K.G. and Fogler, H.S., "Influence of n-Paraffin Composition on the Aging of Wax-Oil Gel Deposits", *AICHE J.*, **49**, 3241-3251 (2003)

Paso, K. and Fogler, H.S., "Bulk Stabilization in Wax Deposition Systems", *Energy & Fuels*, **18**, 1005-1013 (2004)

Paso, K., Senra, M., Yi, Y., Sastry, A.M. and Fogler, H.S., "Paraffin Polydispersity Facilitates Mechanical Gelation", *Ind. Eng. Chem. Res.*, **44**, 7242-7254 (2005)

Qian, J.W., Qi, G.R, Han, L.D. and Yang, S.L., "Influence of Incipient Chain Dimension of EVA Flow Improver on the Rheological Behaviour of Crude Oil", *Fuel*, **75**, 161-163 (1996)

Sangwal, K., "Effects of Impurities on Crystal Growth Processes", *Prog. Cryst. Growth and Charact.*, **32**, 3-43 (1996)

Schmidt, W.F., Barone, J.R., Francis, B. and Reeves III, J.B., "Stearic Acid Solubility and Cubic Phase Volume", *Chem. & Phys. of Lipids* **142**, 23-32 (2006)

Singh, P., Fogler, H.S. and Nagarajan, N.R., "Prediction of the Wax Content of the Incipient Wax-Oil Gel in a Pipeline: an Application of the Controlled Stress Rheometer", *J. Rheol.*, **43**, 1437-1459 (1999)

Singh, P., Venkatesan, R., Fogler, H.S. and Nagarajan, N.R., "Formation and Aging of Incipient Thin Film Wax-Oil Gels", *AICHE J.*, **46**, 1059-1074 (2000)

Turner, W.R., "Normal Alkanes", *Ind. Eng. Chem. Prod. Res. Develop*., **10**, 238-260 (1971)

Venkatesan, R., Singh, P. and Fogler, H.S., "Delineating the Pour Point and Gelation Temperature of Waxy Crude Oils", *SPE J.*, 349-352 (2002)

Venkatesan, R., Nagarajan, N.R., Paso, K., Yi, Y., Sastry, A.M. and Fogler, H.S., "The Strength of Paraffin Gels Formed under Static and Flow Conditions", *Chem. Eng. Sci.*, **60**, 3587-3598 (2005)

Wang, K-S., Creek, J.L., Shuler, P.J. and Tang, Y., “Evaluation of Effect of Selected Wax Inhibitors on Wax Appearance and Dissolution Temperatures”, Proceedings of the 2002 AICHE Spring National Meeting (2002)

CHAPTER V

CONCLUSIONS

This dissertation has provided a fundamental look at how the composition of oil impacts the crystallization, deposition and gelation of n-alkanes in n-alkane solutions. Through the use of a wide number of techniques: thermal analysis via visual inspection, densitometry and differential scanning calorimetry, deposition analysis via a coldfinger apparatus and gelation analysis via visual inspection, rheometry and cross-polarized microscopy, the importance of polydispersity, cocrystallization, solubility and molecular size and type on crystallization, deposition and gelation have been established. Although the systems used in this research are less complex than typical crude oils, the conclusions developed in this work provide fundamental insight into some of the concerns faced by the petroleum industry and can be used for the more complex fluids they handle on a daily basis. The immediate developments of this research are primarily in the realms of thermodynamic modeling of wax deposition, modeling of the resultant gel layer and the development of wax inhibitors. However, a major contribution of this research is that it has laid the groundwork for a wide array of continuing work that can extend this research into even more facets of the petroleum industry. These developments will be discussed in further detail in the following chapter.

Thermodynamic and Kinetic Wax Deposition Modeling

Cocrystallization and polydispersity are issues that must be accounted for when developing appropriate thermodynamic models because both influence the thermodynamics of lower carbon numbers. Materials that are able to cocrystallize with less soluble materials will precipitate at a higher temperature than predicted from solely evaluating their solubility limit. The solubility of the more soluble component becomes dependent on the less soluble component or components that are in the cocrystal. This work has confirmed limitation exists in the composition of cocrystals, based on the criteria set by Turner: molecular size, molecular type and crystal shape when the material self crystallizes in solution (Turner, 1971). For n-alkanes, this limit is dependent on the molecular size of the n-alkanes: longer chained n-alkanes will be capable of cocrystallizing with a wider range of n-alkanes than shorter chained n-alkanes. The major reason is the difference in the molecular length of an n-alkane with a carbon number C_n to the molecular length of an n-alkane number with a carbon number C_{n-2} (C_{n-2} is used because this work has confirmed that although even and odd numbers may be part of a common solid solution, they will not cocrystallize together.). The ratio of the sizes is smaller for higher carbon numbers than for lower carbon numbers. To emphasize this point, Figure 5.1 shows the value of this ratio for a carbon number, C_n, using a correlation for the half length of a carbon chain that is relatively independent of the crystal shape of the n-alkane provided by Dirand (Dirand, et al., 2002).

$$c/2 = 1.2724C_n + 1.8752 \qquad (5.1)$$

Where: c = length of crystallographic c parameter (Angstroms)
C_n = carbon number

Figure 5.1 shows that as the carbon number increases, the difference in size between a molecule with carbon number C_n and a molecule with carbon number C_{n-2} changes from about 15% to about 4% for carbon numbers ranging from 15 to 50. For small carbon numbers, it is physically impossible for a crystal structure to contain a wide range of n-alkanes because of the drastic difference in size between the n-alkanes.

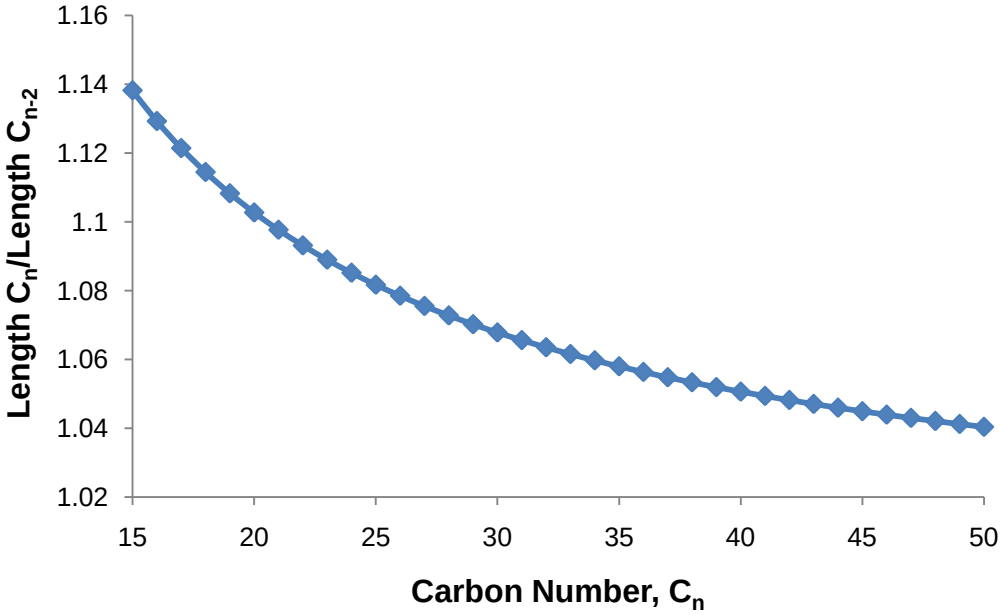

Figure 5.1: Ratio of molecular length for an n-alkane with a carbon number C_n and to an n-alkane with a carbon number C_{n-2} as a function of C_n.

Kravchenko developed his rules for partial and total miscibility of n-alkanes. His results (Table 5.1) show that miscibility is a function of both molecular size and carbon number difference.

Table 5.1: Kravchenko's predictions for miscibility of solid solutions of binary mixtures. Δn represents the difference in carbon number between the two components of the mixture (Dirand et al., 2002). [a] In order for miscibility to occur, the crystalline structures must be identical (for total miscibility) or similar (for partial miscibility)

	Miscibility of Solid Solutions		
Δn	**Total**	**Partial**	**None**
1[a]	n≥17	8<n<17	n≤7
2	n≥34	14<n<34	n≤13
4	n≥68	28<n<68	n≤27

Although Kravchenko focused on solid solutions, this work has shown that his conclusions can be extended to n-alkanes crystallizing in n-alkane solvents.

Unlike the systems used in this research, crude oils will contain consecutive carbon number n-alkanes over a wide range of carbon numbers, meaning that the difference in carbon number will be one and not the higher numbers used in this research. However, this research has shown that cocrystallization is based on the highest carbon number or average carbon number of the n-alkanes present in the cocrystal. Although C_{36} is capable of cocrystallizing with C_{32} and C_{32} is capable of cocrystallizing with C_{28}, C_{36} and C_{28} did not cocrystallize with one another. Therefore, crude oils will contain a large number of different cocrystals. These cocrystals associate and interlock with one another to allow the solid crystals to form a gel. As time progresses, further precipitation will only strengthen the gel, making it more difficult to remediate. To properly predict gel formation, it is crucial to model how both the crystals precipitate out of solution and the composition of the cocrystals.

Thermodynamic models have mostly ignored the interaction effects between the respective n-alkanes and have treated each n-alkane as an independent component. Initial work focused on individual solid/liquid equilibrium for each component, taking into account the Gibbs free energy needed to transition from the liquid phase to the solid phase (Won, 1986). In developing his model, Hansen included a binary interaction parameter that was related to the sum of interactions between a carbon atom of one molecule and a carbon atom of another molecule and later fine tuned the model to better handle the enthalpy change of wax crystallization (Hansen, et al., 1988, Pedersen et al., 1991). However, this work, along with extensive work by Coutinho using activity

coefficient models such as NRTL and UNIQUAC do not completely account for the change in solubility of an n-alkane that undergoes cocrystallization (Coutinho et al., 1995, Coutinho, 1999). Instead, it breaks the deposit into multiple phases containing both even and odd carbon numbers, more accurate than the previous work, but it does not account for cocrystallization in explaining how deposits develop (Heidemann et al., 2005). This research has shown that a compositional model that takes into account not only multiple solid phases but also multiple cocrystals is necessary to properly understand deposition and gelation. This fact becomes more crucial as kinetic models are developed to understand both the crystallization and gelation kinetics of the wax deposit, a point noted recently by Coutinho (Coutinho, 2006).

This work has shown that oil composition plays a very important role in the ability of an n-alkane system to form a gel. Because crude oil contains a continuum of carbon numbers, many at compositions lower than the ones used in this research, the effects would not be expected to be as drastic as the ones seen in this research. However, the mechanisms shown in this work for both polydispersity and cocrystallization will be present in crude oil and must be taken into account when developing a kinetic model for understanding the growth of a gel. The ability to determine the components of a cocrystal will allow for the proper estimation of crystal size, a crucial piece of information for determining gelation. Furthermore, this research has shown that the interaction between different cocrystals and between the crystals and molecules still present in the liquid phase can also greatly influence crystal size.

Understanding Wax Inhibitors and Additives

In the wax inhibitor literature, it is often discussed how the efficacy of an inhibitor is dependent not only on the properties of the inhibitor but also the properties of the crude oil (Garcia, et al., 2000). The inhibitor properties of interest include but are not limited to concentration, backbone chain length, side chain length and functional groups while the crude oil properties of interest include but are not limited to wax content, carbon number distribution, asphaltene content, resin content and temperature. This work shows that the composition of the oil can self-inhibit the formation of a wax-oil gel. This fact emphasizes that the composition of oil is crucial in selecting and developing appropriate wax inhibitors and additives. Crude oil deposits consist of a large number of solid solutions and distinct cocrystals, an effect not seen in this work because of simplicity of the systems used. Previous work has shown that one wax inhibitor will be unable to influence all of the cocrystals because of the differing carbon lengths present in each cocrystal: inhibitors generally can only influence a certain range of carbon numbers (Kuzmic, et al., 2007). Therefore, the efficacy of the inhibitor will be dependent on which cocrystals it can interact with and how important these particular cocrystals are in the thermodynamic, deposition and gelation characteristics of the wax-oil gel.

This research shows the importance of cocrystallization and how it drastically impacts crystal morphology when compared to a single component crystal. Currently, most fundamental research has been focused on understanding how wax inhibitors such as diblock copolymers and microcrystalline poly(ethylene butane) effect monodisperse crystals ranging from C_{24} to C_{36} in decane (Ashbaugh et al., 2002a, 2002b, Guo et al., 2004, 2006). However, when attempting to understand the mechanisms by which a wax

inhibitor works, systems where cocrystallization occurs are necessary. Otherwise, the mechanism that inhibited the growth or formation of C_{36} crystals may not be applicable to a system containing both C_{36} and C_{32} or a system containing a continuum of n-alkanes. This work has shown that multiple carbon numbers must be taken into account when completing this analysis because of the major differences that exist between the formation of single component crystals and multi-component cocrystals.

Finally, the work on stearic acid has shown the effect functional groups have on wax inhibition. Stearic acid is capable of influencing thermodynamics, deposition and gelation only when present in sufficiently high concentrations such that it less soluble than the n-alkane in the solvent. At low concentrations (concentrations much higher than those at which wax inhibitors are typically added), stearic acid did not affect the crystallization of C_{36} and C_{32}. The major reason why stearic acid did not impact the n-alkanes was because of its strong ability to self-associate due to hydrogen bonding. Therefore, stearic acid, along with other straight chained carboxylic acids would make terrible wax inhibitors. However, the strong self association of the carboxyl groups could prove to be very beneficial in developing wax inhibitors because they can cluster and disrupt the formation of crystals and therefore the formation of a gel. However, for these to be useful inhibitors, additional groups would have to be added to the carboxylic acid such that either the molecule is less willing to associate with itself and/or more willing to associate with other molecules. Previous work has shown that the addition of more carbon chains either as a branch or as a replacement for hydrogen in a hydroxyl group can help in improving the interaction with n-alkane molecules (Wang, et al., 2002, Guo, et al., 2004).

References:

Ashbaugh, H.S., Fetters, L.J., Adamson, D.H. and Prud'homme, R.K., "Flow Improvement of Waxy Oils Mediated by Self-Aggregating Partially Crystallizable Diblock Copolymers", *J. Rheol.,* 46, 763-776 (2002)

Ashbaugh, H.S., Radulescu, A., Prud'homme, R.K., Schwahn, D., Richter, D., and Fetters, L.J., "Interaction of Paraffin Wax Gels with Random Crystalline/Amorphous Hydrocarbon Polymers", *Macromolecules,* 35, 7044-7053 (2002)

Coutinho, J.A.P., Andersen, S.I. and Stenby, E.H., "Evaluation of Activity Coefficient Models in Prediction of Alkane Solid-Liquid Equilibria", *Fluid Ph. Equil.,* 103, 23-39 (1995)

Coutinho, J.A.P., "Predictive Local Composition Models: NRTL and UNIQUAC and Their Application to Model Solid-Liquid Equilibrium of n-Alkanes", *Fluid Ph. Equil.,* 158-160, 447-457 (1999)

Coutinho, J.A.P., "Reliable Wax Predictions for Flow Assurance", *Energy & Fuels,* 20, 1081-1088 (2006)

Dirand, M., Bouroukba, M., Chevallier, V., Petitjean D., Behar, E. and Ruffier-Meray, V., "Normal Alkanes, Multialkane Synthetic Model Mixtures and Real Petroleum Waxes: Crystallographic Structures, Thermodynamic Properties and Crystallization", *J. Chem. Eng. Data,* 47, 115-143 (2002)

Garcia, M.d.C., Carbognani, L., Orea, M. and Urbina, A., "The Influence of Alkane Class-Types on Crude Oil Wax Crystallization and Inhibitors Efficiency", *J. Pet. Sci. & Engr,* 25, 99-105 (2000)

Guo, X., Pethica, B.A., Huang, J.S., Prud'homme, R.K., Adamson, D.H. and Fetters, L.J., "Crystallization of Mixed Paraffin from Model Waxy Oils and the Influence of Micro-crystalline Poly(ethylene-butene) Random Copolymers", *Energy & Fuels,* 18, 930-947 (2004)

Guo, X., Pethica, B.A., Huang, J.S., Adamson, D.H. and Prud'homme, R.K., "Effect of Cooling Rate on Crystallization of Model Waxy Oils with Microcrystalline Poly(ethylene butane)", *Energy & Fuels,* 20, 250-256 (2006)

Hansen, J.H., Pedersen, K.S. and Ronnigsen, H.P., "A Thermodynamic Model for Predicting Wax Formation in Crude Oils", *AIChE J.,* 34, 1937-1942 (1988)

Heidemann, R.A., Madsen, J., Stenby, E.H. and Andersen, S.I., "Wax Precipitation Modeled with Many Mixed Solid Phases", *AIChE J.,* 51, 298-308 (2005)

Kuzmic, A.E., Radosevic, M., Bodganic, G., Srica, V. and Vukovic, R., "Studies on the Influence of Long Chain Acrylic Esters Polymers with Polar Monomers as Crude Oil Flow Improver Additives", *Fuel*, 87, 2943-2950 (2008)

Pedersen, K.S., Skovborg, P. and Ronnigsen, H.P., "Wax Precipitation from North Sea Crude Oils. 4. Thermodynamic Modeling", *Energy & Fuels*, 5, 924-932 (1992)

Turner, W.R., "Normal Alkanes", *Ind. Eng. Chem. Prod. Res. Develop.*, 10, 238-260 (1971)

Won, K.W., "Thermodynamics for Solid-Liquid Equilibria: Wax Phase Formation from Heavy Hydrocarbon Mixtures", *Fluid Ph. Equil.*, 30, 265-275 (1986)

Wu, C-H., Wang K-S., Shuler, P. J., Tang, Y., Creek, J. L., Carlson, R. M., and Cheung, S., "Measurement of Wax Deposition in Paraffin Solutions", *AICHE J.*, **48**, 2107-2110 (2002)

CHAPTER VI

FUTURE WORK

The fundamental nature of this research combined with the large number of properties that influence crude oil crystallization, deposition and gelation in subsea pipelines that need a more in-depth understanding makes the possibilities to expand upon this research almost limitless. However, some major areas should be investigated first because additional research could provide an immediate and indelible impact in the petroleum industry. These areas: analysis for more complex systems, gel strength, wax additives/inhibitors, molecular simulations for binary/ternary systems and incorporation of polydispersity in wax deposition modeling are discussed in further detail in this section.

Analysis for More Complex Systems

This research is one of the first to explore how the composition of the oil can greatly influence the characteristics of wax-oil gels seen in subsea oil pipelines. However, the systems used for this research were rather simplistic, primarily focusing on n-alkanes in n-alkane solvents. Actual crude oil systems are far more complex, containing hundreds or even thousands of different components, each of which can impact crystal growth and gel formation (Sangwal, 1996). Although an almost infinite number of ways to conduct this research exist, below are areas of greatest interest. Experiments similar to the ones conducted in this research and those mentioned later in this section could be completed to

investigate these areas.

1.) *Continuous n-alkane systems:* Although this research has accounted for solutions where cocrystaliization between two n-alkanes occur, these cocrystals are much simpler than what is seen in deposits because a continuous set of n-paraffins are present in crude oils (Briard et al., 2006). Wax-oil gels generally contain a number of crystal structures, each containing a number of n-alkanes that cocrystallize with one another, a phenomenon not studied in this research (Dirand et al., 1998). Work has shown that crystal size decreases as the composition of the system becomes more complex, which would influence gelation (Anderson, et al., 2001). An appropriate method of developing such an n-alkane system has been discussed by Paso, where the relative concentrations of the respective n-alkanes are related by a recurrence relationship (Paso, et al., 2006). Initial research could focus on a small continuum of carbon nuumbers (4-8) before expanding to distributions more commonly seen in petroleum.

2.) *Non n-alkane components:* Although n-paraffins are the primary components in wax deposits, they are not the only constituents of the deposit. Branched paraffins and aromatic hydrocarbons are also present in smaller amounts in the deposit (Garcia, 2000). Depending on the crystal shape and solubility of these components, it may be possible for some of these compounds to cocrystallize within a polydisperse n-alkane crystal structure. Initially, work would focus on adding branched alkanes and aromatics, particularly those known to cocrystallize with the n-alkanes used in this research. However, further investigations could incorporate asphaltenes, resins and water, components known to influence the thermodynamic and gelation properties of the deposit (Fuhr et al., 1999, Visintin et al., 2008).

3.) *Solvent:* Although the solvent remains in the liquid phase during wax deposition, it is a crucial part in dictating both the thermodynamics of crystallization and the formation of the wax-oil gel. However, the role of the solvent in crude oil systems has not been extensively studied. The solubility of an alkane or group of alkanes in a particular solvent is dictated by a number of properties including functional groups, polarity, molecular volume and molecular weight (Haulait-Pirson et al., 1987). The more soluble a wax is in a solvent, the lower the cloud point and the amount of wax present at higher temperatures. Work has shown that different solvents have drastically different abilities to form gels (Abdallah and Weiss, 2000). For example, a 0.04M C_{28} system does not gel in heptane, decane and dodecane, but does gel in octanol, ethyl acetate and ethanol at approximate temperatures of 29.5, 33 and 46 degrees Celsius respectively. Because of this, solute-solvent interactions are a major component of any crystallization model, which is discussed in more detail later on in this chapter. Therefore, work could be conducted using longer chained solvents and more complex solvents that contain more complex hydrocarbons.

Gel Strength

This work has conclusively shown that polydispersity and cocrystallization impact the formation of a gel, namely the temperature at which gelation occurs. Another important aspect of the gel is the strength of the gel. The strength of a deposited gel increases over time for two reasons. The first reason is that time allows for greater interactions between the crystals inside the gel with both the solvent and the crystals themselves. The second and more important reason is the aging, where the deposit becomes waxier with the diffusion of higher carbon number alkanes into the deposit and

the counterdiffusion of lower carbon number alkanes out of the deposit (Singh et al., 2000). The ability to model how gel strength changes over time is necessary for proper wax remediation.

As time goes on, the deposit, in addition to becoming stronger, will also grow in size, reducing oil flow and can completely block the pipeline if left untreated. Mechanical pigs are sent into the pipeline to remove the wax from the pipeline wall. However, if the wax becomes too hard, the pigs could become unable to break the gel and get stuck in the pipeline, causing further blockage. To prevent this issue from happening, petroleum companies have utilized a conservative pigging schedule. However, this conservative pigging schedule comes at an expense to the companies. Therefore, a better understanding of the formation of a gel will allow for optimization of the pigging schedule.

To properly understand the strength of the gel, the process by which a gel breaks must be understood. Boger has provided insight into the yielding mechanism of waxy crude oils (Wardhaugh and Boger, 1991, Chang et al., 1998). The yielding process has been broken down into three regimes: elastic response, creep and fracture. In the elastic response regime, the wax deposit acts as a Hookean solid. In the creep phase, the wax-oil gel is being slowly deformed and the internal structure is slowly being broken down. Finally, the fracture regime represents the breaking of the solid and the transition to a liquid. The transition from the creep to fracture regime is very sharp and abrupt. Experimentally, this transition can be seen by a sharp decrease in the viscosity as the shear stress is increased or a sharp decrease in G’ and G” as the stress amplitude is varied. The stress necessary to break a wax-oil gel is commonly referred to as the yield stress.

The yield stress is dependent on a number of variables, many independent of oil composition. Early work showed that both themal history and shear history can impact the rheological behavior of a crude oil (Petrellis and Flumerflet, 1973). Further work has shown that the yield stress is dependent on variables such as the cooling rate, the final temperature the gel is held at before some sort of force is applied, the magnitude of the applied stress, the rate of change of the applied stress, and the strain rate (Chang et al., 2000, Venkatesan et al., 2005).

The ability of a gel to maintain its solid-like characteristics is greatly dependent on the strength and amount of interactions between the wax crystals in the deposit. Although thermal treatment impacts the shape and number of crystals that form, the properties of the crude oil greatly influence both the crystals and the resulting gel network (Chang et al., 2000, Venkatesan et al., 2005). Properties of the oil that can influence the yield stress include the cloud point, the gel point, the wax fraction, the amount of asphaltenes and/or resins present, the presence of water and the presence of additives. One of the mechanisms by which wax inhibitors act is by disrupting these crystal interactions, reducing the strength of the gel as seen in a lower yield stress (Ashbaugh et al., 2002a, 2002b, Guo et al., 2004, 2005, Kuzmic et al., 2008). The further study of wax inhibitors as a future aim of this research will be discussed later.

Paso has provided some initial insight into how polydispersity influences the strength of a gel (Paso et al., 2005). His work showed that a polydisperse system can form stronger gels than a monodisperse system because the sharp, ordered crystals typically seen in monodisperse systems hinders the formation of strong crystal-crystal interactions required to form a strong gel. However, this work is not extensive and does

not evaluate the effects of cocrystallization and independent crystallization that have been shown in this work to impact gel properties.

An issue brought up by the work of Paso is that monodisperse gels may not be very strong and could be broken without much very stress being applied. Therefore, it could be difficult to obtain a yield stress for these gels, which has been confirmed by early work conducted using a cone and plate rheometer. This issue can be overcome in one of two ways: (1) optimizing the operating conditions of the yield stress test such as temperature, shear rate, etc. and (2) using a rheometer such as a Haake or vane rheometer, which have been shown to be more suitable to obtain yield stresses (Wardhaugh and Boger, 1991).

Wax Additives/Inhibitors

Although this work is the first to show how n-alkanes impact the crystallization and gelation of n-alkanes, a large amount of research has been completed in a parallel area: wax additives. Wax additives are materials added to crude oil to alter the properties of the crude. These include but are not limited to wax inhibitors, pour point depressants and flow improvers. n-Alkanes have been shown in this work to act like certain wax additives (although in much greater concentrations than typical wax additives) by altering the properties of crystallizing n-alkanes. Inhibitors such as polalkyleneimines and polymethacrylates can influence the solubility of n-alkanes in n-alkane solvents, similar to the results presented in this work (Wang et al., 2002). A sequestration mechanism has been discussed by Jang to show that inhibitors alter the solubility by associating with the longer chained paraffins (Jang et al., 2007). Similarly, both n-alkanes and certain wax

inhibitors such as poly(ethylene-butene) random copolymers, polymethacrylates, ethylene vinyl acetate copolymers can act as pour point depressants (Wang et al., 2002, Guo et al., 2004, 2006, Soldi et al., 2007, Taraneh et al., 2008). Mechanisms to explain how these inhibitors work are varied: most notable are the ability for an inhibitor to incorporate into the crystal structure and perturb the aggregation of wax molecules, to adsorb onto the wax crystals to block the growth of hard deposits and to sterically hinder the ability of wax molecules to aggregate without incorporating to the crystal structure. Finally, this work has shown that n-alkanes, like wax inhibitors, can act as crystal modifiers, generally decreasing the size of the wax crystals (Guo et al., 2004, 2006). A reduction in crystal size makes it harder for the crystals to aggregate together and form a crystal network, a necessity to form a gel.

Because this work is unique in its analysis of n-alkane polydispersity, very little academic work has been conducted in assessing wax inhibitors with polydisperse n-alkane solutions to allow for a better mechanistic understanding of wax inhibitors. Wax inhibitor studies have generally fallen into two areas. The first area is using wax inhibitors on crude oils (Qian et al., 1996, Wang et al., 2002, Soldi et al., 2007, Kuzmic et al., 2008, Taraneh et al., 2008). Although these works can assist in proper selection of wax inhibitors based on the properties of the oil, little fundamental understanding can be obtained from these works. The other realm of investigation has focused on using wax inhibitors on monodisperse systems (Ashbaugh, et al., 2002a, Guo et al., 2004, 2006). Although gaining mechanistic understanding from these works is feasible, the authors have generally not provided a fundamental understanding into the interaction between the n-paraffin and the wax inhibitor. Additionally, the wax crystals that precipitate out of

these solutions are all monodisperse, a situation not seen in crude oils.

The proposed experimentation would examine wax inhibitor efficacy on binary and ternary systems. Systems where cocrystallization occurs would be of greater interest because of the difference between the morphology of monodisperse crystals and more complex cocrystals. For example, would an inhibitor that is highly effective in modifying C_{36} is crystals be equally effective for C_{36}/C_{32} cocrystals? Systems where cocrystallization does not occur would also be of interest because of the potential for the wax inhibitor to be influenced by the presence of another n-alkane. For example, would the aforementioned inhibitor that impacts C_{36} have a change in efficacy because of the presence of C_{28}? The experimentation completed in this work would provide an effective investigation for this work: the coldfinger apparatus to examine deposition effects, cross-polarized microscopy to examine crystal morphology, differential scanning calorimetry to examine thermodynamic effects and rheometry to explore gelation effects. Inhibitor selection will be extremely important in developing this research because no inhibitor is universally effective (Wang et al., 2002). The efficacy of an inhibitor is not only based on its composition (i.e. length of backbone chain, number of functional groups, types of functional groups, length of functional groups) but also the concentration of the inhibitor and the composition of the crude oil itself.

A few other properties discussed in the inhibitor literature not analyzed in this work that would also be of great interest. As discussed earlier, a variable of interest would be the shear stress, a variable examined in many inhibitor studies (Ashbaugh et al., 2002a, 2002b, Guo et al., 2004, Kuzmic et al., 2008). Many wax additives have been shown to be effective flow improvers, primarily by reducing the viscosity of the solution

(Qian et al., 1995, Dong et al., 2001, Kuzmic et al., 2008, Taraneh et al., 2008). Both of these properties can be explored by use of rheometry. The information obtained from this research could provide a greater mechanistic understanding and be extended to more complex systems.

Molecular Simulations of Binary/Ternary Systems

Cross polarized microscopy has provided a crystal level view of the systems and has shown how composition can affect the overall morphology of the crystals. However, microscopy does not allow for a molecular level view of how the molecules are aggregating together and forming either single crystals or multicomponent crystals via cocrystallization. To obtain a molecular level view, molecular simulations could be used.

Molecular simulations must account for a number of parameters such as crystal (solute) properties, solvent properties, solvent-solute and solute-solute interaction parameters, crystal growth kinetics, transport properties and the degree of supersaturation. Because so many parameters must be taken into account, a significant limitation in using molecular simulations for crude oil systems is the massive computational intensity needed for a mixture such as crude oil. However, work has been conducted on much simpler organic systems and a few of these developments will now be discussed.

Some of the first successful computational work was completed by Liu and Bennema (Bennema et al., 1992, Liu and Bennema, 1993, 1994). In these works, statistical mechanics were used to investigate interfacial interactions between the crystal and the solute and were combined with kinetic growth models and solvent-crystal physical properties obtained from either experimentation or molecular dynamics to predict crystal shapes for systems such as n-C_{24} and n-C_{16} in hexane. To make these

calculations less computationally intensive, Winn and Doherty used pure component properties and an attachment energy model to determine the interfacial interactions between the crystal and the solute (Winn and Doherty, 1998, 2000). In the attachment energy model, the intermolecular forces (primarily Van der Waals repulsive and attractive forces and electrostatic forces) are summed together to find the lattice energy, which obeys the following relationship.

$$E_{latt} = - \Delta H_{sub} - 2RT \qquad (6.1)$$

Where: E_{latt} = lattice energy (kJ/mol)
ΔH_{sub} = heat of sublimation (kJ/mol)
R = universal gas constant (kJ/mol K)
T = temperature (K)

This model has been used to predict the crystal shape of a wide number of organic solvent/solute combinations, most notably the growth of flat biphenyl crystals in the presence of toluene, shapes generally seen in both crude oil systems and simpler n-alkane systems. The major issue with these models is that only single crystal growth is taken into account, ignoring the presence of other n-alkanes present in the solution. However, this work could provide an entry point into simulating the simpler systems used throughout this work.

Using the fact that crystals grown from solvents that are chemically similar form thin crystals, van Hoof performed a Monte Carlo simulation for n-alkane solvent/n-alkane solute combinations (van Hoof et al., 1998a, 1998b). In a Monte Carlo simulation, the probability of breaking and creating a bond are determined and used to determine whether a bond is created, broken or maintained from the previous time step. These

probabilities are shown in Equations 6.2 and 6.3.

$$P^- = k_o \exp(-2i\varphi/kT),\ P^+ = k_0 \exp(-4\varphi/kT)\exp(\Delta\mu/kT) \qquad (6.2, 6.3)$$

Where: P- = probability of breaking a bond
P+ = probability of forming a bond
i = number of first-order nearest neighbors
φ = bond energy (J/mol)
k = Boltzmann constant (J/molec K)
Δμ = change in chemical potential (J/mol)

Δμ/kT represents the driving force and is found using the relationship below.

$$\Delta\mu/kT = (\Delta\mu/kT)^{\infty} - 2\varphi/LkT \qquad (6.4)$$

Where: $(\Delta\mu/kT)^{\infty}$ = driving force for the growth of an infinitely large crystal
L = width of the plate crystal (m)

By comparing their simulations to experimental results, appropriate bond energies were determined, which could be used for more complex systems.

The promising use of Monte Carlo simulations to simulate simple n-alkane systems along with the great potential of molecular dynamics has been used to develop better wax inhibitors. van Enckevort and Los completed work to make a broad class (not solely wax inhibitors) of "tailor-made" inhibitors (van Enckevort and Los, 2008). "Tailor-made" inhibitors retard the growth of particular crystal faces because of selective adsorption, causing a change in crystal morphology. These inhibitors are very similar to the crystal molecules they are modifying, but have a large chemical group on one end of the molecule that causes a change in bond energy because of steric repulsion. Their work showed that these type of inhibitors have the greatest impact on the flat faces of a crystal.

Duffy and Rodger have spearheaded the work for wax inhibitors for n-alkane systems (Duffy and Rodger, 2002a, 2002b). Their work has focused on chained polymers with varying functional groups. An example is modeling the inhibition of n-C_{28}

crystallizing in heptane by a poly(octadecyl acrylate) inhibitor. Molecular dynamics showed how the inhibitor adsorbed onto the (010) surface of a C_{28} crystal, which is shown below.

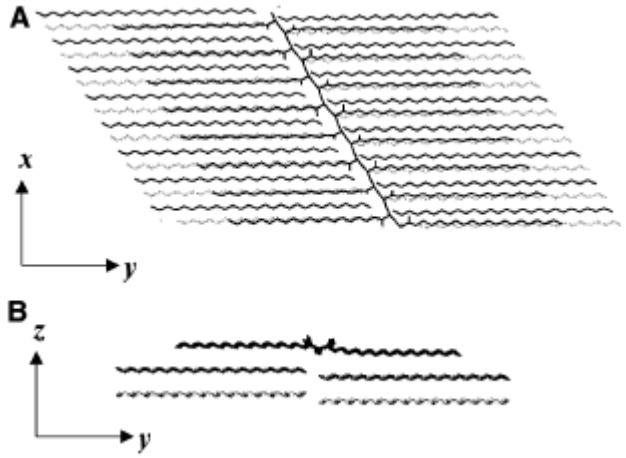

Figure 6.1: Top (a) and side (b) views of a poly(octadecyl acrylate) inhibitor adsorbed on a (010) surface of a C_{28} crystal. The inhibitor is represented in black, the top crystal layer is dark gray and the lower crystal layer is light gray. (from Duffy and Rodger, 2002a)

Using Monte Carlo simulations, this work showed that the inhibitor worked on C_{28} by reducing the growth of a particular crystal face of C_{28} . This reduction significantly limits the ability of these inhibitor affected agglomerates to attract other C_{28} crystals and further grow the crystal. The inhibitor is adsorbed onto the surface and creates a weak interaction between the inhibitor and surrounding crystals.

With molecular dynamics and Monte Carlo simulations, the solutions used in this work could be simulated with dodecane replacing heptane as the solvent and another n-alkane (or multiple n-alkanes) replacing the inhibitor. Although a significant learning curve is involved with properly using these methods and significant computational power is required, this research could provide further insight into the results, analysis and conclusions developed in this work.

Incorporation of Polydispersity Effects in Wax Deposition Modeling

The research presented in this work along with the proposed future work provides a solid backbone to improve the quality of wax deposition modeling. Wax deposition modeling requires the governing principles of thermodynamics, fluid mechanics, heat transfer, mass transfer and precipitation kinetics. Of these areas, the greatest advances this research could provide are in developing more reliable thermodynamic models.

Thermodynamic models for petroleum systems have been around for a lengthy period of time. Abrams and Prausnitz developed the UNIQUAC model that can be used for multicomponent systems that are either partly or completely miscible (Abrams and Prausnitz, 1975). The UNIQUAC model consists of two parameters dependent on structural parameters and deviation from random mixing for each binary combination of materials present in the solution. Although this model provides a starting point, it is severely limited by focusing only on the fluid phase and not rigorously analyzing the solid phase. Coutinho improved on the UNIQUAC model by changing the values of the structural parameters, accounting for the molecular difference between molecules in the fluid phase versus molecules in the solid phase (Coutinho, 1999). Although these models can reasonably match experimental data for relatively simple systems, they are limited by their inability to properly account for the solid phase and ignore the changes in thermodynamics that occurs because of polydispersity and cocrystallization.

Won's work was one of the first to incorporate solid/liquid equilibrium into a thermodynamic model for alkane systems (Won, 1986). Using the fact that the fugacity of the liquid and solid phase must be equivalent at equilibrium, a function can be derived

in terms of the equilibrium between the liquid and solid phases of a particular component.

$$K = \frac{S}{L} = \frac{\gamma_S}{\gamma_L} \exp\left[\frac{\Delta H_f}{RT}\left(1 - \frac{T}{T_f}\right)\right] \qquad (6.5)$$

Where K = solid/liquid equilibrium constant
S = solid phase
L = liquid phase
γ = activity coefficient of the respective phase
ΔH_f = heat of melting (kJ/mol)
T_f = melting point (K)

The activity coefficients were found by using modified solution theory and for many of the alkanes, the ratio of these coefficients was approximately one (Hansen et al., 1988). Therefore, the equilibrium ratios were almost solely dependent on the melting point and heat of melting of the pure components, making the wax appearance temperature dependent on the heaviest component present, independent of the entire composition of the oil, which is known to be false. Hansen built upon Won's model by making three noteworthy additions: (1) initially integrating the presence of non paraffins such as naphthenes and aromatic), (2) using Flory's generalized polymer solution theory to obtain liquid phase activity coefficients by use of a group interaction parameters and (3) beginning to account for the two stages of wax formation: nucleation and crystal growth (Hansen et al., 1993). Coutinho built upon this model by addressing the nonidealities in both the liquid (caused by entropic effects such as difference in size and energetics between dissimilar molecules) and solid (by introducing pair interactions which take into account physical considerations relating molecular interactions with macroscopic effects) phases (Coutinho, 1995, Coutinho and Ruffier-Murray, 1997). These models have done a relatively good job in matching somewhat complex solutions. However, current research has shown that the presence of higher carbon number n-alkanes increases the temperature

at which lower carbon number n-alkanes will change phase. Additionally, a number of crystal phases are actually present in very polydisperse n-alkane systems, each containing a different range of n-alkanes, a fact not accounted for in these models. Therefore, in order for appropriate, physically relevant thermodynamic models to be developed, they must account for (a) how nearby carbon numbers interact with one another and (b) the different crystal phases. The fact that numerous crystal phases are present in a crude system has been shown conclusively in work by Dirand (Dirand, et al., 2002, Briard et al., 2006).

Once a more rigorous thermodynamic compositional model can be developed, it can be incorporated into wax deposition models, which currently base most of their thermodynamic information on solubility curves. Although the complexity of crude oil makes a truly compositional model infeasible both in obtaining appropriate values and interaction parameters and its computational intensity, aspects of it could be integrated into a model either by the use of appropriate pseudo-components or incorporating some facets with a solubility curve when in-depth compositional information is unavailable.

Any useful wax deposition model for the petroleum industry must also provide some insight into the characteristics of the gel deposit that forms on the pipe wall. Using fundamental principles, Singh modeled the formation of gel deposits and their growth by accounting for the convective flux of wax molecules from the bulk to the gel and the diffusive flux into the gel at the gel interface (Singh et al., 2000). These relationships are provided below.

Rate of Change of Wax in Deposit:

$$\frac{d}{dt}\left[\pi(R^2 - r^2)\overline{F}_w(t)L\rho_{gel}\right] = 2\pi r_i L k_l\left[C_{wb} - C_{ws}(T_i)\right] \quad (6.6)$$

Growth Rate of Deposit:

$$\overline{F}_w(t)\rho_{gel}\frac{dr_i}{dt} = D_e\frac{dC_{ws}}{dr}\Big|_i - k_l\left[(C_{wb} - C_{ws}(T_i)\right] \quad (6.7)$$

Where: R = radius of the pipe (m)
r_i = radius of the deposit layer (m)
$\overline{F}_w$ = average mass fraction of the gel
ρ_{gel} = density of gel (kg/m^3)
L = length of the pipeline (m)
k_l = mass transfer coefficient (m/s)
C_{wb} = bulk concentration of the wax (kg/m^3)
C_{ws} = saturation concentration of the wax (kg/m^3)
T_i = interface temperature (K)

Although these equations have been successfully used to predict the size and wax content of the gel for various crude oil systems, it does not provide an accurate means to properly account for the properties of the gel (i.e. gelation temperature, yield stress, etc.). Earlier parts of this section discussed the need for further research into the impact of polydispersity, cocrystallization and overall composition on the properties (particularly strength) of an n-alkane gel in great detail. It would be beneficial to incorporate these effects, either by correlation or theory into a model to provide a better prediction of the gel properties of the system to assist in proper additive addition and/or an optimal pigging schedule.

References:

Abrams, D. S. and Prausnitz, J. M., "Statistical Thermodynamics of Liquid Mixtures: A New Expression for the Excess Gibbs Energy of Partly or Completely Miscible Systems", *AIChE J.*, **21**, 116-127 (1975)

Anderson, T., Peters, H. S., Torres, R. A., Nagy, N. A., and Schruben, D. L., "Wax Crystal Size Distribution Versus Composition", *Fuel*, **80**, 1635-1638 (2001)

Ashbaugh, H. S., Radulescu, A., Prud'homme, R. K., Schwahn, D., Richter, D. and Fetters, L. J., "Interactions of Paraffin Wax Gels with Random Crystalline/Amorphous Hydrocarbon Copolymers", *Macromolecules*, **35**, 7044-7053 (2002)

Ashbaugh, H. S., Fetters, L. J., Adamson, D. H., and Prud'homme, R. K., "Flow Improvement of Waxy Oil Mediated by Self-Aggregating Partially Crystallizable Diblock Copolymets", *J. Rheol.*, **46**, 763-776 (2002)

Bennema, P., Liu, X. Y., Lewtas, K., Tack, R. D., Rijpkema, J. J. K., and Roberts, K. J., "Morphology of Orthorhombic Long Chain Normal Alkanes: theory and observations", *J. Cryst. Growth*, **121**, 679-696 (1992)

Briard, A-J., Bouroukba, M., Petitjean, D., Hubert, N., Moise, J-C., and Dirand, M., "Thermodynamic and Structural Analyses and Mechanisms of the Crystallisation of Multi-Alkane Model Mixtures Similar to Petroleum Cuts", *Fuel*, **85**, 764-777 (2006)

Chang, C., Boger, D. V., and Nguyen, Q. D., "The Yielding of Waxy Crude Oils", *Ind. Eng. Chem. Res.*, **37**, 1551-1559 (1998)

Chang, C., Boger, D. V., and Nguyen, Q. D., "Influence of Thermal History on the Waxy Structure of Statically Cooled Waxy Crude Oil", *SPE J.*, **5**, 148-157

Coutinho, J. A. P., "Predictive Local Composition Models: NRTL and UNIQUAC and Their Application to Model Solid-Liquid Equilibrium of n-Alkanes", *Fluid Ph, Equil.*, **158-160**, 447-457 (1999)

Coutinho, J. A. P. and Ruffier-Murray, V., "Experimental Measurements and Thermodynamic Modeling of Paraffinic Wax Formation in Undercooled Solutions", *Ind. Eng. Chem. Res.*, **36**, 4977-4983 (1997)

Dirand, M., Chevallier, V., Provost, E., Bouroukba, M., and Petitjean, M., "Multicomponent Paraffin Waxes and Petroleum Solid Deposits: Structural and Thermodynamic State", *Fuel*, **77**, 1253-1260 (1998)

Dirand, M., Bouroukba, M., Chevallier, V., Petitjean, D., Behar, E., and Ruffier-Murray, V., "Normal Alkanes, Multialkane Synthetic Model Mixtures and Real Petroleum Waxes: Crystallographic Structures, Thermodynamic Properties and Crystallization", *J. Chem. Eng. Data.*, **47**, 115-135 (2002)

Dong, L., Xie, H., and Zhang, F., "Chemical Control Techniques for the Paraffin and Asphaltene Deposition", *SPE 65380,* (2001)

Duffy, D. M., and Rodger, P. M., "Modeling the Activity of Wax Inhibitors: A Case Study of Poly(octadecylacrylate)", *J. Phys. Chen. B,* **106**, 11210-11217 (2002)

Duffy, D. M., and Rodger, P. M., "Hydrogen Bonding and the Conformations of Poly(alkly acrylamides)", *J. Am. Chem. Soc.,* **124**, 5206-5212 (2002)

Fuhr, B. J., Holloway, L. R. and Hammami, A., "Analytical Considerations Related to Asphaltenes and Waxes in the Same Crudes", *Energy & Fuels,* **13**, 336-339 (1999)

Garcia, M.d.C., "Crude Oil Waxy Crystallization. The Effect of Heavy n-Paraffins and Flocculated Asphaltenes", *Energy & Fuels,* **14**, 1043-1048 (2000)

Guo, X., Pethica, B. A., Huang, J. S., Prud'homme, R. K., Adamson, D. H., and Fetters, L. J., "Crystallization of Mixed Paraffin from Model Waxy Oils and the Influence of Micro-crystalline Poly(ethylene-butene) Random Copolymers", *Energy & Fuels*, **18**, 930-937 (2004)

Guo, X., Pethica, B. A., Huang, J. S., Adamson, D. H., and Prud'homme, R. K., "Effect of Cooling Rate on Crystallization of Model Waxy Oils with Microcrystalline Poly(ethylene butane)", *Energy & Fuels,* **20**, 250-256 (2006)

Hansen, J. H., Pedersen, K. S. and Ronningsen, H. P., "A Thermodynamic Model for Predicting Wax Formation in Crude Oils", *AIChE J.,* **34**, 1937-1942 (1988)

Haulait-Pirson, M-C., Huys, G., and Vanstraelen, E., "New Predictive Equation for the Solubility of Solid n-Alkanes in Organic Solvents", *Ind. Eng. Chem. Res.,* **26**, 447-452 (1987)

Jang, Y. H., Blanco, M., Creek, J., Tang, Y. and Goddard, W. A., "Wax Inhibition by Comb-like Polymers: Support of the Incorporation-Perturbation Mechanism from Molecular Dynamics Simulations, *J. Phys. Chem. B,* **111**, 13173-13179 (2007)

Kuzmic A. E., Radosevic, M., Bogdanic, G., Srica, V., and Vukovic, R., "Studies on the Influence of Long Chain Acrylic Esters Polymers with Polar Monomers as Crude Oil Flow Improver Additives", *Fuel,* **87**, 2943-2950 (2008)

Liu, X.Y., and Bennema, P. "The Relationship Between Macroscopic Quantities and the Solid-Fluid Interfacial Structure", *J. Chem Phys.,* **98**, 5863-5883 (1993)

Liu, X.Y., and Bennema, P. "On the Morphology of Crystals of Triclinic Even Normal Alkanes: Theory and Observation", *J. Cryst. Growth,* **135**, 209-223 (1994)

Paso, K. G., and Fogler, H. S. "Bulk Stabiliziation in Wax Deposition Systems", *Energy & Fuels,* **18**, 1005-1013 (2004)

Paso, K, Senra, M., Yi, Y., Sastry, A. M., and Fogler, H. S., "Paraffin Polydispersity Facilitates Mechanical Gelation", *Ind. Eng. Chem. Res.,* **44**, 7242-7254 (2005)

Petrellis, N. C., and Flumerfelt, R. W., "Rheological Behavior of Shear Degradable Oils: Kinetic and Equilibrium Properties", *Can. J. Chem. Eng.,* **51**, 291-301 (1973)

Qian, J. W., Qi, G. R., Han, D. L. and Yang, S. L., "Influence of Incipient Chain Dimension of EVA Flow Improver on the Rheological Behaviour of Crude Oil", *Fuel,* **75**, 161-163 (1996)

Sangwal, K., "Effects of Impurities on Crystal Growth Processes", *Prog. Cryst. Growth and Proc.,* **32**, 3-43 (1996)

Singh, P., Venkatesan, R., Fogler, H. S., and Nagarajan, N., "Formation and Aging of Incipient Thin Film Wax-Oil Gels", *AIChE J.,* **46**, 1059-1074 (2000)

Soldi, R. A., Oliveira, A. R. S., Barbosa, R. V., and Cesar-Oliveira, M. A. F., "Polymethacrylates: Pour Point Depressants in Diesel Oil", *European Polymer Journal,* **43**, 3671-3678 (2007)

Taraneh, J. B., Rahmatollah, G., Hassan, A., and Alireza, D., "Effect of Wax Inhibitors on Pour Point and Rheological Properties of Iranian Waxy Crude Oil", *Fuel Processing Technology,* **89**, 973-977 (2008)

van Hoof, P. J. C. M., Grimbergen, R. F. P., Meekes, H., van Enckevort, W. J. P. and Bennema, P., "Morphology of Orthorhombic n-Paraffin Crystals: A Comparison Between Theory and Experiments", *J. Cryst. Growth,* **191**, 861-872 (1998)

van Enckevort, W. J. P. and Los, J. H. "'Tailor-Made' Inhibitors in Crystal Growth: A Monte Carlo Simulation Study", *J. Phys. Chem. C,* **112**, 6380-6389 (2008)

van Hoof, P. J. C. M., van Enckevort, W. J. P. and Schoutsen, M. "The Growth of Extremely Thin Crystals: A Monte Carlo Study and an Application to n-Paraffins", *J. Cryst. Growth*, **193**, 679-691 (1998)

Venkatesan, R., Nagarajan, N. R., Paso, K., Yi, Y.-B., Sastry, A. M., and Fogler, H. S., "The Strength of Paraffin Gels Formed Under Static and Flow Conditions", *Chem. Eng. Sci.,* **60**, 3587-3598 (2005)

Visintin, R. F. G., Lockhart, T. P., Lapasin, R. and D'Antona, P., "Structure of Waxy Crude Oil Emulsion Gels", *J. Non-Newt. Fluid Mech.,* **149**, 34-39 (2008)

Wang, K-S., Creek, J. L., Shuler, P. J. and Tang, Y, "Evaluation of Effects of Selected Wax Inhibitors on Wax Appearance and Dissolution Temperatures", *Pet. Sci. & Tech.,* **21**, 359-368 (2003)

Wardhaugh, L. T., and Boger, D. V., "The Measurement and Description of the Yielding Behavior of Waxy Crude Oil", *J. Rheol.,* **35**, 1121-1156 (1991)

Winn, D. and Doherty, M. F. "A New Technique for Predicting the Shape of Solution-Grown Organic Crystals", *AICHE J.,* **44**, 2501-2514 (1998)

Winn, D. and Doherty, M. F. "Modeling Crystal Shapes of Organic Materials Grown from Solution", *AICHE J.,* **46**, 1348-1367 (2000)

Won, K. W., "Thermodynamics for Solid-Liquid Equilibria: Wax Phase Formation from Heavy Hydrocarbon Mixtures" *Fluid Ph. Equil.,* **30**, 265-275 (1986)

APPENDIX A

CALCULATION OF EXPECTED ENTHALPY OF CRYSTALLIZATION FOR POLYDISPERSE SYSTEMS

In order to evaluate an expected enthalpy of crystallization (Table 4), it is assumed that the heat released by the n-alkanes is the same for the monodisperse and polydisperse system. For the 4% C_{36}/4% C_{28} system, the heat released by each component can be determined using the enthalpies of crystallization shown in Table 2 and then combined to find the expected enthalpy of crystallization. By using a basis of 100 grams, there is 4 grams of both C_{36} and C_{28}

Heat released by C_{36}:

$$(4.0gC_{36})(\frac{molC_{36}}{506g})(\frac{174kJ}{molC_{36}}) = 1.38kJ$$

Heat released by C_{28}:

$$(4.0gC_{28})(\frac{molC_{28}}{394g})(\frac{107kJ}{molC_{28}}) = 1.09kJ$$

Therefore, a total of 2.47 kJ of heat would be expected to be released. In order to find the enthalpy of crystallization on a molar basis, the total number of moles must be determined.

Total moles in the system:

$$(4.0gC_{36})(\frac{molC_{36}}{506g}) + (4.0gC_{28})(\frac{molC_{28}}{394g}) = .0181mol$$

Dividing the amount of heat released by the total moles in the system yields the enthalpy of crystallization, which is 137 kJ/mol.

This calculation also enables the determination of what percent of the heat would be released by the respective alkanes in a polydisperse system as done in Figure 5. The percent of the heat in the 4% C_{36}/4% C_{28} system that would be released by C_{36} is:

$$\%\ \text{heat released by}\ C_{36} = \frac{\text{heat released by}\ C_{36}}{\text{heat released by}\ C_{36}\ \&\ C_{28}} = \left(\frac{1.38kJ}{2.57kJ}\right)(100) = 56\%$$

APPENDIX B

INTERMEDIATE MICROSCOPY IMAGES FOR CROSS-POLARIZED MICROSCOPY EXPERIMENTS

Work in Chapter 3 on cross polarized microscopy was completed to show how polydispersity and cocrystallization changed the crystal morphology of the systems, altering the gelation characteristics of the system. For wide temperature ranges, the microscopy images remained relatively constast with the exception of some crystal growth. This appendix is devoted to showing some of the images at intermediate temperatures not shown in Chapter 3.

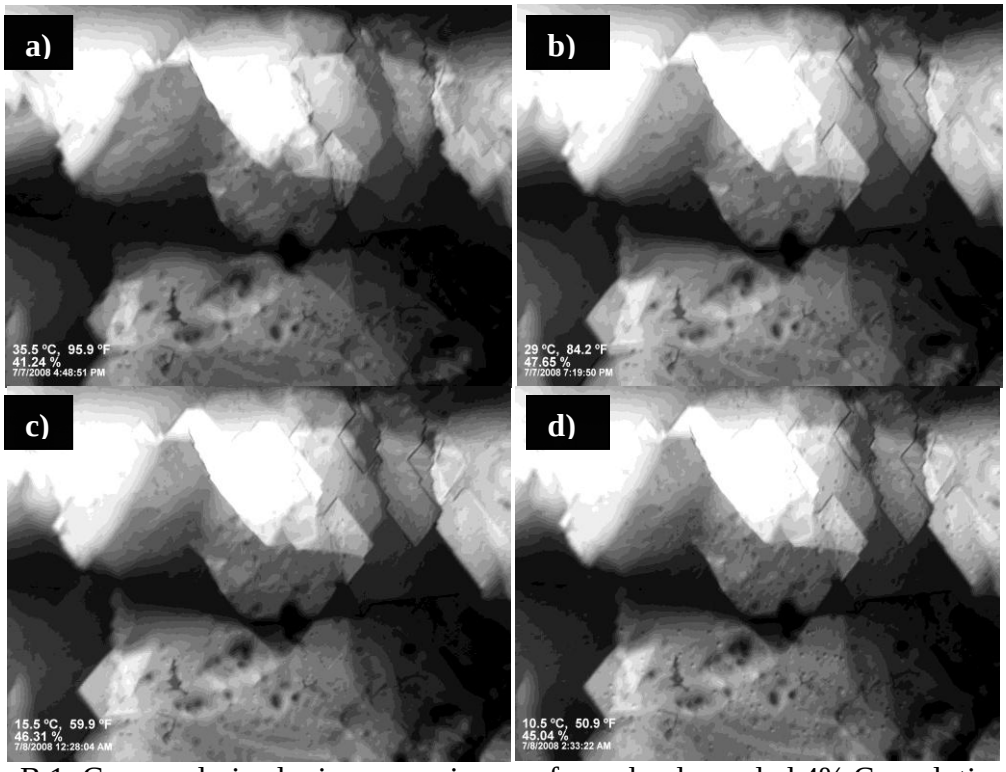

Figure B.1: Cross-polarized microscopy images for a slowly cooled 4% C_{36} solution. The temperatures of the respective micrographs are 33.5° C for a), 29° C for b), 15° C for c) and 10.5° C for d).

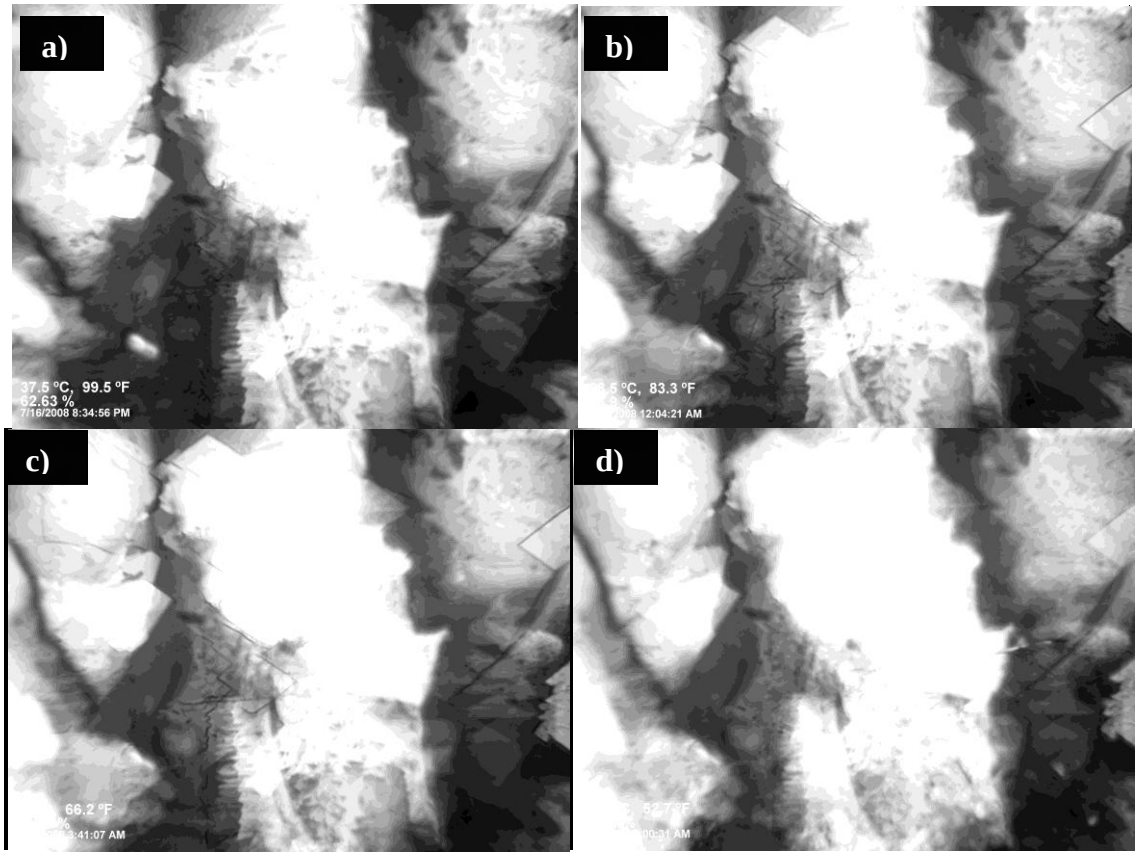

Figure B.2: Cross-polarized microscopy images for a slowly cooled 4% C_{36}/2% C_{28} solution. The temperatures of the respective micrographs are 37.5° C for a), 28.5° C for b), 19° C for c) and 11.5° C for d).

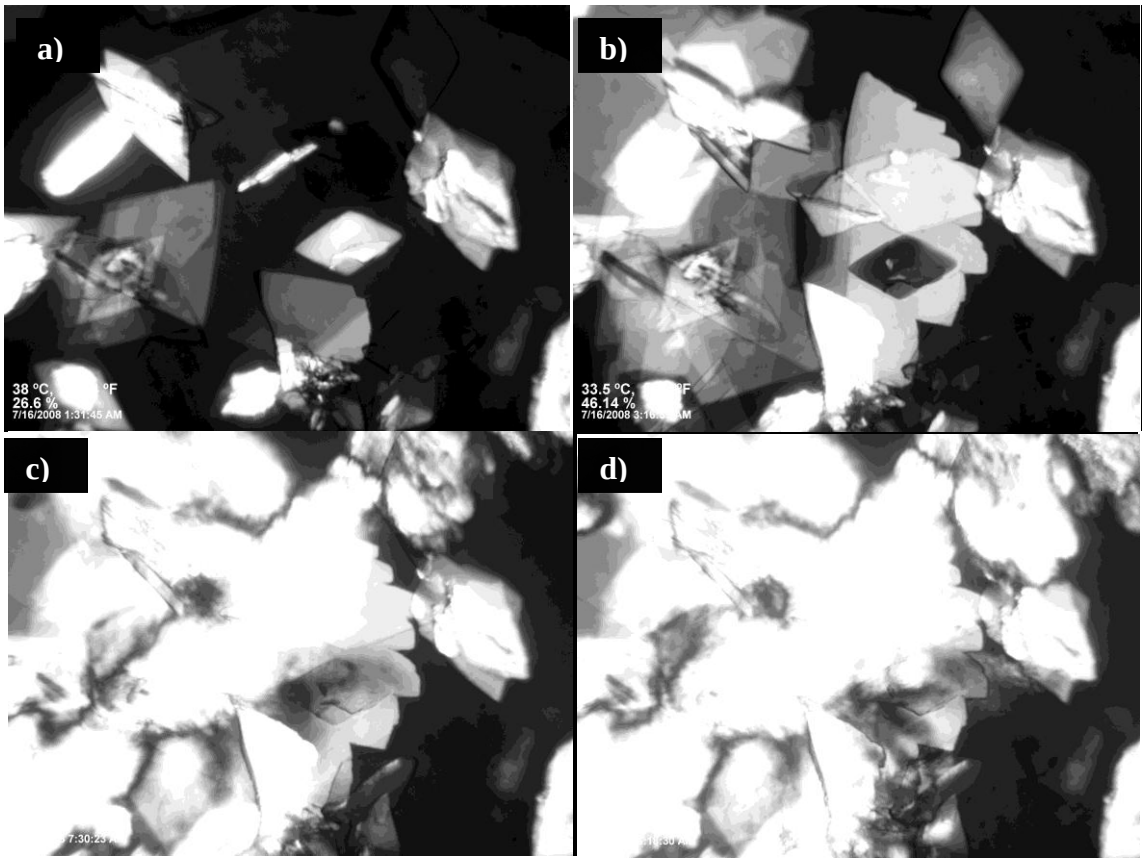

Figure B.3: Cross-polarized microscopy images for a slowly cooled 4% C_{36}/5% C_{28} solution. The temperatures of the respective micrographs are 38° C for a), 33.5° C for b), 22° C for c) and 20° C for d).

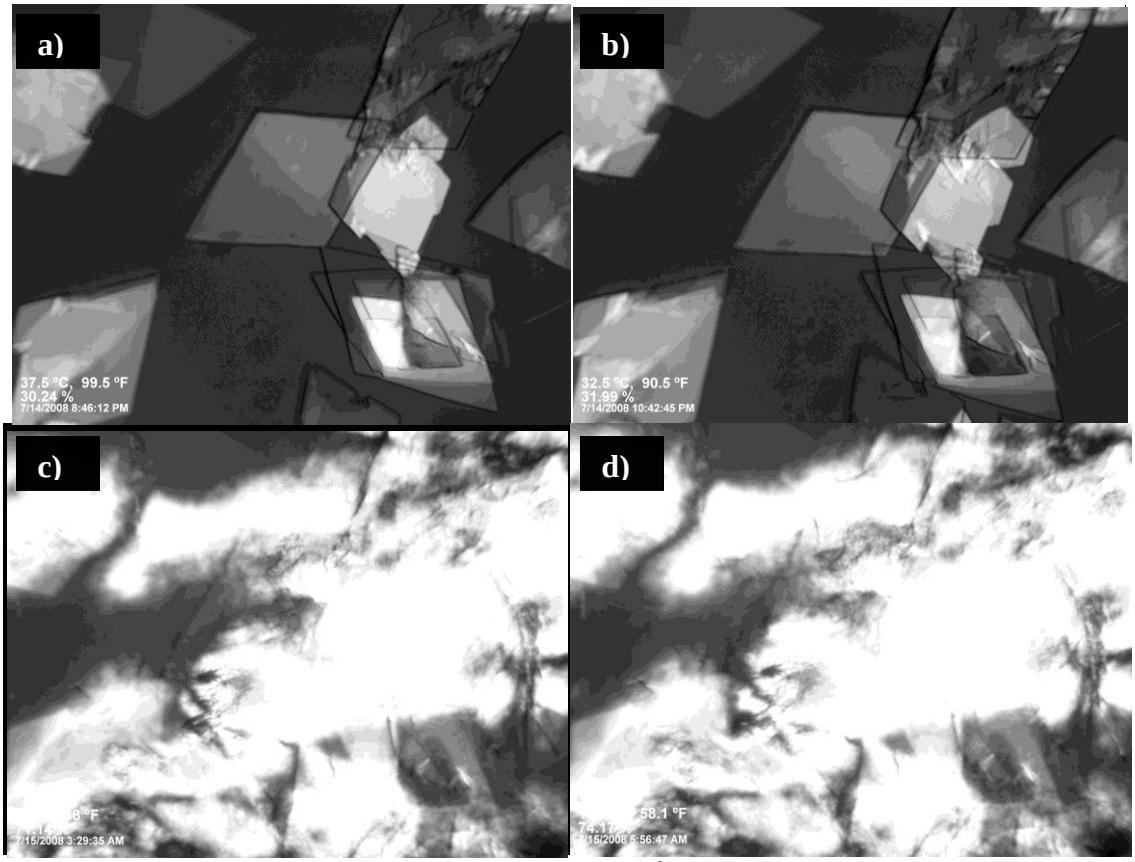

Figure B.4: Cross-polarized microscopy images for a slowly cooled 4% C_{36}/8% C_{28} solution. The temperatures of the respective micrographs are 37.5° C for a), 32.5° C for b), 20° C for c) and 14.5° C for d).

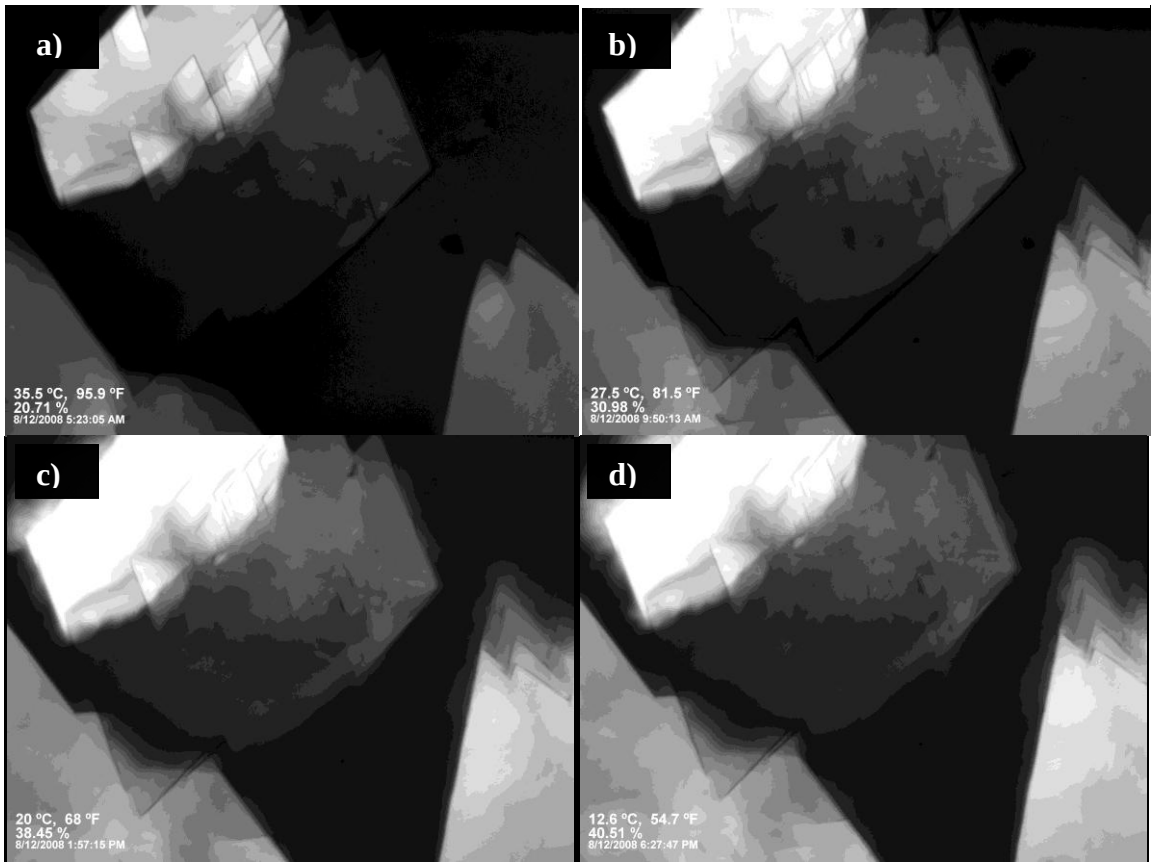

Figure B.5: Cross-polarized microscopy images for a slowly cooled 4% C_{36}/3% C_{32} solution. The temperatures of the respective micrographs are 35.5° C for a), 27.5° C for b), 20° C for c) and 12.6° C for d).

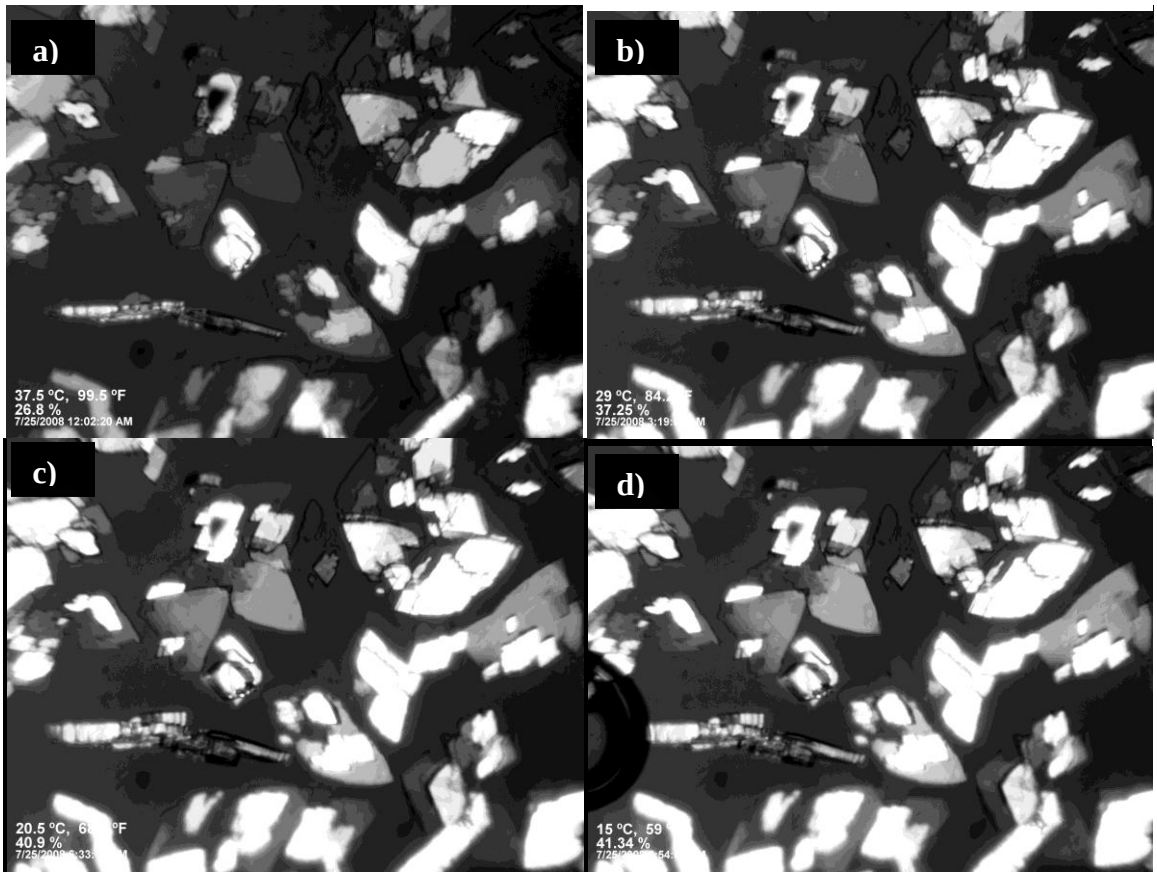

Figure B.6: Cross-polarized microscopy images for a slowly cooled 4% C_{36}/6% C_{32} solution. The temperatures of the respective micrographs are 37.5° C for a), 29° C for b), 20.5° C for c) and 15° C for d).